Note on a Null Method for the Direct Measurement of Pressure Coefficients

L. H. TANNER, B.A.

(National Physical Laboratory)

SUMMARY: Values of the pressure coefficient C_p between $+1$ and -1 can be measured directly in incompressible flow by comparison with the known pressures on a circular cylinder placed in the tunnel working section. The development of the method and the apparatus required are described. The method gives more consistent and accurate readings than can easily be obtained with normal manometer measurements, particularly when the pressure differences are small and the tunnel speed not very steady. Since the coefficients depend on Reynolds number only, less precise measurement and control of tunnel speed are required, unless the coefficients to be measured are subject to critical scale effects. Possible ways of extending the range of coefficients which can be measured are suggested.

1. Introduction

In almost all aerodynamic experiments which involve pressure measurements, a pressure ratio, or a ratio of pressure differences, is required, rather than the actual value of the pressure. In high-speed work the quantity required is sometimes the ratio of the pressure on the model to the stagnation pressure, but in low-speed work pressure coefficients—ratios of two pressure differences—are almost always used.

In view of this it seems surprising that methods for measuring these ratios directly are so rarely used. The only instruments for this purpose in general use seem to be the various types of Machmeter; these are normally used only for setting or measuring the free stream Mach numbers of wind tunnels or aeroplanes, not for routine pressure measurements. The reason why such pressure ratio instruments are so little used clearly lies in the simplicity and convenience of liquid manometers, particularly of multiple manometers for rapid reading of pressures at many different points. Such manometers have, however, some disadvantages which are worth remembering. With an ordinary multi-tube manometer, each result involves three meniscus readings, each of which contains an error. This error arises from the reading error and from the effects of surface tension, clamping the tubes, before reading, and errors in the tube position in the case of an inclined manometer. The accuracy depends largely on the magnitude of the pressure differences to be measured and becomes poor if these are small.

[Aeronautical Quarterly, Vol. VI, November 1955]
Received June 1955

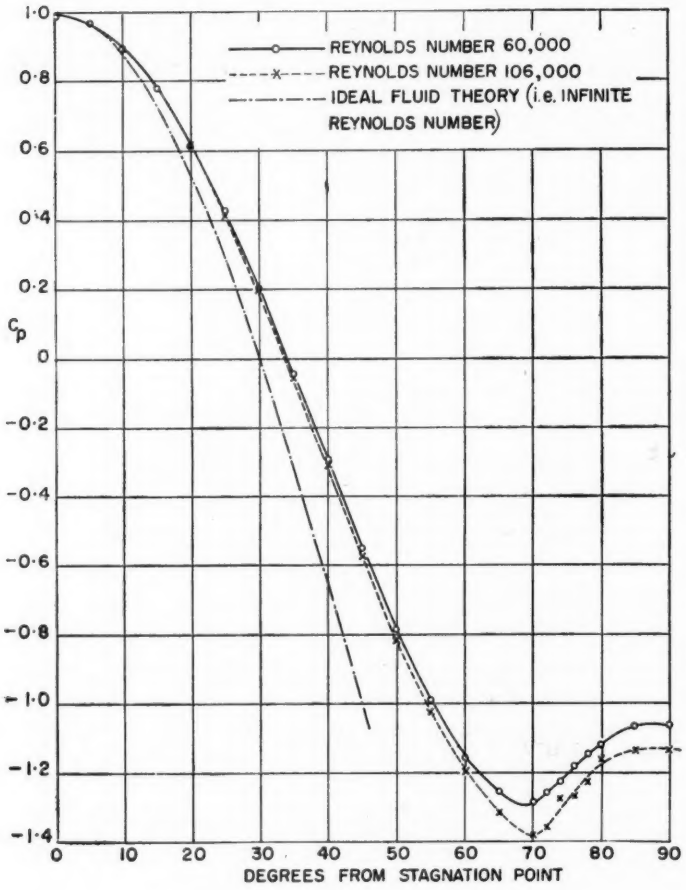

Fig. 1.

Pressure distributions round a circular cylinder (Ref. 3).

When small pressure differences are to be measured, when great accuracy is required or when a single Pitot or static tube is traversed, it is necessary to use a single manometer, usually of the type in which one limb is raised on a micrometer screw. The tunnel speed usually varies slightly with time, so it is often necessary to have a second observer measuring the tunnel dynamic pressure, which is to be used in reducing the pressure measurements to coefficient form. Even then, rapid fluctuations in tunnel speed appear as random errors in the results. The actual coefficients may be much more steady, since they would be affected only by fluctuations of flow direction, and not by speed fluctuations.

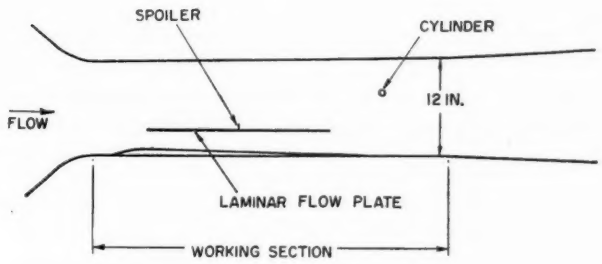

Fig. 2.

The tunnel, showing the cylinder position for the experiment on the flow past spoilers attached to a flat plate.

Thus it appears that a pressure ratio instrument would have two main advantages, namely:—

(*i*) Accuracy and ease of operation under unsteady conditions. Only one operator is required as against two for accurate work with normal manometers. With such manometers high accuracy may be obtained if the tunnel conditions are steady enough to allow the use of very sensitive gauges; these gauges, however, require skilled operators. A null indicator gives the same sensitivity more simply, and should give high accuracy with less experimental difficulty and under less perfect conditions.

(*ii*) Independence of tunnel speed. The pressure coefficient, at incompressible flow speeds, is a function of Reynolds number only, so unless there are critical Reynolds number effects only a rough estimate of tunnel speed is needed, and the speed need not be kept accurately constant. It should be noted, however, that the lack of sensitivity to tunnel speed and hence to speed fluctuations is due to the fact that these have the same effect on the model and on the instrument. The same will not normally be true of fluctuations in flow direction, and the presence of such fluctuations will limit the sensitivity of the instrument.

In the experiment for which the instrument was developed, the pressure rise ahead of a spoiler in the laminar boundary layer of a flat plate was being measured. This involved measuring coefficients of the order of 0·1 at speeds down to 15 ft./sec. So to get 5 per cent. accuracy the pressure measurement would have to be accurate to 3×10^{-4} in. of water. At first a Chattock gauge was used, but the experimental scatter was large, the results were clearly erratic and could not be consistently repeated. It was therefore decided to replace the Chattock by some instrument which would be easier to use and also more sensitive. The only way of achieving this seemed to be to use a pressure ratio instrument combined with a null indicator. The instrument developed and described here enabled accurate measurements to be made, and with reasonable ease. The principle involved may have wider applications and some possibilities for its development are discussed.

NOTATION

C_p	a pressure coefficient, $=(P-P_0)/(H-P_0)$
P	local static pressure at the point under consideration
P_0	free stream static pressure
H	free stream total pressure
θ	the angle between the cylinder radius through the pressure hole and that through the zero C_p position
n	a factor depending on the cylinder Reynolds number (*see* Section 4.1(3))
m	a factor depending on the thickness of the wake produced by the model (*see* Section 4.1(4))

2. The Circular Cylinder as a Pressure Coefficient Meter

Pressure distributions round circular cylinders have been measured by Schiller and Linke[1], and by Fage and Falkner[2, 3], some of whose results are shown in Fig. 1. These show that the pressure coefficient varies from $+1$ at the stagnation point to about $-1{\cdot}3$ just ahead of the laminar separation. Suppose that such a cylinder, with one pressure hole in its surface, is placed in the working section of the tunnel in which tests are being made on a model. The speed of flow past the cylinder will automatically be proportional to that past the model (subject to certain reservations noted later). So if the cylinder is rotated so that the pressure at its pressure hole is the same as that at a point on the model, the angle of rotation (from the zero C_p position) will be a measure of the pressure coefficient. This is the basis of the instrument to be described.

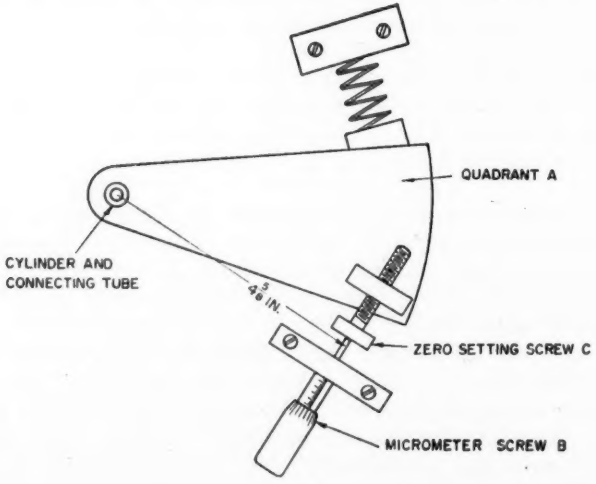

Fig. 3.
The cylinder and adjusting screws.

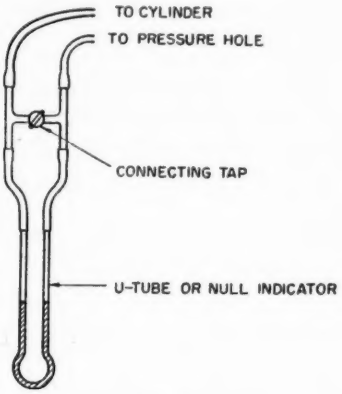

Fig. 4..
Connections to the null indicator.

3. Apparatus and Experimental Details

3.1. The Cylinder

The apparatus was developed in a 12 in. × 8 in. open-return tunnel which gives a maximum speed of 90 ft./sec. The instrument is an approximately circular and cylindrical length of copper gas-pipe, $\frac{3}{8}$ in. diameter, spanning the 8 in. tunnel width and rotating in two holes in the wooden tunnel walls. It is placed at the rear of the working section near the centre line of the tunnel, as shown in Fig. 2. The cylinder has one pressure hole, about 0·01 in. diameter, in the surface. One end of the cylinder is fixed to the quadrant *A* as shown in Fig. 3, and it can be rotated about its axis by the micrometer screw *B*, or by the zero-setting screw *C*. The micrometer screw is $4\frac{5}{8}$ in. from the axis, so a travel of 0·1 in. corresponds to a rotation of 1·27°.

Initially the cylinder was set relative to the quadrant so that, with screw *B* at zero and *C* at about its mid-position, the pressure at the hole was approximately equal to the tunnel static pressure. It was then fixed to the quadrant and further adjustments were made entirely by the two screws.

In use, the zero-setting screw *C* is adjusted until the pressure at the hole is equal to the tunnel static or datum pressure, with screw *B* at zero. For this purpose the hollow cylinder is connected to one side of a null pressure indicator; the other side is connected to the datum pressure hole. Next this datum pressure hole is disconnected, and the indicator is connected to the pressure to be measured. The micrometer screw *B* is adjusted until the cylinder pressure is equal to this, and the micrometer reading then gives a measure of the pressure coefficient required. The effect of the choice of the datum pressure is discussed in Section 4.2.

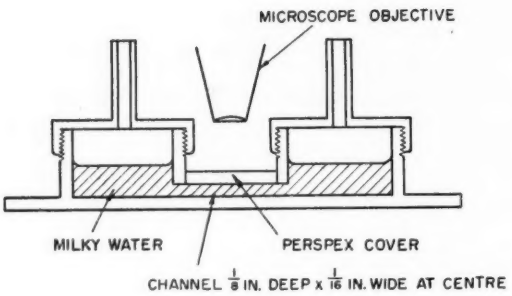

Fig. 5.
The null indicator. Sectional view. Half size.

3.2. The Null Indicator

The type of indicator used for detecting a pressure difference will depend mainly on the magnitude of the pressure differences involved. For most ordinary low-speed work a simple inclined U-tube, with a tap to connect the limbs, as shown in Fig. 4, would probably be suitable. For the experiment considered here, however, a much more sensitive device was required, and Fig. 5 shows a sectional view of the type used. Essentially this is also a U-tube. The two limbs are brass capsules $1\frac{1}{8}$ in. diameter and the connecting channel, about $\frac{1}{8}$ in. $\times \frac{1}{16}$ in. in cross section, has its roof and one side made of Perspex. A beam of light from a projector lamp illuminates particles in the fluid in this channel, and these are viewed through a low power microscope as shown. The area ratio is such that a pressure difference of 0·001 in. of water gives a mean particle movement of about 0·06 in., and the corresponding travel in the microscope field is about 2 in. It is therefore easy to detect a pressure difference of 10^{-4} in. of water. The sensitivity, in this sense, could be increased almost indefinitely by increasing the area ratio, or the power of the microscope, but in use the sensitivity is limited by the fluctuations in the stream.

The fluid used is water with the addition of two or three drops of milk to provide suitable particles. This needs changing every few days as the particles coagulate. Possibly a more stable material could be found, but the milk is the best of those tried. The capsules have screw tops so that the fluid can be easily replaced.

One side of the instrument is connected to the cylinder hole and the other to the pressure hole with which this is to be compared. A tap, as in Fig. 4, is arranged so that the two sides may also be connected directly together. The cylinder is rotated until opening or closing the tap causes no appreciable movement of the particles. This is a trial and error process which is, however, very rapidly convergent, particularly when the required cylinder position is roughly known as, for example, when taking readings at consecutive holes along the plate. The main practical difficulty is due to the fluctuations. It is best not to try to observe the mean direction of motion when the tap is closed, but rather to check that there is little movement on opening the tap.

Obtaining a reading takes about as long as with a Chattock gauge, owing to the trial and error process and the fluctuations. The apparatus, however, follows pressure changes much more rapidly than a normal Chattock, as is evident from the fact that the null indicator is affected by rapid fluctuations. This is probably due mainly to the fact that the connecting channel of the null indicator can be much smaller in area than the Chattock meniscus, so that less air has to flow through the pressure hole to cause a given movement.

4. The Calibration of the Cylinder, and the Assumptions Involved

4.1. The Calibration Measurements Required

There are four points to check in calibrating the cylinder, namely:—

(1) The position of zero pressure coefficient. This depends on tunnel speed (*i.e.* on cylinder Reynolds number) and on the model in the tunnel, since this may alter the flow direction at the cylinder. To allow for this the cylinder is adjusted by the zero-setting screw until the pressure is equal to the datum static pressure. This is normally done at each run of the tunnel, although this may not be necessary if the speed and model are the same in the next run.

(2) The variation of pressure coefficient with micrometer reading. This will probably be linear if the required range is small; otherwise a complete calibration is necessary.

(3) The variation of micrometer reading with Reynolds number, at a given pressure coefficient.

The pressure distribution round the front part of a circular cylinder varies very little with Reynolds number, so long as this is always below, or always above, that of the change from laminar to turbulent separation. The cylinder size used should be such as to avoid the critical range of Reynolds number. Normally, Reynolds numbers below the critical would be used, except perhaps in a compressed air tunnel. For example in a normal tunnel at 300 ft./sec. and with a cylinder diameter of 1 in., the Reynolds number would be about 160,000, which would probably still be below the critical value. With the cylinder diameter of $\frac{3}{8}$ in. and the tunnel speeds used in the present experiment, the Reynolds number ranges from 3,000 to 18,000.

Points (2) and (3) are properties of a given cylinder and tunnel only, and to a first order are independent of the model under test. So it would not be too difficult to obtain a complete set of readings giving C_p as a function of micrometer reading and Reynolds number. This is not necessary, however. The variation with Reynolds number is such that it can be assumed, for C_p between $+1$ and -1 at least, that the pressure distribution has the same shape at all Reynolds numbers, the sensitivity (rate of variation of C_p with θ) alone varying. That is, it can be assumed that C_p is a function of $n\theta$ or $n \times$ the micrometer reading, where n is a factor depending on the Reynolds number. It is then only necessary to measure n, which

involves one measurement only at each speed. This can be the reading at the highest C_p, positive or negative, in the required range, which can be done accurately even at low speeds. The shape of the distribution, (2), can be determined with good accuracy at the highest speed.

Alternatively, the factor n could be determined by measuring the angle between the two positions of zero C_p, one on each side of the front stagnation point. No manometer readings would then be needed except at the highest tunnel speed, but a device for measuring the angle of rotation over the range of about 70° would be required.

Thus the calibration measurements could all be done at the highest tunnel speed, and so the accuracy of the method is not limited to that obtainable with normal manometers, even though these have to be used for the calibration.

(4) Variation of sensitivity with the configuration of the model. There are two possible effects namely:—

(*a*) If the model produces a wake, the sensitivity will increase, since the velocity at the cylinder will be raised.

Once again the shape of the curve of C_p against θ should be unchanged, so C_p will be a function of $m\theta$, where m depends on the thickness of the wake. This will depend on the model and possibly also on its Reynolds number, as for example with a wing stalled at low speeds but not at high speeds. Again, if m has to be measured at low speeds this could be done most accurately by measuring the angle between the two positions of zero C_p.

This dependence on the wake produced by the model could be eliminated by placing the cylinder ahead of the model, at the front instead of the rear of the working section. The front position would thus be better, so long as no trouble arises from the turbulent wake of the cylinder.

(*b*) If the cylinder is too near the model, the model will produce a velocity gradient affecting the cylinder pressure distribution. The sensitivity will be affected differently on the two sides of the stagnation point, so the change cannot be measured by measuring the angle between the zero C_p positions. In practice the cylinder should be made small and placed sufficiently far from the model to ensure that the effect will be negligible.

These effects will probably be most serious if the model is an aerofoil at incidence. The flow direction at the cylinder will vary with the aerofoil incidence, so the zero C_p position must be readjusted after any change of incidence. The most serious effect, however, is that the circulation round the aerofoil produces a velocity gradient at the cylinder. In the present tunnel, if the $\frac{3}{8}$ in. diameter cylinder were placed 12 in. from the centre of an aerofoil of 4 in. chord, at a lift coefficient of unity, the variation of velocity from one side of the cylinder to the other would be roughly 0·001 of the stream velocity. Thus the effect can be made fairly small.

4.2. The Method of Calibration

The cylinder is first adjusted so that the pressure at its pressure hole is equal to the datum static pressure, by means of the zero-setting screw. The tunnel dynamic pressure is then measured on a Chattock or other manometer. Then the Chattock is set to a definite fraction, for example $\frac{1}{5}$, of the reading obtained, and the cylinder is connected to it in place of the Pitot tube. The micrometer screw is then adjusted to balance the Chattock, and the reading obtained is that corresponding to a pressure coefficient of 0·2. Finally the Pitot tube is replaced to check the dynamic pressure.

It should be noted that the pressure coefficient measured is $(P-P_1)/(H-P_2)$, where P_1 is the datum pressure used for setting the cylinder when taking measurements on the model, and P_2 is the datum used in the calibration. The method should give an accurate measure of this quantity. It is an accurate measure of C_p only if P_1 and P_2 are both equal to the true free stream static pressure, and this will depend on the design and location of the static tubes or holes in the usual way.

5. Results

5.1. Calibration

The range of pressure coefficients required for the experiment on the flow ahead of spoilers was small, and so calibration was carried out over the range of C_p from 0 to +0·2 only. The results at various speeds given in Table I show that the variation with micrometer reading was linear and that the sensitivity was independent of Reynolds number in this range (3,000 to 12,000). The factor n is thus constant and may be taken as unity.

TABLE I

READINGS FOR $C_p=0{\cdot}1$ AND 0·2 AT VARIOUS SPEEDS, WITH A $\frac{1}{4}$ IN. SPOILER IN POSITION

Dynamic Pressure (in. water)		*Micrometer Reading*		$\frac{C_p}{\text{Micrometer Reading}}$	
Before Reading	*After Reading*	$C_p=0{\cdot}1$	$C_p=0{\cdot}2$	$C_p=0{\cdot}1$	$C_p=0{\cdot}2$
0·0685	0·0682	0·167	0·340	0·599	0·588
0·1028	0·1028	0·170	0·330	0·588	0·606
0·171	0·172	0·167	0·330	0·599	0·606
0·360	0·361	0·167	0·330	0·599	0·606
0·627	0·626	0·165	0·330	0·606	0·606
0·912	0·915	0·167	0·335	0·599	0·596
				Mean 0·600	

TABLE II

READINGS AT TOP SPEED AND $C_p=0{\cdot}2$, WITH VARIOUS SPOILERS

Spoiler Height	*Dynamic Pressure (in. water)*		*Cylinder Pressure*	*Micrometer Reading*	$\frac{C_p}{\text{Micrometer Reading}}$
	Before Reading	*After Reading*			
No Spoiler	0·884	0·880	0·179	0·354	0·571
$\frac{1}{4}$ in.	0·858	0·852	0·172	0·348	0·576
$\frac{1}{2}$ in.	0·852	0·852	0·171	0·338	0·593

KRESGE-HOOKER WAYNE UNIVERSITY SCIENTIFIC LIBRARY

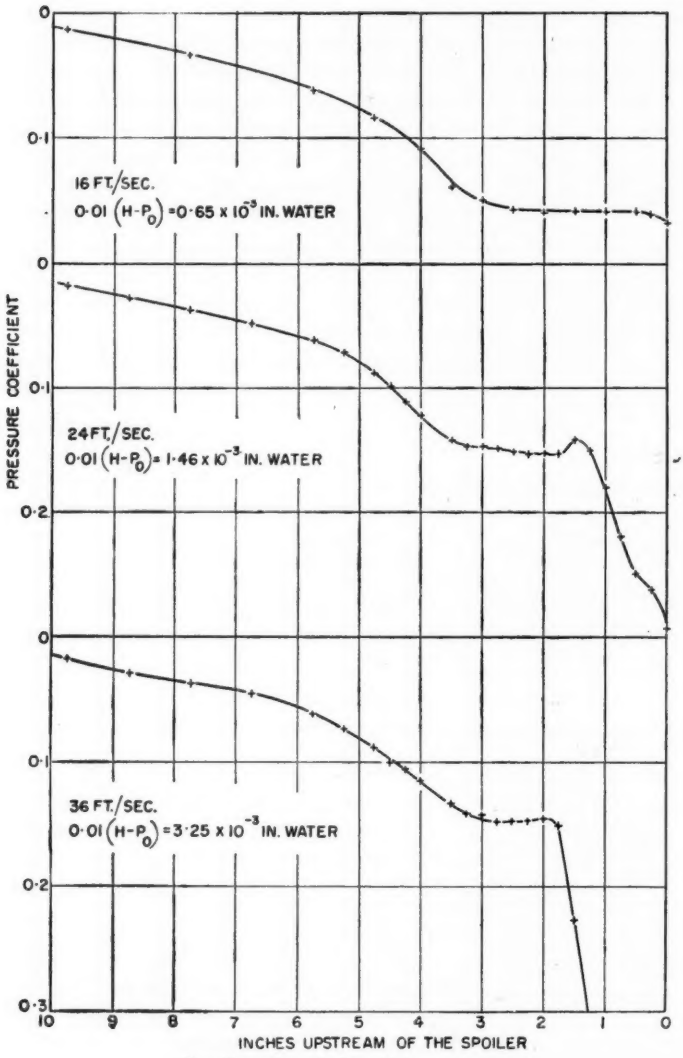

(Leading edge of plate 12 in. upstream)

Fig. 6.

Pressure distributions upstream of a $\frac{1}{2}$ in. spoiler on a flat plate with laminar boundary layer.

A set of readings with different spoilers in position was taken, at the highest speed and a C_p of 0·2. These show that a $\frac{1}{2}$ in. high spoiler in the 12 in. high tunnel increases the sensitivity by about 4 per cent., corresponding to an increase in displacement thickness of the wake of about $\frac{1}{4}$ in. The factor m thus varies from unity with no spoiler to 0·96 with the $\frac{1}{2}$ in. spoiler. The slight discrepancy between the

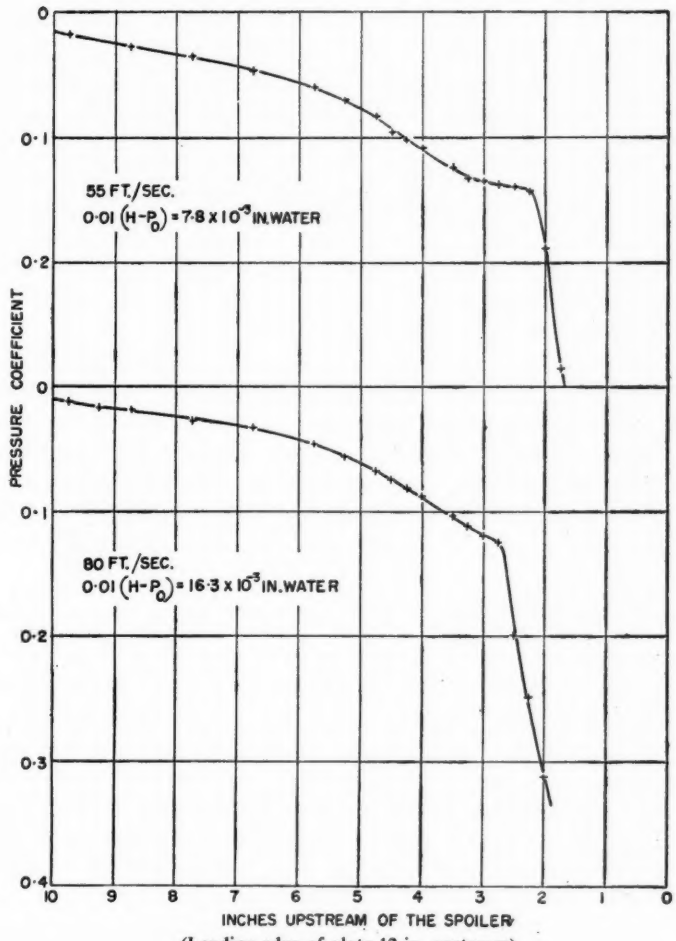

Fig. 7.

Pressure distributions upstream of a ½ in. spoiler on a flat plate with laminar boundary layer.

two readings given in Tables I and II for the ½ in. spoiler is probably due to a difference in the incidence of the plate on the two occasions.

5.2. Pressure Distributions

Figures 6 and 7 give pressure distributions at various speeds from 16 to 80 ft./sec., which show that the readings are consistent and the random errors small, even at low speeds and small pressure coefficients. The pressure difference corresponding to a coefficient of 0·01 is shown on each graph, and ranges from $0{\cdot}65 \times 10^{-3}$ in. to $16{\cdot}3 \times 10^{-3}$ in. of water.

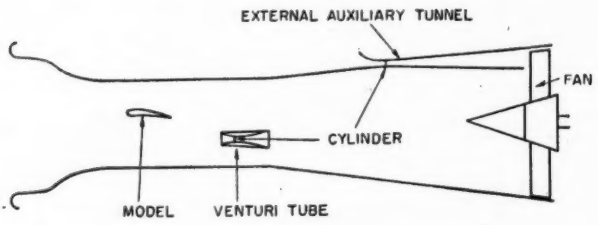

Fig. 8.
Methods of increasing the measurable range of C_p.

5.3. General Behaviour of the Apparatus

It is perhaps worth noting that the cylinder part of the apparatus was assembled in a few hours, that no modifications or development were needed, and that no trouble has been experienced in routine experimental use. The development of the null indicator proved more difficult, but since the design shown in Fig. 5 was made, and a suitable fluid found, no trouble has occurred. Despite initial difficulties with the null indicator, the complete equipment was in routine use within about a fortnight of the initial decision to try the idea.

6. Further Possibilities for Development

The arrangement described could be used over a range of C_p from $+1$ to about -1. For still larger negative coefficients there seem to be two possible ways of extending this range, namely:—

(*i*) An aerofoil, with a pressure hole at or near the leading edge on the upper surface, could be used instead of the cylinder. This should give large negative coefficients, but more care would be needed in calibrating to find any Reynolds number effects. In particular, the simplifying assumptions made in Section 4.1 in calibrating the cylinder at varying Reynolds numbers would probably not be applicable.

(*ii*) A very small auxiliary tunnel could be used, driven by the main tunnel fan but with a more efficient diffuser giving a higher speed. This could be separate from the main tunnel, except for the end of the diffuser, or alternatively it could be in the form of a venturi tube held in the tunnel, as Fig. 8 shows. For example, if the small tunnel ran at twice the speed of the main tunnel, a circular cylinder placed in it would give a range of C_p, based on main tunnel speed, from $+1$ to -7, which should be adequate for most uses. Further advantages would be that the sensitivity should depend less on the wake produced by the model in the tunnel and that the effect of fluctuations in flow direction may be reduced.

The method could probably be made automatically self-balancing with little difficulty, by using some type of null indicator to control a motor rotating the cylinder.

7. Conclusions

Pressure coefficients ranging from $+1$ to -1 can be measured by comparing the pressure on the model with that on a circular cylinder placed at the front or rear of the working section. The method has two main advantages:——

(*i*) It gives more consistent readings than normal manometer measurements, particularly for small pressure differences or in unsteady conditions. The instrument is insensitive to fluctuations in tunnel speed, although it is affected by fluctuations in flow direction. The calibration needed may often be done entirely at high speeds, so the accuracy is practically independent of manometer measurements. Being a null method it can be used over a wide range of pressure differences while a very high sensitivity is retained.

(*ii*) Since it measures coefficients directly, the reading usually varies only slowly with speed, so no precise measurement or regulation of tunnel speed is needed.

The possible range of coefficients might be greatly increased by using an aerofoil instead of the cylinder, or by placing the cylinder in a small auxiliary tunnel running at higher speed.

The apparatus is simple and convenient, requires little development and has given very little trouble in use.

Acknowledgments

Miss C. M. Tracy, B.A., has done most of the experimental work with the apparatus, including that summarised in Figs. 6 and 7. The work formed part of the research programme of the Aerodynamics Division of the National Physical Laboratory and is published with the permission of the Director.

References

1. Linke, *Physikalische Zeitschrift*, Vol. 32, pp. 900-914, 1931; Schiller and Linke, *Zeitschrift für Flugtechnik und Motorluftschiffahrt*, Vol. 24, pp. 193-198, 1933.
Goldstein, S. (Editor). *Modern Developments in Fluid Dynamics.* First Edition, Oxford University Press. Vol. II, pp. 423-4, 1938.

2. Fage, A. The Airflow around a Circular Cylinder in the Region where the Boundary Layer Separates from the Surface. R. & M. 1179, 1928.

3. Fage, A. and Falkner, V. M. Further Experiments on the Flow around a Circular Cylinder. R. & M. 1369, 1930.

Compressible Subsonic Flow in Two-dimensional Channels

Part II: The Application of the Theory to Problems of Channel Flow*

L. C. WOODS, D.Phil., A.F.R.Ae.S.

(Department of Applied Mathematics, University of Sydney)

SUMMARY: The theory developed in Part I* is applied to a number of problems of aeronautical interest, the most important of which is to the setting of "streamline" walls about a symmetrical aerofoil placed in the centre of a channel. It is shown how the position of the streamline wall can be deduced from the (experimentally determined) position of a constant pressure wall. This theory is applicable to symmetrical aerofoils of any given shape, and makes allowance for the presence of the aerofoil's wake. To illustrate the theory, and to test it by an extreme example, the flow is calculated about a circular cylinder, with a diameter about half the tunnel height, for both straight and constant pressure walls. The solid blockage is calculated in each case and compared with the standard first order theory. For this extreme example the standard theory fails badly for straight walls, but is reasonably accurate for constant pressure walls.

NOTATION (Additional to that defined in Part I*)

$\mathrm{gd}\, x = 2\tan^{-1}(\tanh \frac{1}{2}x)$, the Gudermannian function

R radius of curvature of a solid boundary

A cross-sectional area of an aerofoil

ε blockage factor, $(q-q_t)/q_t$

$\sigma = y_t/y_p$, on the walls

c aerofoil chord

C_D drag coefficient

Suffixes "p" and "f" denote values appropriate to "constant pressure walls" and "streamline walls," respectively.

7. Summary of Equations

Let (q, θ) be the velocity vector in polar co-ordinates, ϕ, ψ be the velocity potential and stream functions, $\lim_{\phi\to-\infty}(q, \theta)=(U, 0)$ (upstream), $\lim_{\phi\to\infty}(q, \theta)=(V, \tau)$,

*Part I of this paper was published in August 1955 (pp. 205-220).

Received June 1955.

M_∞ be the Mach number at $\phi=-\infty$, $\beta_\infty=(1-M_\infty^2)^{\frac{1}{2}}$, $m_\infty=\beta_\infty\rho_0/\rho_\infty$, where ρ_∞, ρ_0 are the fluid densities at $\phi=-\infty$ and a stagnation point respectively,

$$\varepsilon=\sinh^{-1}(\beta_\infty/M_\infty), \quad . \quad . \quad . \quad . \quad . \quad (1)$$

and Ω is defined by

$$\frac{q}{U}=\sinh\varepsilon\,\mathrm{cosech}\,(\Omega+\varepsilon). \quad . \quad . \quad . \quad . \quad (2)$$

Then it has been shown in Part I that the flow through a given channel can be calculated from

$$f(w)=-\frac{1}{\pi}\int_{\phi=-\infty}^{\infty}\log\sinh\frac{\pi}{2h}(\phi-w)\,d\theta_0(\phi)+\frac{1}{\pi}\int_{\phi=-\infty}^{\infty}\log\cosh\frac{\pi}{2h}(\phi-w)\,d\theta_h(\phi)+\frac{1}{2}\log\frac{U}{V}, \quad . \quad . \quad . \quad . \quad (3)$$

$$\log\frac{U}{V}=\frac{1}{h}\int_{\phi=-\infty}^{\infty}\phi\,d\theta_0(\phi)-\frac{1}{h}\int_{\phi=-\infty}^{\infty}\phi\,d\theta_h(\phi), \quad . \quad . \quad . \quad (4)$$

$$h=UH\beta_\infty, \quad . \quad . \quad . \quad . \quad . \quad . \quad (5)$$

where $f=\Omega+i\theta$, $w=\phi+im_\infty\psi$, H is the channel width at $\phi=-\infty$, and θ_0, θ_h are the values of θ on the walls $\psi=0$, $\psi=h/m_\infty$ respectively.

It has also been shown that the physical or $z(=x+iy)$-plane is related to the w-plane by

$$Udz=\frac{1+\beta_\infty}{2\beta_\infty}e^f\,dw-\frac{1-\beta_\infty}{2\beta_\infty}e^{-\bar{f}}\,d\bar{w}, \quad . \quad . \quad . \quad (6)$$

and that the channel width K downstream at infinity is given by

$$\frac{K}{H}=\frac{1+\beta_\infty}{2\beta_\infty}\frac{U}{V}+\frac{1-\beta_\infty}{2\beta_\infty}\frac{V}{U}. \quad . \quad . \quad . \quad . \quad (7)$$

If the wall $\psi=h/m_\infty$ is a constant pressure wall, it has been shown in Part I that

$$f=\frac{1}{2h}\int_{-\infty}^{\infty}\theta_0\,\mathrm{cosech}\frac{\pi}{2h}(\phi-w)\,d\phi. \quad . \quad . \quad . \quad . \quad (8)$$

Also, for channel design the equations

$$f=\frac{-i}{2h}\int_{-\infty}^{\infty}\left\{\Omega_0\coth\frac{\pi}{2h}(\phi-w)-\Omega_h\tanh\frac{\pi}{2h}(\phi-w)\right\}d\phi+\frac{1}{2}i\tau, \quad . \quad (9)$$

and

$$\tau=\frac{1}{h}\int_{-\infty}^{\infty}(\Omega_0-\Omega_h)\,d\phi, \quad . \quad . \quad . \quad . \quad . \quad . \quad . \quad . \quad . \quad . \quad (10)$$

have been established.

One final result required in this paper is that when $\theta_0(\phi)$ is differentiable we can write

$$d\theta_0=-\frac{d\phi}{Rq_0}, \quad . \quad . \quad . \quad . \quad . \quad (11)$$

where $R(=ds/d\theta)$ is the radius of curvature of the wall, and q_0 is the velocity at the wall: a similar result holds for $d\theta_h$.

8. Boundary Conditions Prescribed as Simple Step-Functions

There are many problems in which the boundary values are specified as simple step-functions. For example, in the direct problem of calculating the flow through a given channel the walls may be composed of a number of straight sections; in this case the direction of flow, θ, is a step-function on the walls; Fig. 1 shows such a case. A similar case is shown in Fig. 2, except that here one wall is at constant pressure.

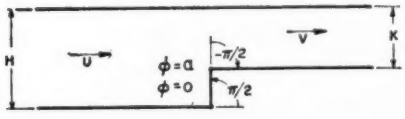

Fig. 1.
Channel with rectilinear walls.

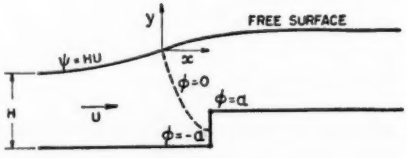

Fig. 2.
Flow of a stream up a step.

Similarly, in the indirect or design problem it may be considered desirable to prescribe constant pressure over a number of intervals, for this avoids adverse pressure gradients except those occurring at points of pressure discontinuity, and flow separation at these points could be prevented by some form of boundary layer control. Lighthill[1] has used this principle to design wind tunnel bends; Fig. 3 shows such a bend, obtained by prescribing $q=U$ on $E_{-\infty}CE_{\infty}$, $E_{-\infty}A$ and BE_{∞}, and $q=V$ on AB.

8.1. Flow Through a Channel with Rectilinear Walls

The following theory is not strictly applicable to compressible flow, as with flow past a sharp projecting corner the local Mach number exceeds unity in the neighbourhood of the corner; however, outside such neighbourhoods the theory will yield reasonably accurate results.

Suppose that θ_0 is constant except for discontinuities of amount τ_j at $\phi=\phi_j$, $j=1, 2, \ldots m$, and that θ_h is likewise constant except for jumps τ_i at $\phi=\phi_i$, $i=1, 2, \ldots n$, then the Riemann-Stieltjes integrals in (3) and (4) degenerate to give

$$f=\frac{1}{2}\log\frac{U}{V}-\frac{1}{\pi}\sum_j \tau_j \log\sinh\frac{\pi}{2h}(\phi_j-w)+\frac{1}{\pi}\sum_i \tau_i \log\cosh\frac{\pi}{2h}(\phi_i-w),$$

$$\text{and}\qquad h\log\frac{U}{V}=\sum_j \tau_j\phi_j-\sum_i \tau_i\phi_i.$$

Hence from (2), (5) and (6) the required solution is contained in

$$Uz=\frac{1+\beta_\infty}{2\beta_\infty}\int A(w)\,dw-\frac{1-\beta_\infty}{2\beta_\infty}\int\frac{d\overline{w}}{A(\overline{w})}, \qquad \ldots \quad (12)$$

$$\frac{U}{V}=\prod_j \exp(\tau_j\phi_j/HU\beta_\infty)\prod_i \exp(-\tau_i\phi_i/HU\beta_\infty)$$

$$q=U\left\{\frac{1+\beta_\infty}{2\beta_\infty}\,|A(w)|-\frac{1-\beta_\infty}{2\beta_\infty}\,|A(\overline{w})|^{-1}\right\}^{-1},$$

$$\text{and}\qquad A(w)=\left(\frac{U}{V}\right)^{\frac{1}{2}}\prod_j\left[\cosh\frac{\pi}{2HU\beta_\infty}(\phi_i-w)\right]^{\frac{\tau_i}{\pi}}\prod_j\left[\sinh\frac{\pi}{2HU\beta_\infty}(\phi_j-w)\right]^{-\frac{\tau_j}{\pi}},$$

where the ratio U/V is determined from (7). The constants ϕ_i, ϕ_j are calculated from (12) and the known corresponding values of z. Notice the simplification that occurs when $\beta_\infty=1$, that is when the flow is incompressible.

The usual method of solving these problems is by means of the Schwarz-Christoffel mapping theorem, which yields the same results, but with more labour.

8.2. Design of a Channel with Wall Pressures Sectionally Constant

The calculation is similar to that given in Section 8.1. From (9) and (10),

$$f=\frac{1}{2}i\tau+\frac{i}{\pi}\left\{\sum_j \Omega_j\log\sinh\frac{\pi}{2HU\beta_\infty}(\phi_j-w)-\sum_i \Omega_i\log\cosh\frac{\pi}{2HU\beta_\infty}(\phi_i-w)\right\}, \qquad \ldots \quad (13)$$

$$\text{and}\qquad \tau=\frac{1}{HU\beta_\infty}\left(\sum_i \Omega_i\phi_i-\sum_j \Omega_j\phi_j\right), \qquad \ldots \quad (14)$$

where Ω_j are the jumps in Ω_0 at $\phi=\phi_j$, and Ω_i are the jumps in Ω_h at $\phi=\phi_i$.

As a simple example, suppose Ω_0 jumps from 0 to σ at $\phi=-a$, and from σ to 0 at $\phi=a$, and that $\Omega_h=0$ for all ϕ; then, from (13) and (14),

$$f=\frac{1}{2}i\tau+\frac{i\sigma}{\pi}\log\frac{\sinh\{\pi(w+a)/2HU\beta_\infty\}}{\sinh\{\pi(w-a)/2HU\beta_\infty\}}, \quad . \quad . \quad . \quad . \quad (15)$$

$$\tau=2a\sigma/(HU\beta_\infty). \quad . \quad . \quad . \quad . \quad . \quad (16)$$

As indicated at the beginning of Section 8, these equations can be used to design an efficient bend in a channel; σ and a are chosen to give the desired value of τ (equation (16))—the angle of the bend—then (15) yields the required wall shape.

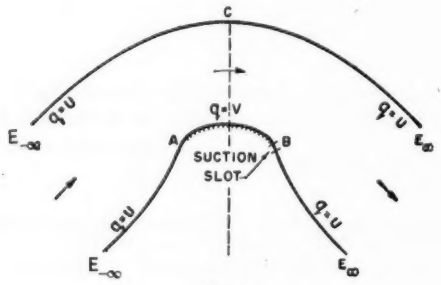

Fig. 3.
Design of a right-angled bend.

For example on $\psi=0$, $|\phi|<a$, equations (15), (1) and (2) yield the intrinsic equation

$$\theta_0=\frac{1}{2}\tau+\frac{\sigma}{\pi}\log\left|\frac{\sinh\{\pi(Vs+a)/2HU\beta_\infty\}}{\sinh\{\pi(Vs-a)/2HU\beta_\infty\}}\right|,$$

$$\text{where} \quad \sigma=\sinh^{-1}\left(\frac{\beta_\infty U}{M_\infty V}\right)-\sinh^{-1}\left(\frac{\beta_\infty}{M_\infty}\right),$$

and s is distance measured along the wall.

The incompressible flow form of these equations was obtained by Lighthill[1] by means of the Schwarz-Christoffel theorem. Fig. 3 gives some idea of the type of bend achieved.

8.3. Mixed Boundary Conditions: Flow of a Stream up a Step

Equation (8) can be reduced similarly to give results corresponding to those of Sections 8.1 and 8.2; we omit this calculation but consider the simple example shown in Fig. 3, the flow of a stream over a right-angled step.

From equation (8) it is readily found that the intrinsic equation of the free surface is

$$\theta_h = \frac{1}{2}\left\{ \mathrm{gd}\,\frac{\pi(Us+a)}{2HU\beta_\infty} - \mathrm{gd}\,\frac{\pi(Us-a)}{2HU\beta_\infty} \right\}, \quad . \quad . \quad . \quad (17)$$

where a is defined in the figure, and gd x $(=2\tan^{-1}(\tanh \frac{1}{2}x))$ is the Gudermannian function.

The co-ordinates of the free surface are

$$x = \int_0^s \cos\theta_h ds, \qquad y = \int_0^s \sin\theta_h ds, \quad . \quad (18)$$

and eliminating s from these, by (17), gives

$$x(\theta_h) = \frac{H\beta_\infty}{\pi} \log \left| \frac{(\sin^2\theta' + k^2\cos^2\theta')^{\frac{1}{2}} + k\,(\sin^2\theta_h + k^2\cos^2\theta_h)^{\frac{1}{2}} - k}{(\sin^2\theta' + k^2\cos^2\theta')^{\frac{1}{2}} - k\,(\sin^2\theta_h + k^2\cos^2\theta_h)^{\frac{1}{2}} + k} \right|, \quad . \quad (19)$$

$$y(\theta_h) = \frac{2Hk\beta_\infty}{\pi} \left\{ \mathrm{F}[\tfrac{1}{2}\pi - \theta', \sqrt{(1-k^2)}] - \mathrm{F}[\tfrac{1}{2}\pi - \theta_h, \sqrt{(1-k^2)}] \right\}, \quad . \quad (20)$$

where $\theta' = \mathrm{gd}\,[(\pi a/(2HU\beta_\infty)]$, $k = \sinh[\pi a/(2HU\beta_\infty)]$, and F is the elliptic integral of the first type. If λ is the total depth of the step, then from (20)

$$\lambda = \frac{4Hk\beta_\infty}{\pi} \left\{ \mathrm{F}[\tfrac{1}{2}\pi - \theta', \sqrt{(1-k^2)}] - \mathrm{F}[\tfrac{1}{2}\pi, \sqrt{(1-k^2)}] \right\},$$

which gives the relation between λ and a.

This example shows how soon difficult algebra appears, even in the simplest cases. For curved boundaries, even if simple functional relations $\theta_0 = \theta_0(\phi)$ were assumed, the algebra would be excessive; there is no real alternative to the numerical methods given in the next section.

9. Curved Boundaries

It has been shown in Section 4.1 of Part I that with *given* curved walls two integral equations must be solved in order to determine the flow; if one wall is straight or at constant pressure a single integral equation suffices, and for simplicity of exposition it is this case which is considered here.

TABLE I

$$J(y) = \int_0^y \log \tanh x \, dx$$

y	$J(y) - y \log y$	δ^2	y	$J(y)$	δ^2
0	0	0	0·50	−0·86000	+426
0·05	−0·05001	− 9	0·55	−0·89656	+375
0·10	−0·10011	− 16	0·60	−0·92937	+332
0·15	−0·15037	− 25	0·65	−0·95886	+295
0·20	−0·20088	− 33	0·70	−0·98540	+263
0·25	−0·25172	− 40	0·75	−1·00931	+234
0·30	−0·30296	− 48	0·80	−1·03088	+212
0·35	−0·35468	− 56	0·85	−1·05033	+189
0·40	−0·40696	− 61	0·90	−1·06789	+169
0·45	−0·45985	− 69	0·95	−1·08376	+154
0·50	−0·51343	− 74	1·00	−1·09809	+138
0·55	−0·56775	− 80	1·05	−1·11104	+124
0·60	−0·62287	− 86	1·10	−1·12275	+113
0·65	−0·67885	− 90	1·15	−1·13333	+101
0·70	−0·73573	− 94	1·20	−1·14290	+ 92
0·75	−0·79355	− 99	1·25	−1·15155	+ 82
0·80	−0·85236	−102	1·30	−1·15938	+ 75
0·85	−0·91219	−105	1·35	−1·16646	+ 67
0·90	−0·97307	−108	1·40	−1·17287	+ 62
0·95	−1·03503	−110	1·45	−1·17866	+ 55
1·00	−1·09809	−112	1·50	−1·18390	+ 50
			1·55	−1·18864	+ 45
			1·60	−1·19293	+ 41
			1·65	−1·19681	+ 37
			1·70	−1·20032	+ 33
			1·75	−1·20350	+ 31
			1·80	−1·20637	+ 26
			1·85	−1·20898	+ 26
			1·90	−1·21133	+ 22
			1·95	−1·21346	+ 21
			2·00	−1·21538	+ 17
			2·05	−1·21713	+ 18
			2·10	−1·21870	+ 14
			2·15	−1·22013	+ 14
			2·20	−1·22142	+ 12
			2·25	−1·22259	+ 11
			2·30	−1·22365	+ 10
			2·35	−1·22461	+ 10
			2·40	−1·22547	+ 8
			2·45	−1·22625	+ 7
			2·50	−1·22696	+ 7
			2·55	−1·22760	+ 6
			2·60	−1·22818	+ 5
			2·65	−1·22871	+ 6
			2·70	−1·22918	+ 4
			2·75	−1·22961	+ 4
			2·80	−1·23000	+ 4
			2·85	−1·23035	+ 3
			2·90	−1·23067	+ 3
			2·95	−1·23096	+ 3
			3·00	−1·23122	+ 2

Note: For $y > 3$,

$$J(y) = e^{-2y} - \frac{\pi^2}{8} \text{ (to 9 decimal places).}$$

9.1. The Numerical Solution of the Integral Equation

(a) *One Wall a Constant Pressure Wall*

First we show how to determine the velocity on the given curved wall $\psi=0$. On $\psi=0$ equation (8) yields

$$\Omega_0(\phi)=-\frac{1}{\pi}\int_{\phi'=-\infty}^{\infty}\log\left|\tanh\frac{\pi}{4h}(\phi'-\phi)\right|d\theta_0(\phi'), \quad . \quad . \quad . \quad (21)$$

on integrating by parts and denoting the variable of integration by ϕ'. Now where θ_0 is continuous, (11) is applicable; elsewhere suppose θ_0 has simple discontinuities of amount τ_k at $\phi=\phi_k$, $k=1, 2, \ldots m$; then (21) gives

$$\Omega_0(\phi)=\frac{1}{\pi}\int_{-\infty}^{\infty}\log\left|\tanh\frac{\pi}{4h}(\phi'-\phi)\right|\frac{d\phi'}{Rq_0}-\frac{1}{\pi}\sum_k\tau_k\log\left|\tanh\frac{\pi}{4h}(\phi_k-\phi)\right|.$$

Equation (2), which gives the relation between Ω_0 and q_0, shows just how complicated this integral equation is.

In most practical examples $1/R=0$ outside some finite range $-2a\leqslant\phi\leqslant 2a$, say. If this range is divided into n parts thus $(2a, \phi_{n-\frac{1}{2}}, \phi_{n-1\frac{1}{2}}, \ldots \phi_{i-\frac{1}{2}}, \ldots \phi_{1\frac{1}{2}}, -2a)$, such that $1/(Rq_0)$ can be taken as constant, say $1/(Rq)_i$, in the i^{th} interval $(\phi_{i+\frac{1}{2}}, \phi_{i-\frac{1}{2}})$, with negligible error (excluding the points where θ_0 is discontinuous), then we can write

$$\Omega_0(\phi)=\sum_{i=1}^{r}\left(\frac{h}{Rq}\right)_i\frac{4}{\pi^2}\left[J\left\{\frac{\pi}{4h}(\phi'-\phi)\right\}\right]_i-\frac{1}{\pi}\sum_{k=1}^{m}\tau_k\log\left|\tanh\frac{\pi}{4h}(\phi_k-\phi)\right|,$$

where $J(y)=\int_0^y \log\tanh x\,dx$, and $[X]_i$ denotes the first difference, or jump in value of the bracketed function over the i^{th} interval. $J(y)$ is tabulated in Table I.

If $\quad A_{ij}=\frac{4}{\pi^2}\left[J\left\{\frac{\pi}{4h}(\phi'-\phi_j)\right\}\right]_i, \qquad A_{kj}=\frac{1}{\pi}\log\left|\tanh\frac{\pi}{4h}(\phi_k-\phi_j)\right|,$

and $\quad B_i=\left(\frac{h}{Rq}\right)_i, \qquad B_k=-\tau_k,$

then the formula for Ω_0 can be written concisely

$$\Omega_0(\phi_j)=\sum_{i=1}^{n}B_iA_{ij}+\sum_{k=1}^{m}B_kA_{kj}. \quad . \quad . \quad . \quad . \quad . \quad (22)$$

TABLE II

$$I(y)=\int_0^y \mathrm{gd}\, x\,dx$$

y	$\int_0^y \mathrm{gd}\, x\,dx$	δ^2	y	$\int_0^y \mathrm{gd}\, x\,dx$	δ^2
0	0	1000	2·5	2·25911	163
0·1	0·00500	993	2·6	2·40060	147
0·2	0·01993	981	2·7	2·54356	135
0·3	0·04467	955	2·8	2·68787	121
0·4	0·07896	925	2·9	2·83339	109
0·5	0·12250	886	3·0	2·98000	101
0·6	0·17490	844	3·1	3·12762	89
0·7	0·23574	795	3·2	3·27613	81
0·8	0·30453	749	3·3	3·42545	74
0·9	0·38081	697	3·4	3·57551	67
1·0	0·46406	649	3·5	3·72624	61
1·1	0·55380	599	3·6	3·87758	54
1·2	0·64953	553	3·7	4·02946	49
1·3	0·75079	507	3·8	4·18183	46
1·4	0·85712	465	3·9	4·33466	39
1·5	0·96810	425	4·0	4·48788	38
1·6	1·08333	389	4·1	4·64148	32
1·7	1·20245	354	4·2	4·79540	31
1·8	1·32511	321	4·3	4·94963	27
1·9	1·45098	293	4·4	5·10413	24
2·0	1·57978	267	4·5	5·25887	23
2·1	1·71125	241	4·6	5·41384	19
2·2	1·84513	218	4·7	5·56900	19
2·3	1·98119	200	4·8	5·72435	16
2·4	2·11925	180	4·9	5·87986	16
			5·0	6·03553	12

Note: For $y>5$, $I(y)=2e^{-y}+\frac{\pi}{2}y-2\sum_{n=1}^{\infty}\frac{(-1)^{n+1}}{(2n-1)^2}$

i.e. $I(y)=2e^{-y}+\frac{\pi}{2}y-1{\cdot}8319312$ (to 7 decimal places).

Besides (22) there is another equation necessary in the numerical calculations; it is the self-evident result $\int_{-\infty}^{\infty} d\theta_0(\phi')=\tau$, where τ is the total angle of deflection of the channel. By (11) and the approximations already introduced this can be written

$$\frac{1}{h}\sum_{i=1}^{n} B_i[\phi]_i=\sum_{k=1}^{m} B_k+\tau. \quad . \quad . \quad . \quad . \quad . \quad (23)$$

Equation (23) must be satisfied exactly if the overall deflection angle τ is to be achieved. This can be done most simply by modifying the values of B_k (*see* the example in Section 9.2).

Similarly, from (8) and (11), it is found that the slope of the free surface can be calculated from

$$\theta_h(\phi_j)=\frac{1}{2}\tau+\sum_{i=1}^{n}B_iC_{ij}+\sum_{k=1}^{m}\mathcal{B}_kC_{kj}, \quad . \quad . \quad . \quad . \quad (24)$$

where $C_{ij}=\frac{2}{\pi^2}\left[I\left\{\frac{\pi}{2h}(\phi'-\phi_j)\right\}\right]_i$, $C_{kj}=\frac{1}{\pi}\,\mathrm{gd}\,\frac{\pi}{2h}(\phi_k-\phi_j)$,

and $I(y)=\int_0^y \mathrm{gd}\,x\,dx$. $I(y)$ is given in Table II.

Since the values of B_i in (22) are unknown until Ω_0 has been calculated, it is necessary to solve the equation by iteration. If reasonable values of q_0/U are assumed at $\phi=\phi_j$, $j=1, 2, \ldots n$, then

$$sU=\int\frac{U}{q_0}d\phi, \quad . \quad . \quad . \quad . \quad . \quad (25)$$

enables the distance s to be determined as a function of ϕ. $R(\phi)$ now follows from this relationship and the given wall shape. Then $B_i=[HU\beta_\infty/(Rq)]_i$ can be obtained and used in (22) to yield values of $\Omega_0(\phi)$, and hence q_0/U from (2). This calculation is now repeated until an iteration does not alter q_0/U.

When this has been done the final values of B_i can be used directly in (24) to give θ_h; the co-ordinates of the constant pressure wall then follow from

$$Ux=\int^{\phi}\cos\theta_h d\phi, \qquad Uy=\int^{\phi}\sin\theta_h d\phi. \quad . \quad . \quad . \quad (26)$$

Two further points in connection with the application of equations (25) and (26) need be mentioned.

First, near a stagnation point, at $\phi=b$, say, produced by a jump in θ of τ, U/q_0 becomes infinite, when instead of (26) the approximate equation[2]

$$sU=(\phi'-b)\frac{U}{q'}\left(\frac{1}{1-\tau/\pi}\right), \quad . \quad . \quad . \quad . \quad (27)$$

must be used to calculate the distance s from the stagnation point to $\phi=\phi'$, where the velocity is q'.

Secondly, since $(\phi_h - \tau)$ will in general vanish only at $\phi = \infty$, it is useful to have a formula from which to calculate y at some large value of ϕ, say ϕ_0. In this case the second equation of (26) can be replaced by

$$Uy = Uy(\phi_0) + \int_{\phi_0}^{\phi} \sin \theta_h d\phi.$$

Consider, for simplicity, the case $\tau = 0$; then

$$Uy(\phi_0) = Uy(\infty) + \int_{\infty}^{\phi_0} \sin \theta_h d\phi$$

$$= Uy(\infty) + \int_{\infty}^{\phi_0} \theta_h d\phi,$$

provided ϕ_0 is "reasonably" large (*see* later). Therefore inserting the value of θ_h given by the imaginary part of (8) gives

$$y(\phi_0) - y(\infty) = \frac{1}{2hU} \int_{\infty}^{\phi_0} \left\{ \int_{-2a}^{2a} \theta_0 \operatorname{sech} \frac{\pi}{2h} (\phi' - \phi) \, d\phi' \right\} d\phi$$

$$= \frac{-1}{\pi U} \int_{-2a}^{2a} \theta_0 \left\{ \frac{1}{2} \pi + \operatorname{gd} \frac{\pi}{2h} (\phi' - \phi_0) \right\} d\phi'.$$

Integration by parts gives

$$y(\phi_0) - y(\infty) = \frac{1}{\pi U} \int_{\phi' = -2a}^{2a} \left[\frac{1}{2} \pi (\phi' - \phi_0) - \frac{2h}{\pi} I \left\{ \frac{\pi}{2h} (\phi' - \phi_0) \right\} \right] d\theta_0(\phi'),$$

where I is the function already defined, and (5) has been used. Now for $x > 4$, $I(x) = 2e^{-x} + \frac{1}{2}\pi x - 1{\cdot}8319$ is accurate to four decimal places, and so in the calculations it is sufficient to take

$$\frac{y(\phi_0) - y(\infty)}{H} = -\frac{4\beta_\infty}{\pi^2} \int_{\phi' = -2a}^{2a} \exp \left\{ \frac{2h}{\pi} (\phi' - \phi_0) \right\} d\theta_0(\phi'),$$

provided that $\pi(\phi_0 + 2a)/(2HU\beta_\infty) > 4$.

Thus in the notation of the first part of this section we can write

$$\frac{y(\phi_0)}{H}=\frac{y(\infty)}{H}+\frac{8\beta_\infty{}^2}{\pi^3}\left\{\sum_{i=1}^{n}B_i\left[\exp\left\{\frac{\pi}{2h}(\phi'-\phi_0)\right\}\right]_i+\sum_{k=1}^{m}B_k\frac{\pi}{2\beta_\infty}\exp\left\{\frac{\pi}{2h}(\phi_k-\phi_0)\right\}\right\}. \quad . \quad . \quad . \quad (28)$$

(*b*) *One Wall Straight*

Suppose $\theta_h=0$, then the velocity on the other wall ($\psi=0$) can be found from

$$\Omega_0(\phi_j)=\sum_{i=1}^{n}B_iD_{ij}+\sum_{k=1}^{m}B_kD_{kj}, \quad . \quad . \quad (29)$$

where B_i, B_k have already been defined,

$$D_{ij}=\frac{2}{\pi^2}\left[F\left\{\frac{\pi}{2h}(\phi'-\phi_j)\right\}\right]_i, \qquad D_{kj}=\frac{1}{\pi}\log\left|\sinh\frac{\pi}{2h}(\phi_k-\phi_j)\right|.$$

and $F(y)=\int_0^y \log\sinh x\,dx$. This function is given in Table III. Equation (29) follows from (3) and (11) by making the same approximations as in (*a*).

In the present case, besides the auxiliary equation (23), it is also necessary to satisfy

$$\frac{1}{h}\sum_{i=1}^{n}B_i\left[\frac{1}{2}\phi^2\right]_i+\sum_{k=1}^{m}\phi_kB_k+\log\frac{U}{V}=0, \quad . \quad . \quad . \quad (30)$$

which comes from (4). The ratio U/V can be determined from (7).

9.2. Example: Flow about a Circular Cylinder in a Channel

Consider the incompressible flow about a circular cylinder placed centrally in a stream of total width $2H$ at infinity. As the flow is symmetrical about the stagnation streamline, say $\psi=0$, only that half of the flow pattern lying between the streamlines $\psi=0$ and $\psi=HU$ need be considered; this can be regarded as a "channel" flow. Compressible flows can be determined by making only minor modifications to the following calculations.

The flow about a circular cylinder may seem to be an unpractical example, but it does serve to test the theory severely, for the larger the thickness ratio of the body the more slowly does the iterative process described in Section 9.1 converge.

TABLE III

$$F(y)=\int_0^y \log \sinh x\,dx$$

y	$F(y)-y\log y$	δ^2	y	$F(y)$	δ^2
0	0	0	0·50	−0·83966	541
0·05	−0·04999	4	0·55	−0·86962	500
0·10	−0·09994	8	0·60	−0·89458	466
0·15	−0·14981	12	0·65	−0·91488	438
0·20	−0·19956	18	0·70	−0·93080	414
0·25	−0·24913	20	0·75	−0·94258	394
0·30	−0·29850	25	0·80	−0·95042	376
0·35	−0·34762	28	0·85	−0·95450	362
0·40	−0·39646	34	0·90	−0·95496	350
0·45	−0·44496	37	0·95	−0·95192	337
0·50	−0·49309	41	1·00	−0·94551	329
0·55	−0·54081	44	1·05	−0·93581	320
0·60	−0·58809	50	1·10	−0·92291	312
0·65	−0·63487	52	1·15	−0·90689	306
0·70	−0·68113	57	1·20	−0·88781	300
0·75	−0·72682	60	1·25	−0·86573	294
0·80	−0·77191	64	1·30	−0·84071	291
0·85	−0·81636	68	1·35	−0·81278	286
0·90	−0·86013	71	1·40	−0·78199	282
0·95	−0·90319	74	1·45	−0·74838	279
1·00	−0·94551	79	1·50	−0·71198	277
			1·55	−0·67281	273
			1·60	−0·63091	271
			1·65	−0·58630	270
			1·70	−0·53899	267
			1·75	−0·48901	265
			1·80	−0·43638	265
			1·85	−0·38110	262
			1·90	−0·32320	262
			1·95	−0·26268	260
			2·00	−0·19956	259
			2·05	−0·13385	259
			2·10	−0·06555	257
			2·15	+0·00532	258
			2·20	0·07877	255
			2·25	0·15477	256
			2·30	0·23333	256
			2·35	0·31445	253
			2·40	0·39810	255
			2·45	0·48430	254
			2·50	0·57304	253
			2·55	0·66431	253
			2·60	0·75811	253
			2·65	0·85444	253
			2·70	0·95330	251
			2·75	1·05467	253
			2·80	1·15857	252
			2·85	1·26499	251
			2·90	1·37392	252
			2·95	1·48537	251
			3·00	1·59933	252

Note: For $y > 3$,

$$F(y) = -y\log_e 2 + \tfrac{1}{2}y^2 + \tfrac{1}{2}e^{-2y} - \frac{\pi^2}{12}$$

(to 5 decimal places).

(*a*) *One Wall a Constant Pressure Wall*

This case is obtained if the cylinder (radius R) is placed centrally in a jet of fluid, as shown in Fig. 4. The deflection angle τ is zero for this case. It is assumed that $2a=HU$, which yields a ratio of approximately $1/2$ for R/H, as in a stream of infinite width it is a standard result that $R=a/U$.

The range $(2a, -2a)$ is divided into sixteen equal parts, while ϕ_j are taken to be at the mid-points of these intervals (*see* the first column of Table IV). A_{ij} are then simply the first differences of

$$\frac{4}{\pi^2} J\left(\frac{\pi}{64}\right), \quad \frac{4}{\pi^2} J\left(\frac{3\pi}{64}\right), \quad \frac{4}{\pi^2} J\left(\frac{5\pi}{64}\right), \ldots.$$

A good initial assumption for $q/U(\phi)$ is the infinite stream distribution q_t/U, namely

$$\frac{q_t}{U}=2\left\{1-\left(\frac{\phi}{2a}\right)\right\}^{\frac{1}{2}} \quad . \quad . \quad . \quad . \quad . \quad (31)$$

From the definition of B_i and (5)

$$B_i=\left(\frac{HU}{Rq}\right)_i=\left(\frac{2a}{RU}\right)\left(\frac{U}{q}\right)_i.$$

With the assumption (31), $RU=a$, and hence

$$B=\left\{1-\left(\frac{\phi}{2a}\right)^2\right\}^{-\frac{1}{2}}, \quad \left(\frac{\phi}{2a}\right)=\pm\frac{1}{16}, \ \pm\frac{3}{16}, \ldots \pm\frac{15}{16}.$$

For the present example θ has two discontinuities (τ_k), one at each stagnation point, and hence (23) yields

$$2\tau_k=\left(\frac{4a}{HU}\right)\sum_{i=1}^{16} B_i\left[\frac{\phi}{4a}\right]_i=\frac{1}{8}\sum_{i=1}^{16} B_i,$$

as $$\left[\frac{\phi}{4a}\right]_i=\frac{1}{8}.$$

Thus $$B_k=-\frac{1}{16}\sum_{i=1}^{16} B_i, \quad . \quad . \quad . \quad . \quad . \quad . \quad (32)$$

as $B_k=-\tau_k$. As the number of intervals into which $(2a, -2a)$ is divided tends to infinity, τ_k tends to $\frac{1}{2}\pi$; for the division adopted here τ_k is found to be $82{\cdot}31°$. An application of (22), in which $\Omega_0=\log(U/q_0)$ as the flow is incompressible, completes the first iteration. Notice that in this example it is unnecessary to use (25) during the iterative process, due to the constancy of R.

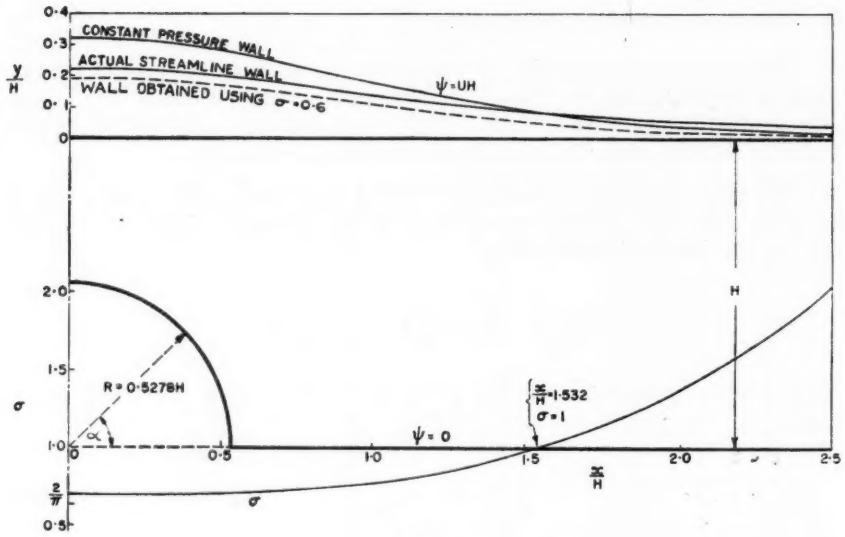

Fig. 4.
Flow about a circular cylinder.

The final values of q_0/U, obtained after five iterations, are given in column 1 of Table IV. Column 2 gives the values of $sU/(4a)$, obtained from column 1 and equation (25). From the first entry in this column it follows that

$$RU/(2a)=4\times 0{\cdot}4145/\pi=0{\cdot}5278, \text{ and so } R/H=0{\cdot}5278 \text{ as } HU=2a.$$

Column 3 gives the value of α, defined in Fig. 4, while column 4 gives the free stream value $q_t=2U\sin\alpha$.

Column 5 sets out the solid blockage ε, defined by $\varepsilon=(q-q_t)/q_t$, which agrees closely with the first order term used in the standard theory. In the general case this first order term can be calculated as follows.

For slender cylinders $\theta_0\simeq dy/dx$, $\phi\simeq Ux$, so on $\psi=0$ equations (5) and (8) yield

$$\Omega\simeq\frac{1}{2H\beta_\infty}\int_{x'=-c/2}^{c/2}\operatorname{cosech}\frac{\pi}{2H\beta_\infty}(x'-x)\,dy(x'),$$

where c is the "chord" length of the cylinder. Allowing H to tend to infinity gives

$$\Omega_t\simeq\frac{1}{\pi}\int_{x'=-c/2}^{c/2}\frac{dy(x')}{x'-x}.$$

TABLE IV

FLOW ABOUT A CYLINDER WITHIN CONSTANT PRESSURE WALLS; $R/H=0{\cdot}5278$

TABLE IV

FLOW ABOUT A CYLINDER WITHIN CONSTANT PRESSURE WALLS: $R/H = 0{\cdot}5278$

	1	2	3	4	5	6	7	8	9	10
$\left(\frac{\phi}{4a}\right)\times 32$	$\frac{q}{U}$	$\frac{sU}{4a}$	α	$\left(\frac{q_1}{U}\right)$ *(infinite stream)*	*Solid Blockage* ε	θ_h *(radians)*	$\frac{y_p}{H}$	$\frac{x}{H}$	$\frac{y_t}{H}$	σ
0	1·8544	0·4145	90·0°	2·0000	−0·0728	0	0·3255	0	0·2271	0·6977
1	1·8510	0·3980	86·42°	1·9961	−0·0727	0·0246	0·3247	0·0625	0·2266	0·6979
3	1·8237	0·3634	78·89°	1·9625	−0·0707	0·0725	0·3186	0·1873	0·2226	0·6987
5	1·7676	0·3293	71·49°	1·8966	−0·0680	0·1164	0·3067	0·3118	0·2151	0·7013
7	1·6786	0·2924	63·48°	1·7896	−0·0620	0·1541	0·2898	0·4356	0·2045	0·7057
9	1·5495	0·2544	55·24°	1·6430	−0·0569	0·1834	0·2687	0·5588	0·1917	0·7134
11	1·3669	0·2109	45·80°	1·4338	−0·0467	0·2028	0·2446	0·6815	0·1772	0·7244
13	1·1023	0·1611	34·98°	1·1467	−0·0387	0·2117	0·2188	0·8038	0·1622	0·7413
15	0·6530	0·0882	19·15°	0·6561	−0·0047	0·2106	0·1925	0·9260	0·1471	0·7642
16	0	0	0	0	—					
						0·2010	0·1669	1·0483	0·1333	0·7987
						0·1853	0·1429	1·1710	0·1194	0·8355
						0·1659	0·1210	1·2941	0·1067	0·8818
						0·1451	0·1016	1·4176	0·0953	0·938
						0·1248	0·0848	1·5414	0·0852	1·005
						0·1058	0·0705	1·6656	0·0764	1·084
						0·0889	0·0583	1·7900	0·0686	1·177
						0·0742	0·0482	1·9146	0·0617	1·280
						0·0616	0·0397*	2·0393	0·0558	1·41
						0·0421	0·0270	2·2891	0·0460	1·70
						0·0286	0·0182	2·5389	0·0385	2·11
						0·0193	0·0123	2·7888	0·0325	2·64
						0·0131	0·0083	3·0387	0·0278	3·35
						0·0088	0·0056	3·2886	0·0240	4·3
						0·0060	0·0037*	3·5386	0·0209	5·5
						0·0040	0·0025	3·7886	0·0185	7·4
						0·0027	0·0017	4·0386	0·0164	9·7
						0·0018	0·0011	4·2886	0·0146	13
						0·0012	0·0007	4·5386	0·0131	19
						0·0008	0·0005	4·7886	0·0118	24
						0·0006	0·0003	5·0386	0·0107	36
						0·0004	0·0002	5·2886	0·0097	49
						0·0003	0·0001	5·5386	0·0089	89
						0·0002	0·0001	5·7886	0·0081	
						0·0001	0·0001*	6·0386	0·0077	

*These figures compare with the check made in Section 9.2.

Now to first order in Ω, from (1), (2) and the definition of ε it is found that $\varepsilon=(\Omega_t-\Omega)/\beta_\infty$.

Thus
$$\varepsilon=\frac{1}{2H\beta_\infty{}^2}\int_{x'=-c/2}^{c/2}\left[\left\{\frac{\pi}{2H\beta_\infty}(x'-x)\right\}^{-1}-\operatorname{cosech}\frac{\pi}{2H\beta_\infty}(x'-x)\right]dy(x')$$

$$=\frac{\pi}{6(2H)^2\beta_\infty{}^3}\int_{x'=-c/2}^{c/2}(x'-x)\,dy(x'),$$

provided that c/H is small. An integration by parts now gives

$$\varepsilon=-\frac{\pi A}{12(2H)^2\beta_\infty{}^3}, \qquad (33)$$

where A is the cross-sectional area of the cylinder.

This theory would appear to be applicable only to conventional aerofoil shapes in jets of width large compared to the aerofoil chord. For the circular cylinder

$$\varepsilon=-\frac{\pi^2}{48}\left(\frac{R}{H}\right)^2\simeq 0{\cdot}0472.$$

The average value in column 4 of Table IV is 0·0525, and so, even for the extreme case of the flow of a relatively narrow jet about a circular cylinder, the first order term is still a fair approximation.

Column 6 of Table IV is obtained directly from equation (24), while columns 7 and 8 follow from equations (26). The value of y_p/H at $\phi/(4a)=97/32$, was calculated from equation (28). As a check equation (28) was also used to calculate y_p/H at $\phi/(4a)=53/32$ and $\phi/(4a)=33/32$, with the satisfactory results 0·0038 and 0·0399 respectively (*cf.* the figures marked with an asterisk in column 7).

In an infinite stream

$$\phi+i\psi=U\left\{x+iy+\frac{R^2(x-iy)}{x^2+y^2}\right\},$$

and so on $\qquad \psi=HU, \qquad \frac{H}{y_t}=1-\frac{(H/R)^2}{(x/H)^2+(y_t/H)^2},$

which enables column 9 to be calculated. Column 10 is the ratio $\sigma=y_t/y_p$, and this ratio becomes unity at $x/H=1{\cdot}532$, which is in close agreement with the value deduced for an aerofoil of the same chord in Section 10.

TABLE V

FLOW ABOUT A CYLINDER WITHIN STRAIGHT WALLS: $R/H=0{\cdot}4749$

	1	2	3	4	5
$32\left(\frac{\phi}{4a}\right)$	$\frac{q}{U}$	$\frac{sU}{4a}$	α	$\left(\frac{q_1}{U}\right)$ *(infinite stream)*	*Solid Blockage* ε
0	2·5609	0·3141	90·00°	2·0000	0·2805
1	2·5551	0·3019	86·50°	1·9963	0·2799
3	2·5087	0·2772	79·44°	1·9662	0·2759
5	2·4142	0·2519	72·18°	1·9040	0·2680
7	2·2696	0·2252	64·53°	1·8055	0·2570
9	2·0687	0·1964	56·29°	1·6638	0·2434
11	1·7988	0·1642	47·04°	1·4637	0·2289
13	1·4273	0·1255	35·95°	1·1743	0·2154
15	0·8315	0·0691	19·81°	0·6779	0·2266
16	0	0	0	0	—

(*b*) *One Wall Straight*

The equations appropriate to this case are (29), (23) and (30), the first of which is satisfied identically in virtue of the symmetry about $\phi=0$. Equation (23) is used, as in (*a*), to define B_k. The assumption $HU=1{\cdot}68396a$ (selected in an effort to obtain R/H nearly equal to 1/2), and the division of the range into sixteen equal parts, leads eventually to the solution set out in Table V. For this case it is found that $R/H=0{\cdot}4749$. The last entry in column 5 is not reliable as it changes rapidly with change in α; in fact increasing α from 19·81° to 20·31° reduces ε from 0·227 to 0·198. Some small error in α at $\phi/(4a)=15/32$ is an inevitable consequence of using the approximation (27) to calculate $sU/(4a)$ at this point. The same remarks apply to the last entry in column 5 of Table IV.

The standard result for the first order term in solid blockage is

$$\varepsilon=\frac{\pi A}{6(2H)^2\beta_\infty{}^3},$$

which may be established from equation (3) by an argument parallel to that already given for constant pressure walls. For the circular cylinder

$$\varepsilon=\frac{\pi^2}{24}\left(\frac{R}{H}\right)^2=0{\cdot}0927,$$

which is only about 37 per cent. of the average result obtained from column 5—in marked contrast to the result obtained for constant pressure walls. Fig. 5 shows q/U and ε as functions of α.

The results obtained for the blockage factor lead to the conclusion that, as far as drag corrections are concerned, relatively larger models can be safely used in open-jet tunnels than in closed tunnels.

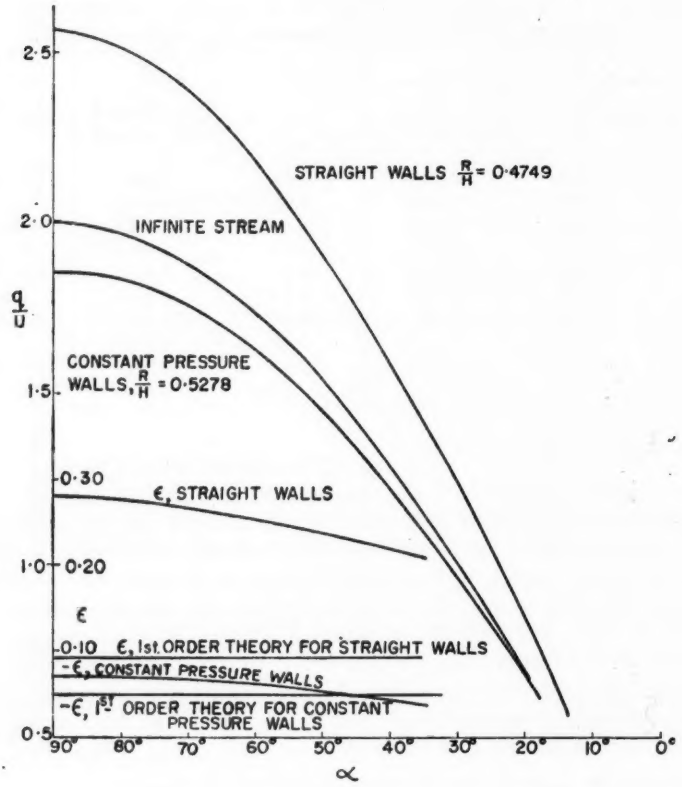

Fig. 5.

Solid blockage and velocity distributions for a circular cylinder.

10. The Setting of "Streamline" Walls

Equation (8) has an important application to the theory of flexible-wall wind tunnels. In such tunnels the wall shape can be changed as required, and the principle adopted is to set them, as nearly as possible, to lie along streamlines of the infinitely deep stream. This eliminates any need to apply wind tunnel corrections, and, more important, avoids that defect of straight-walled tunnels at high subsonic Mach numbers known as "choking."

The method of setting these walls is shown in Fig. 6. In this figure ABC is the constant pressure wall in the absence of the aerofoil, $A_pB_pC_p$ is the constant pressure wall in the presence of the aerofoil (assumed to be at zero incidence on the tunnel centre line), while $A_fB_fC_f$ is the corresponding free streamline about the aerofoil.

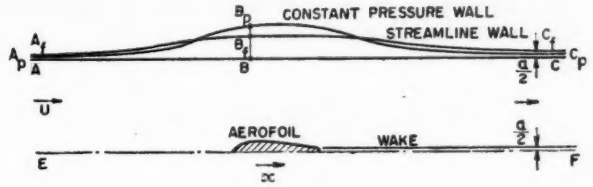

Fig. 6.

The setting of streamline walls.

These curves have a common point at an infinite distance upstream, but downstream the existence of the aerofoil's wake causes a displacement of the constant pressure and free streamline walls from the wall position of the empty tunnel. The constant pressure wall is obtained experimentally, so the displacement BB_p at any point will be known. The required streamline wall $A_fB_fC_f$ can now be determined from the equation $BB_p = \sigma BB_f$, provided that the value of σ is known. The present purpose is to determine the theoretical value of this ratio σ.

Present practice, based on calculations of Lock and Beavan[4], is to take σ as constant and equal to 0·6. The calculations of Lock and Beavan (for doublets, vortices and sources instead of aerofoils) are not consistent with the method actually used in practice for setting streamline walls. In their calculations they made the constant pressure and streamline walls pass through the same point *opposite* the doublet (source or vortex), whereas in experimental practice the walls pass through a common point effectively an infinite distance *upstream* ($x = -\infty$). Thus for the doublet their method results in values of σ of $\frac{1}{2}\pi$ and $16/\pi^3$ ($=0{\cdot}516$), at $x = -\infty$ and $x = 0$ respectively, whereas if the walls have a common point at an infinite distance upstream it is shown later that the values of σ are ∞ and $2/\pi$ ($=0{\cdot}637$) respectively. Furthermore it is shown later that in the presence of a wake $\sigma = 1$ at an infinite distance downstream, whereas Lock and Beavan recommended a factor of 0·6 *throughout* the range of x. The effect of this is not serious when applied upstream, but downstream, where the wake produces a permanent displacement of the tunnel wall from the empty tunnel position, to return the wall 0·4 of the displacement will plainly result in the reappearance of some of the wake blockage. This may not, of course, materially affect the experimental results.

It is suggested in this paper that for symmetrical aerofoils at zero incidence σ should be taken as $2/\pi$ along the wall opposite the aerofoil, and then parabolically increased such that it becomes unity at $\frac{1}{4}\beta_\infty$ tunnel widths up and down stream from the centre of area of the aerofoil. Outside this range the constant pressure walls could probably be left undisturbed ($\sigma = 1$) with little resulting error. The analysis leading to these conclusions is as follows.

By considering, as in Section 9, only that half of the flow for which $\psi \geqslant 0$, the flow can be regarded as being one in a "channel," the aerofoil surface being $\psi = 0$, and the constant pressure or streamline wall being $\psi = h/m_\infty$. The equations

appropriate to this case are (5), in which H is now *half* the tunnel height, and (8). In the limit, $H \longrightarrow \infty$, these equations yield

$$f = \frac{1}{\pi} \int_{-\infty}^{\infty} \frac{\theta_0 d\phi'}{\phi' - w},$$

which applies to a symmetrical aerofoil in an infinite stream. On the streamline $\psi = h/m_\infty$ the imaginary part of this equation gives

$$\theta_t(\phi) = \frac{1}{\pi h} \int_{-\infty}^{\infty} \frac{\theta_0 d\phi'}{1 + \{(\phi' - \phi)/h\}^2}, \quad . \quad . \quad . \quad (34)$$

which enables the shape of the streamline wall to be calculated directly. The approximation of thin aerofoil theory is now made by replacing θ_0, ϕ' and ϕ in (34) by dy_0/dx, Ux' and Ux. Then from (5) and (34)

$$\frac{dy_t}{dx} = \frac{1}{\pi H \beta_\infty} \int_{x'=-c/2}^{c/2} \frac{dy_0(x')}{1 + \{(x' - x)/(H\beta_\infty)\}^2}, \quad . \quad . \quad . \quad (35)$$

where c is the chord length, and y_t is the displacement of the wall $\psi = h/m_\infty$ from its original straight position in the empty tunnel. The origin of x is taken at the mid-chord point, and the range of integration is reduced, as $\theta_0 = 0$ outside $-\frac{1}{2}c \leqslant x \leqslant \frac{1}{2}c$. Now $y_t = 0$ at $x = -\infty$, so integrating (35) gives

$$y_t = \frac{1}{\pi} \int_{x'=-c/2}^{c/2} \left\{ \frac{1}{2}\pi + \tan^{-1}\left(\frac{x - x'}{H\beta_\infty}\right) \right\} dy_0(x'). \quad . \quad . \quad . \quad (36)$$

Similarly it is found that on $\psi = h/m_\infty$ equations (5) and (8) yield the displacement

$$y_D = \frac{1}{\pi} \int_{x'=-c/2}^{c/2} \left\{ \frac{1}{2}\pi + \mathrm{gd}\, \frac{\pi}{2H\beta_\infty}(x - x') \right\} dy_0(x'), \quad . \quad . \quad . \quad (37)$$

for the constant pressure wall (*cf.* the third equation after (27)).

Now $y_0 = 0$ at $x = -\frac{1}{2}c$ (the leading edge), but at the trailing edge ($x = \frac{1}{2}c$) $y_0 = \frac{1}{2}cC_D$, where C_D is the drag coefficient. Here it has been assumed that a "sting" of thickness $\frac{1}{2}cC_D$ is attached to the trailing edge to represent the wake displacement thickness (*see* the theory in Ref. 3).

For large z,

$$\mathrm{gd}\,(z)=\frac{1}{2}\pi-\mathrm{sech}\,z-\frac{1}{6}\,\mathrm{sech}^3 z\ldots,\quad\text{and}\quad\tan^{-1}(z)=\frac{1}{2}\pi-\frac{1}{z}+\frac{1}{6z^3}-\ldots.$$

and it therefore follows from (36) and (37) that well downstream ($x=\infty$) both y_t and y_p tend to $\frac{1}{4}cC_D$, that is $\sigma(\equiv y_t/y_p)$ tends to unity, whereas well upstream σ tends to infinity like $(\cosh z)/z$.

The value of σ is now calculated in the neighbourhood of the aerofoil. From (36) and (37),

$$y_t-\frac{2}{\pi}y_p=\frac{\pi-2}{4\pi}cC_D+\frac{1}{\pi}\int_{x'=-c/2}^{c/2}\left\{\tan^{-1}\left(\frac{x-x'}{H\beta_\infty}\right)-\frac{2}{\pi}\,\mathrm{gd}\,\frac{\pi}{2h\beta_\infty}(x-x')\right\}dy_0(x').$$

For small z,

$$\mathrm{gd}\,(z)=\frac{1}{2}z\left(1-\frac{z^2}{6}+\ldots\right),\quad\tan^{-1}(z)=z\left(1-\frac{z^2}{3}+\ldots\right),$$

so that for small values of x/H we can write

$$y_t-\frac{2}{\pi}y_p=\frac{\pi-2}{4\pi}cC_D+\frac{(\frac{1}{8}\pi^2-1)}{3\pi}\int_{x'=-c/2}^{c/2}\left\{\left(\frac{x-x'}{H\beta_\infty}\right)^3+O\left(\frac{x}{H}\right)^5\right\}dy_0(x').$$

Integrating by parts and ignoring terms of order $(c/H)^5$, it is found that

$$y_t=\frac{2}{\pi}y_p+\frac{\pi-2}{4\pi}cC_D+\frac{(\frac{1}{8}\pi^2-1)}{2\pi H^3\beta_\infty{}^3}\left\{J(x)-\frac{c}{6}C_D(\tfrac{1}{2}c-x)^3\right\},\qquad(38)$$

where $J(x)$ is the second moment of the profile section about x. It is clear from (38) that σ will always exceed $2/\pi$, but not by very much in the neighbourhood of the aerofoil. Whitehead[5] has also obtained the first order result $\sigma=2/\pi$ by applying conformal transformations to special aerofoil profiles.

It is of some interest to determine the value of x at which σ becomes unity. From (36) and (37) this occurs where

$$\int_{x'=-c/2}^{c/2}F\left(\frac{x-x'}{H\beta_\infty}\right)dy_0(x')=0,\qquad(39)$$

where $F(y)=\mathrm{gd}\,(\pi/2)\,y-\tan^{-1}y$. This equation can be solved numerically for a given aerofoil if C_D is known. A good estimate of the value of x can be found as follows.

For the rectangle $y_0=\frac{1}{2}t$, $-\frac{1}{2}c \leqslant x \leqslant \frac{1}{2}c$, relation (39) gives

$$F\left(\frac{x+\frac{1}{2}c}{H\beta_\infty}\right) = \left(1-\frac{cC_D}{4t}\right) F\left(\frac{x-\frac{1}{2}c}{H\beta_\infty}\right), \quad . \quad . \quad (40)$$

which is easily solved graphically. When $cC_D/(4t)$ can be ignored, corresponding values of $c/(H\beta_\infty)$ and $x/(H\beta_\infty)$ satisfying (40) are

$c/(H\beta_\infty)$	0	0·2	0·4	0·6	0·8	1·0	1·2
$x/(H\beta_\infty)$	±1·43	±1·44	±1·45	±1·46	±1·48	±1·51	±1·54

This shows that $x/(H\beta_\infty)$ is practically independent of $c/(H\beta_\infty)$ and, since an aerofoil can be constructed from a number of rectangular strips of varying chord, it is reasonable to apply this table to any aerofoil shape. In fact even for the extreme case of the cylinder of Section 9.2, where $c/(H\beta_\infty)=2\times 0{\cdot}5278$, the table yields $x/(H\beta_\infty)=1{\cdot}52$, a value less than one per cent. in error from the true value of 1·532 (*see* Fig. 4). If C_D is not made zero the values of $x/(H\beta_\infty)$ are reduced downstream and increased upstream, but the effect appears to be small for typical values of the ratios $c/(H\beta_\infty)$ and $cC_D/(4t)$. Thus it would probably be a satisfactory rule in experimental work to take σ as unity outside the range $-\frac{1}{4}\beta_\infty \leqslant x/(2H) \leqslant \frac{1}{4}\beta_\infty$, say, as the adjusting of the constant pressure wall to the "streamline" position has to stop somewhere upstream and downstream, and the points where $\sigma=1$ are convenient for this purpose.

Acknowledgments

Tables I, II and III were calculated for the author by the Mathematics Division of the National Physical Laboratory, Teddington, Middlesex. The work described in the paper was done early in 1952 in the Aerodynamics Division of the National Physical Laboratory, and it is published by permission of the Director of the Laboratory.

References

1. Lighthill, M. J. Notes on the Deflection of Jets by Insertion of Curved Surfaces, and on the Design of Bends in Wind Tunnels. R. & M. 2105, 1945.

2. Woods, L. C. The Numerical Solution of Two-dimensional Fluid Motion in the Neighbourhood of Stagnation Points and Sharp Corners. R. & M. 2726, 1949.

3. Woods, L. C. The Second Order Terms in Two-dimensional Tunnel Blockage. *The Aeronautical Quarterly*, Vol. IV, pp. 361-372, February 1954.

4. Lock, C. N. H. and Beavan, J. A. Tunnel Interference at Compressibility Speeds using the Flexible Walls of the Rectangular High Speed Tunnel. R. & M. 2005, 1944.

5. Whitehead, L. G. Two-dimensional Wind Tunnel Interference. R. & M. 2802, 1950.

Effect of Yielding on the Fatigue Properties of Test Pieces Containing Stress Concentrations

K. GUNN, B.Sc., A.R.S.M.

(*Aluminium Laboratories, Banbury*)

SUMMARY: A method of estimating the fatigue properties of notched test pieces when cyclic loads are applied in the presence of mean stresses is described. The method takes into account the local yielding which occurs near the base of the notch when the nominal stresses are sufficiently high. The general form of the predicted R/M diagrams closely resembles those obtained experimentally in previously published work.

1. Introduction

A large number of investigations have been made in the past on the effect of mean stresses on the fatigue properties of aluminium alloys. The published reports of these investigations have not formulated general relationships, since for the most part they have been merely a description of test results. An attempt is made here to rationalise the results of tests on notched test pieces which are subjected to mean stress by postulating simple relationships between the nominal applied stress and the actual stress present in the test pieces.

A description of the derivation of a general relationship applied to idealised materials is given and the predicted values of fatigue strength are compared with actual results obtained by experiment in work previously published by other investigators.

NOTATION

R	semi-range of stress under mean stress M
R_0	semi-range of stress under zero mean stress
M	mean stress
U	ultimate tensile stress
K_t	elastic stress concentration factor
K_p	"plastic" stress concentration factor
E	Young's modulus
E_s	secant modulus at base of notch

Received June 1955.

E_∞ secant modulus at a point away from notch but in weakest section of test piece

K_r strength reduction factor $\left(=\dfrac{\text{fatigue strength of plain test pieces}}{\text{fatigue strength of notched test pieces}}\right)$

$q=\dfrac{K_r-1}{K_t-1}$

Y yield stress

f_1 nominal stress in weakest section of test piece

f_2 local stress at base of notch

e_1, e_2 total strains corresponding to f_1 and f_2 respectively

2. Initial Assumptions Based on Modified Goodman Relationship

For simplicity it may be assumed that when plain test pieces are subjected to fatigue loads in the presence of mean stresses, the relationship between Range of Stress and Mean Stress for a given endurance is

$$R=R_0\left(1-\frac{M}{U}\right). \quad . \quad . \quad . \quad . \quad . \quad . \quad (1)$$

This relationship is known as the modified Goodman relationship. (It is not necessary to assume that this relationship is correct; it does, however, make the development of the theory more easily understood).

In a notched test piece under static stresses which are entirely elastic, the maximum stress at the base of the notch (termed "local" stress in this paper) is given by

$$f_2=f_1\times K_t.$$

It is assumed for the present that this stress concentration factor K_t can also be applied to fatigue test results. The nominal semi-range of stress under zero mean stress which can be applied to the test piece for a given endurance will be reduced from R_0 for plain test pieces to R_0/K_t for notched test pieces. The mean stress at the base of the notch will be increased over the mean stress M in the body of the test piece by the factor K_t and will equal K_tM. These values, substituted in equation (1), give for notched test pieces the equivalent relationship to the Goodman rule:—

$$R=\frac{R_0}{K_t}\left(1-K_t\frac{M}{U}\right). \quad . \quad . \quad . \quad . \quad . \quad . \quad (2)$$

The equations (1) and (2) are illustrated diagrammatically in Fig. 1. This diagram is here called an R/M diagram.

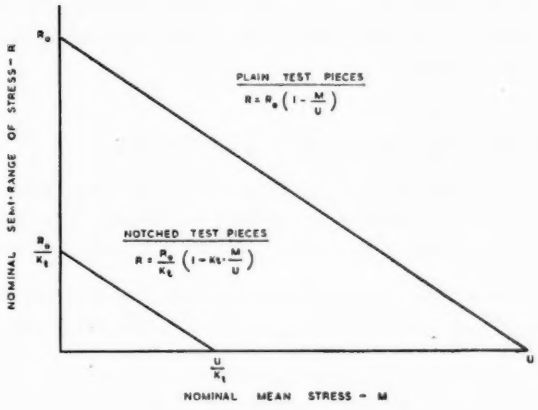

Fig. 1.

Modified Goodman relationship for plain and notched test pieces in the absence of local yielding.

Equation (2) is only applicable when a test piece is stressed purely elastically, for once yielding occurs the relationship $f_2 = f_1 \times K_t$ is no longer valid. The effect on equation (2) of local yielding in notched test pieces is discussed in the next section, where it will be seen that higher values for the nominal range of stress than those predicted by equation (2) can be tolerated, once yielding occurs.

3. Effect of Yielding on Mean Stress

In a notched test piece under cyclically varying loads, the material which yields at the base of the notch will be hardened sufficiently to prevent further plastic deformation* (*see* Appendix I). (The hardening may be completed in the first cycle or in several cycles; the actual number of cycles will depend on the properties of the test piece and the applied stresses). When the test piece has "settled down" and is stressed purely elastically the stress amplitude at the base of the notch will have the same value as it would have had if the body had been purely elastic from the beginning (*see* Appendix I). Although the actual range of stress at the base of the notch will be equal to K_t times the nominal range of stress, the local maximum stress will be less than the stress derived from purely elastic considerations because the local maximum stress will be limited by yielding, its actual value depending on the shape of the stress-strain curve. As a result of the diminution of the local maximum stress, but the maintenance in full of the local range of stress, the local mean stress in the cycle will be reduced below the value

$$K_t \times \text{nominal mean stress.}$$

*The material is assumed to be a homogeneous isotropic solid and plastic deformation under apparently purely elastic stresses is not considered.

With this relief of local mean stress the range of stress which can be withstood under a given nominal mean stress will be greater than that predicted if local yielding had not been taken into account.

4. The R/M Diagram of Notched Test Pieces

Using the concept that due to local yielding the local mean stress diminishes, it is possible to derive R/M diagrams for notched test pieces. The method based on the theory outlined in the previous section is presented in this section.

Under purely elastic stresses the range of stress, related to the mean stress by the equation $R=(R_0/K_t)[1-K_t(M/U)]$, decreases with increasing mean stress along the line AB in Fig. 2. After point B the maximum stress in the local stress cycle at the base of the notch exceeds the yield point of the material and so the local stress is no longer directly proportional to the nominal stress in the body of the test piece.

The stress concentration factor after yielding has occurred can be calculated (*see* Appendix II) from the following formula[1]

$$K_p=1+(K_t-1)\frac{E_s}{E_\infty}. \quad . \quad . \quad . \quad . \quad . \quad . \quad (3)$$

Using values of K_p derived by means of this expression, the local maximum stress can be calculated from each chosen nominal maximum stress. From the now known local maximum stress the corresponding local range of stress can be obtained from Fig. 3, which relates the semi-range of stress and the maximum stress. This diagram

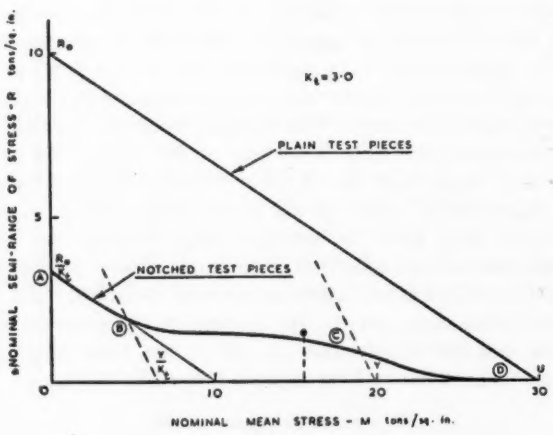

Fig. 2.
The influence of local yielding in notched test pieces on the R/M diagram.

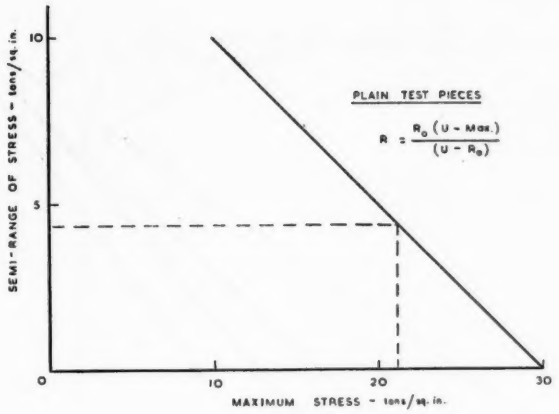

Fig. 3.
Semi-range of stress *v.* maximum stress.
Modified Goodman relationship.

is easily derived from the modified Goodman relationship $R=R_0(1-M/U)$ illustrated in Fig. 1. The nominal semi-range of stress and the nominal mean stress in the body of the test piece are obtained directly by

$$\text{Nominal semi-range of stress} = \frac{\text{Local semi-range of stress}}{K_t}$$

and

$$\text{Nominal mean stress} = \text{Nominal maximum stress} - \left(\frac{\text{Local semi-range of stress}}{K_t}\right).$$

Instead of using the "semi-range/maximum stress" diagram of Fig. 3, the local range of stress can be obtained from the diagram in Fig. 4, where the maximum and minimum stresses are plotted directly against the mean stress. The nominal range of stress and the nominal mean stress can be derived as before.

The post-yielding relationship between nominal mean stress and nominal semi-range of stress (calculated in this manner), is illustrated in Fig. 2 by the curve *BCD* and in Fig. 4 by *BCD* and *B′C′D*. The curve *BC* in Fig. 2 (or the curves *BC* and *B′C′* in Fig. 4) illustrate the relationship when the body of the material is elastic and only the material at the base of the notch undergoes plastic deformation. At *C* in Fig. 2 (or *C* and *C′* in Fig. 4) the body of the test piece also begins to yield and this causes the corresponding range of stress to diminish rapidly as the ultimate stress is approached.

5. Secondary Modifications to the Theory

It is obvious that the idealised curves derived from the simplest assumptions can be modified to cover a number of additional factors. Some of these factors are now discussed.

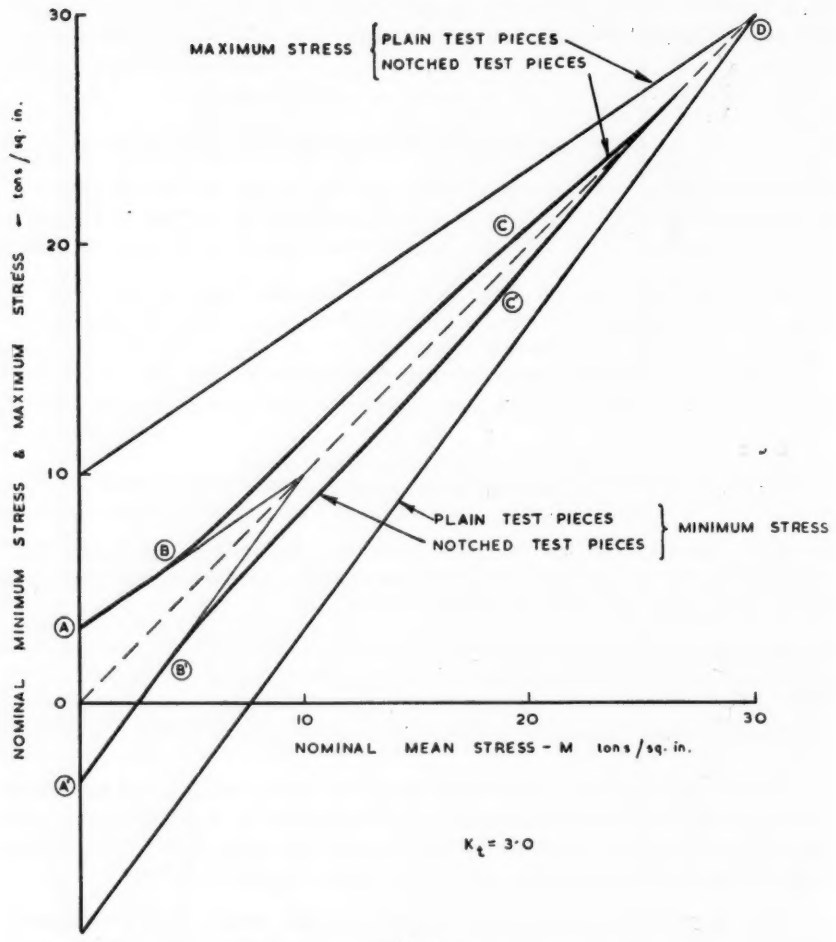

Fig. 4.
The influence of local yielding on the fatigue properties of notched test pieces.

5.1. Modified Goodman Relationship

The initial assumption which was mentioned earlier was only included to demonstrate the theory more easily. Any relationship between R and M for plain test pieces can be used, since the shape of the R/M diagram for notched test pieces is determined by graphical methods.

5.2. Stress Concentration Factor

The expression in equation (3) for the "plastic" stress concentration factor K_p cannot be solved directly for any chosen nominal stress. Either a graphical method

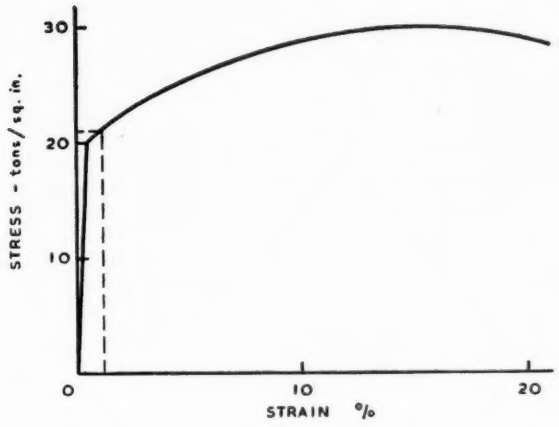

Fig. 5.

Stress-strain curve used in deriving Fig. 2.

or a process of successive approximations must be used once yielding has occurred. A simpler, but less accurate, conception is to assume that the strain concentration factor is equal to the elastic stress concentration factor after local yielding, as well as before local yielding occurs. A value for the local maximum stress can be obtained directly from the stress-strain curve as shown in the example in Fig. 5. In this example a nominal stress of 17 tons/in.^{2} was chosen—its associated elastic strain being 0·36 per cent. With an elastic stress concentration factor of $K_t=3{\cdot}0$, the local strain is taken as $3\times0{\cdot}36$ per cent.$=1{\cdot}08$ per cent. The stress corresponding to this strain is 21·2 tons/in..^{2}. The semi-range of stress, 4·35 tons/in.^{2}, associated with this maximum stress can be read from Fig. 3. The nominal semi-range of stress is 1·45 tons/in.^{2} and the nominal mean stress is therefore 15·55 tons/in.^{2}. These values can be compared with the curve in Fig. 2, where it can be seen that the error due to the simpler method is small.

A comparison of the stress concentration factors calculated by both methods, using the stress-strain curve in Fig. 5 and an elastic stress concentration factor $K_t=3{\cdot}0$, is shown in Fig. 6. Only at high stresses is there appreciable divergence in the two curves and so the simpler method has been adopted in the examples illustrating the theory.

5.3. Stress at which General Yielding Begins

The shape of the curve *CD* in Fig. 2 is not accurately defined. The first uncertain part is the point at which general yielding occurs. Often with notches there are triaxial stresses induced in the material away from the notch, as for example at the centre of a cylindrical test piece containing a circumferential notch.

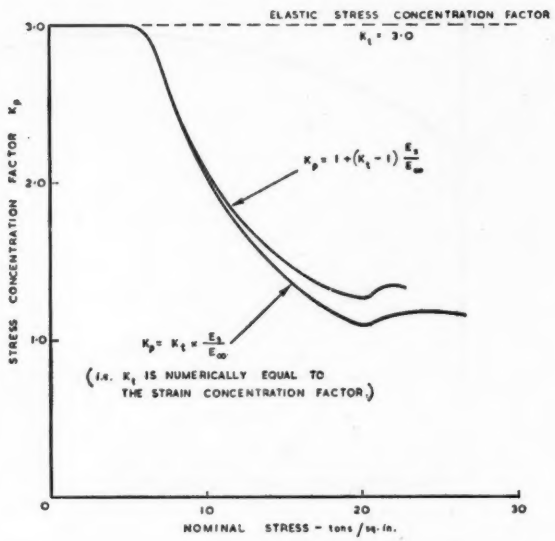

Fig. 6.

Variation of stress concentration factor when local stresses are greater than the yield point.

Two expressions for K_p are illustrated.

Under triaxial stresses, assuming all are in tension, the nominal yield stress will rise and therefore there will be a prolongation of the flattened portion *BC* of the *R/M* diagram. This may be partly an explanation of the large range of stress which is sometimes obtained experimentally under extremely high mean stress as in Fig. 9(*b*) (this figure is discussed later).

5.4. The *R/M* Diagram under High Mean Stresses

The high value for the points under high mean stress discussed in Section 5.3 is but one example of the uncertainty of this part of the diagram. The precise shape of the *R/M* diagram for plain test pieces under very high mean stresses is virtually unknown. Indeed it is likely to depend on the testing technique employed in the fatigue tests. The application of static test results or dynamic test results from plain test pieces under mean stresses approaching the ultimate stress, to a prediction of the behaviour of notched test pieces in fatigue is therefore unreliable.

It is possible that true stress-strain curves derived from tests on notched test pieces, together with the true stress-strain curves obtained on plain test pieces, could be used in determining the maximum local stress in a loading cycle, but no attempt has been made to do so in this paper.

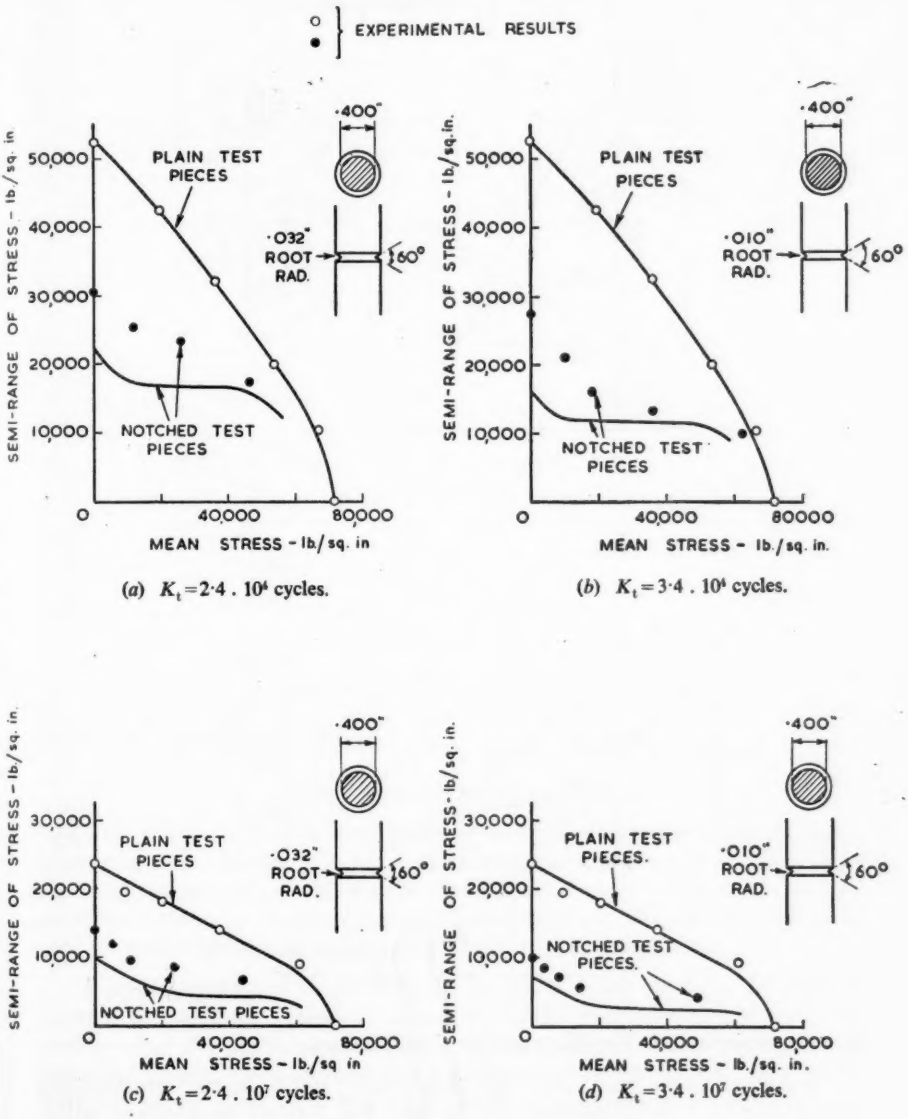

(*a*) $K_t = 2{\cdot}4 \cdot 10^4$ cycles.

(*b*) $K_t = 3{\cdot}4 \cdot 10^4$ cycles.

(*c*) $K_t = 2{\cdot}4 \cdot 10^7$ cycles.

(*d*) $K_t = 3{\cdot}4 \cdot 10^7$ cycles.

Fig. 7.
Comparison of theoretical R/M diagrams for notched test pieces and experimental results. 14S-T6, an alloy similar to B.S. L65[2].

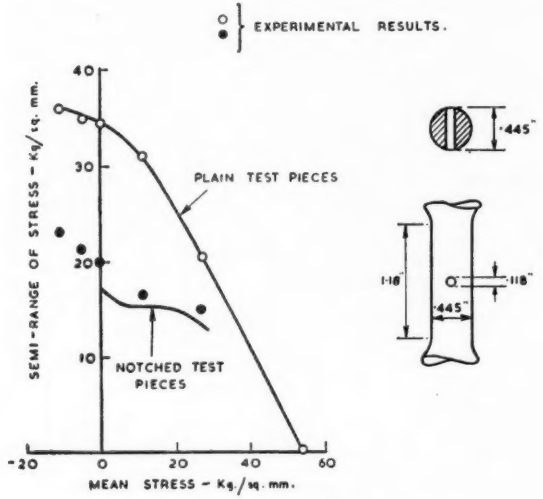

(*a*) $K_t = 2{\cdot}05$. 10^4 cycles.

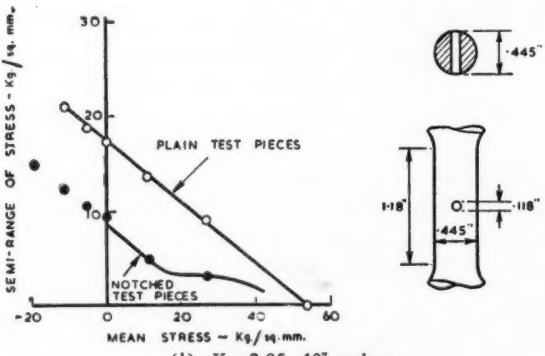

(*b*) $K_t = 2{\cdot}05$. 10^7 cycles.

Fig. 8.
Comparison of theoretical R/M diagrams for notched test pieces and experimental results. 24S-T4[3].

6. Experimental Verification of the Theory

Test results taken from Lazan and Blatherwick[2], and Wållgren[3], are illustrated in Figs. 7 and 8 in the form of R/M diagrams. Fig. 7 shows the results of fatigue tests on both plain and notched test pieces in 14S-T6 (an alloy similar to those conforming to B.S. L65) subjected to various mean stresses. Two designs of notched test pieces were tested and the fatigue strengths for two endurances, 10^4 and 10^7 cycles, are given for each notch. Figs. 7(*a*) and 7(*c*) illustrate the results for a notched test piece with an elastic stress concentration factor of $K_t = 2{\cdot}4$ and

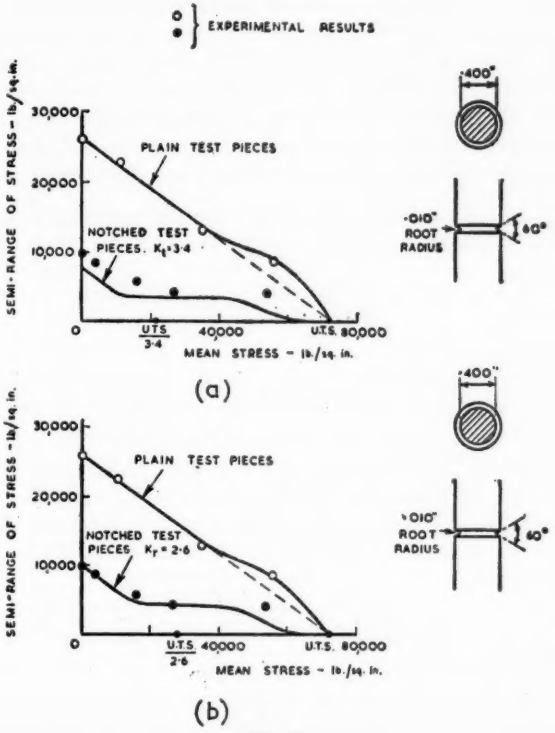

Fig. 9.

Comparison of experimental test results and theoretical curves assuming (*a*) $K_t = 3{\cdot}4$ and (*b*) $K_f = 2.6$.
Alcoa 24S-T4. 10^7 cycles endurance[2].

Figs. 7(*b*) and 7(*d*) illustrate the results for a notched test piece with an elastic stress concentration factor of $K_t = 3{\cdot}4$. Similarly in Figs. 8(*a*) and 8(*b*) the results of plain and notched ($K_t = 2{\cdot}05$) test pieces in 24S-T4 are illustrated for 10^4 and 10^7 cycles endurance. Superimposed on the diagrams are calculated curves derived from the results from plain test pieces and the elastic stress concentration factors.

A striking feature of all the experimental results is the presence of a more or less well defined knee similar to that shown by the calculated curves. In most cases however the calculated curves fall below the experimental results, because in deriving the curves it was assumed that the elastic stress concentration factors would exert their effects to the full. It is a well known experimental observation that this is generally not so and that the strength reduction factor K_f is often less than the elastic stress concentration factor K_t. A relation between these two factors has been expressed[4] as the "sensitivity index" q defined by

$$q = \frac{K_f - 1}{K_t - 1}.$$

The sensitivity index is often called the notch sensitivity factor. The numerical value of q depends, for any alloy, on the condition of heat treatment, on the test piece size and shape, on the magnitude of the mean stress and on the number of cycles endurance. By ignoring q in the development of the theory it has been tacitly assumed that its numerical value is always unity. This can cause the effective stress concentration factor to be overestimated (by unknown amounts) with consequent discrepancy between the experimental and calculated curves.

If instead of K_t the value K_r calculated from the tests results under zero mean stress were used, it would for example modify the equation (2) so that it became

$$R=\frac{R_0}{K_r}\left(1-K_r\frac{M}{U}\right). \quad . \quad . \quad . \quad . \quad . \quad . \quad (4)$$

It would also modify the R/M diagrams for notched test pieces obtained graphically; for example Fig. 9(*a*) shows experimental results[2] (plotted in the form of R/M diagrams) for plain and notched test pieces in 24S-T4, together with the calculated R/M diagram obtained by using K_t to its full extent, *i.e.* $K_t=3{\cdot}4$. In Fig. 9(*b*) however, the calculated R/M diagram obtained by using the value $K_r=2{\cdot}6$ instead of K_t is compared with the same experimental results. In this figure the experimental results are seen to lie close to the theoretical curve, especially at low and intermediate mean stresses.

7. Simplified Procedure

The derivation of the complete R/M diagram for notched test pieces entirely by graphical methods is both complicated and tedious. A simplified procedure is outlined here which is rapid when graphical methods are used and is amenable to algebraic treatment.

First, the R/M diagram for plain test pieces is drawn. The first part (*i.e.* before local yielding) of the R/M diagram for notched test pieces (*AB* in Figs. 2 and 10) is drawn from the plain test piece curve by reducing both the semi-range of stress and the mean stress by the elastic stress concentration factor K_t. The point of local yielding is obtained by the intersection of this R/M curve and the straight line joining the points "stress=(yield)/K_t" plotted on both axes (*i.e.* the straight line that is the locus of maximum stress=(yield)/K_t). "Yield," itself, is taken as the 0·1 per cent. proof stress in aluminium alloys.

It is now assumed, to simplify the diagram, that the range of stress does not change with increase in mean stress after local yielding has occurred (line *BC* in Fig. 10). There is little error in this assumption until general yielding is approached, but as such high stresses are outside the scope of normal design it is convenient to ignore this region of the diagram. The simplified diagram is shown in Fig. 10 and under a different method of plotting in Fig. 11. The R/M diagram obtained by considering work-hardening (*i.e.* the curve *BC* in Fig. 2) is superimposed on these figures to illustrate the small degree of error which the simplification entails.

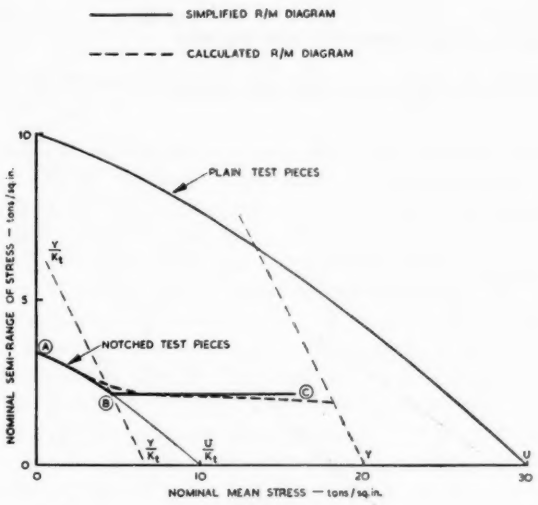

Fig. 10.
A simplified R/M diagram.

$$AB: \quad R=\frac{R_0}{K_t}\left[1-\left(K_t\frac{M}{U}\right)^{4/3}\right]$$

$$BC: \quad R=\frac{R_0}{K_t}\left[1-\left(\frac{Y-K_tR}{U}\right)^{4/3}\right]$$

The algebraic treatment is straightforward, since the R/M diagrams for plain test pieces can be expressed by a number of equations, one group being of the form

$$R=R_0\left[1-\left(\frac{M}{U}\right)^n\right]. \qquad . \quad . \quad . \quad . \quad (5)$$

Equation (1) is of this form, n being taken as 1. Similarly equation (2) can be obtained by putting $n=1$ in equation (6), which is the equation for the first part of the R/M diagram for notched test pieces:—

$$R=\frac{R_0}{K_t}\left[1-\left(\frac{K_tM}{U}\right)^n\right]. \qquad . \quad . \quad . \quad . \quad (6)$$

The intersection of this curve and the straight line representing

$$\text{maximum stress}=(\text{yield})/K_t,$$

i.e.

$$\frac{Y}{K_t}=M+R \qquad . \quad . \quad . \quad . \quad . \quad (7)$$

gives the start of local yielding. This point (and hence the horizontal line BC in Fig. 10) is obtained by substituting equation (7) in equation (6).

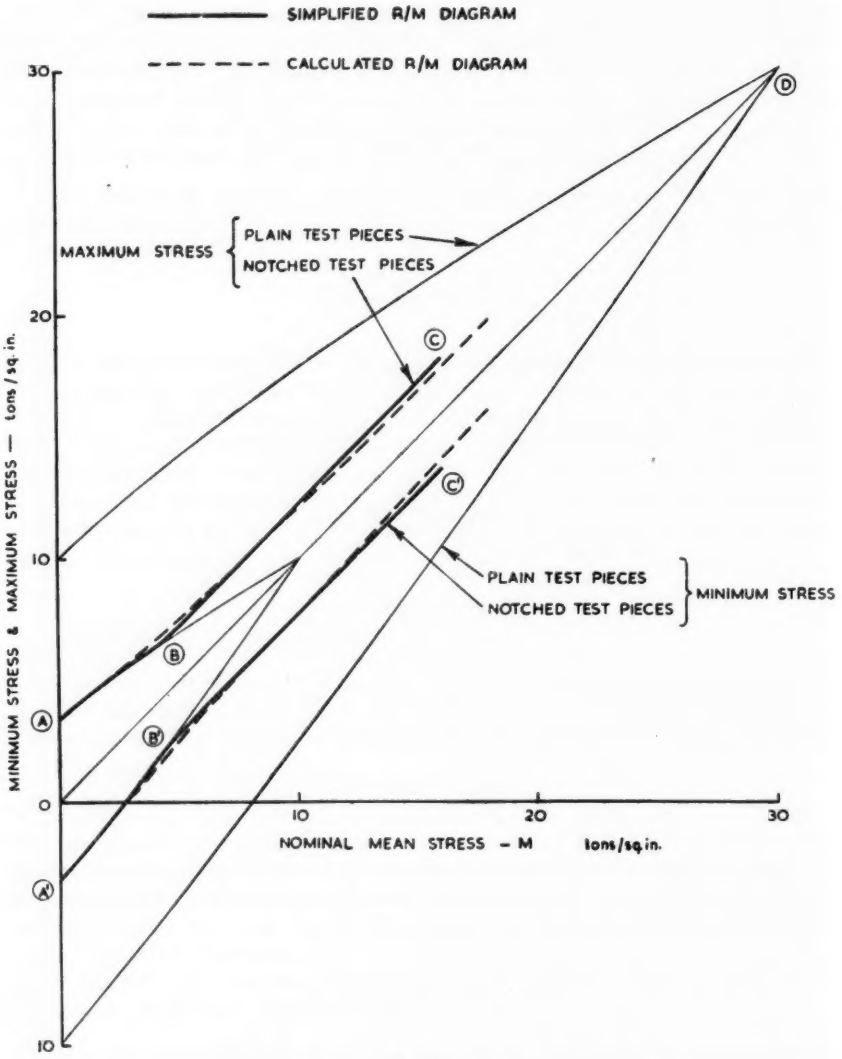

Fig. 11.
Simplified maximum and minimum stress diagram.

$$AB \text{ and } A'B': \quad R = \frac{R_o}{K_t}\left[1-\left(\frac{M}{U}\right)^{4/3}\right]$$

$$BC \text{ and } B'C': \quad R = \frac{R_o}{K_t}\left[1-\left(\frac{Y-K_tR}{U}\right)^{4/3}\right]$$

This gives $$R = \frac{R_n}{K_t}\left[1 - \left(\frac{Y - K_t R}{U}\right)^n\right] . \quad . \quad . \quad . \quad . \quad . \quad (8)$$

The curves for these equations, with the constant n taken as 4/3, are illustrated in Figs. 10 and 11.

In the previous section an example was given of the use of the strength reduction factor K_r in the place of the elastic stress concentration factor K_t. A word of warning is necessary against the unreserved use of this procedure in practice. There is evidence to suggest that the notch sensitivity factor q approaches unity (*i.e.* the strength reduction factor K_r approaches the elastic stress concentration factor K_t) as the volume of highly stressed material increases. If the factor K_r were obtained from test pieces of the same order of size as a service member, then it is possible that it could be used with safety. When the service member is large compared with the test pieces, then it is advisable to use the elastic stress concentration factor to its full extent. A further warning is required against an optimistic interpretation of plain test piece results, since the location of the point of local yielding, occurring as it does at the intersection of two steeply sloping lines, may be critically dependent on minor changes in shape of the initial R/M diagram.

This application of K_r or K_t disregards other factors which may be important in promoting the onset of fatigue failure. For example, if corrosion or fretting corrosion cannot be ignored then they must be taken into account by multiplying the stress concentration factor K_t by an empirical factor. Apart from these adverse service conditions it is expected that it may be difficult to determine the value for the stress concentration factor itself; however, it is necessary to have specific details of designs before this can be discussed.

8. Discussion

In the development of the theory it has been assumed that the static stress-strain curve adequately describes the behaviour of the material under dynamic loads. Insufficient information is available at present to enable a more accurate estimation of the stress-strain relationship under fatigue conditions, but it must be borne in mind that a dynamic stress-strain relationship may modify the final R/M diagrams appreciably.

However the qualitative agreement between the theory and actual test results justifies further speculation on the behaviour of notched test pieces. It is evident that the theory lends some support to the belief that for good fatigue properties a large difference is needed between the proof stress and the ultimate tensile stress (as in material where the ratio (proof stress)/(ultimate tensile stress) is low). The redistribution of stress near the base of a notch will be more easily accomplished in such a material than in a material with a high ratio (proof stress)/(ultimate tensile stress), and so under certain mean stresses it is possible that the former will have relatively higher fatigue properties than the latter, purely because of the difference in yield strength. It is necessary, however, that this suggestion be supported by experimental evidence before it can be accepted.

ACKNOWLEDGMENT

Acknowledgment is made to Aluminium Laboratories Limited for permission to publish this paper.

REFERENCES

1. HARDRATH and OHMAN. A Study of Elastic and Plastic Stress Concentration Factors due to Notches and Fillets in Flat Plates. N.A.C.A. Report 1117.
2. LAZAN and BLATHERWICK. Strength Properties of Rolled Aluminium Alloys under Various Combinations of Alternating and Mean Axial Fatigue Stresses. A.S.T.M. Preprint No. 74, 1953.
3. WÅLLGREN. Direct Fatigue Tests with Tensile and Compressive Mean Stresses on 24ST Aluminium Plain Specimens and Specimens Notched by a Drilled Hole. Flygtekniska Försöksanstalten FFA Meddelande Nr. 48, 1953.
4. PETERSON. Methods of Correlating Data from Fatigue Tests of Stress Concentration Specimens. Stephen Timoshenko, 60th Anniversary Volume. Macmillan, 1938.

Appendix I

A test piece containing a notch, when subjected to tensile stresses, will eventually undergo plastic deformation round the notch, as in the shaded area in Fig. 12. The local stress at the base of the notch will be given by the point *A* on the stress-strain curve of Fig. 13, when the nominal stress is increased from zero (point *O*) to point *P*. On releasing the load, if the volume of material plastically deformed is very small compared with that still purely elastic, the local stress will be *B* and the stress in the body of the test piece *O*. On similar subsequent applications of tensile stress the local stress at the notch will cycle between *B* and *A*, *i.e.* purely elastically but with a lower mean stress than that in the body of the test pieces multiplied by the stress concentration factor.

It is possible that yielding in compression could occur round the notch on releasing the load. In this case, several cycles must elapse before the local stresses are purely elastic, but the mean stress is still less than that given by $K_t \times$ the nominal mean stress.

With zero nominal mean stress the local mean stress will also be zero if the properties in compression are the same as in tension.

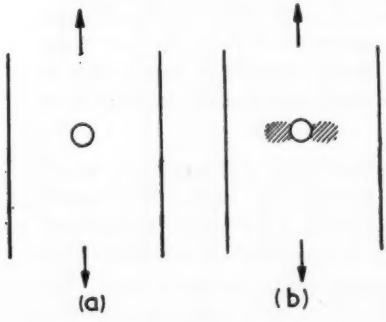

Fig. 12.
Notched test pieces under tensile stress. (*a*) Purely elastic. (*b*) Partially plastic ($K_t \times$ nominal stress is greater than the yield point).

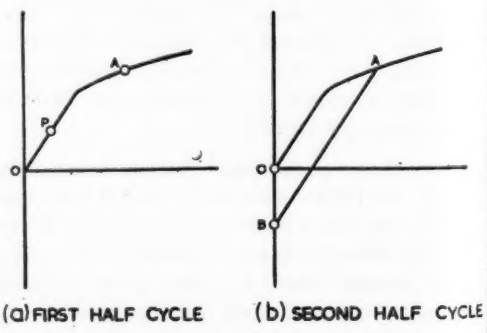

Fig. 13.
Stress in body of test piece: *P* and *O*.
Local stress round notch: *A* and *B*.

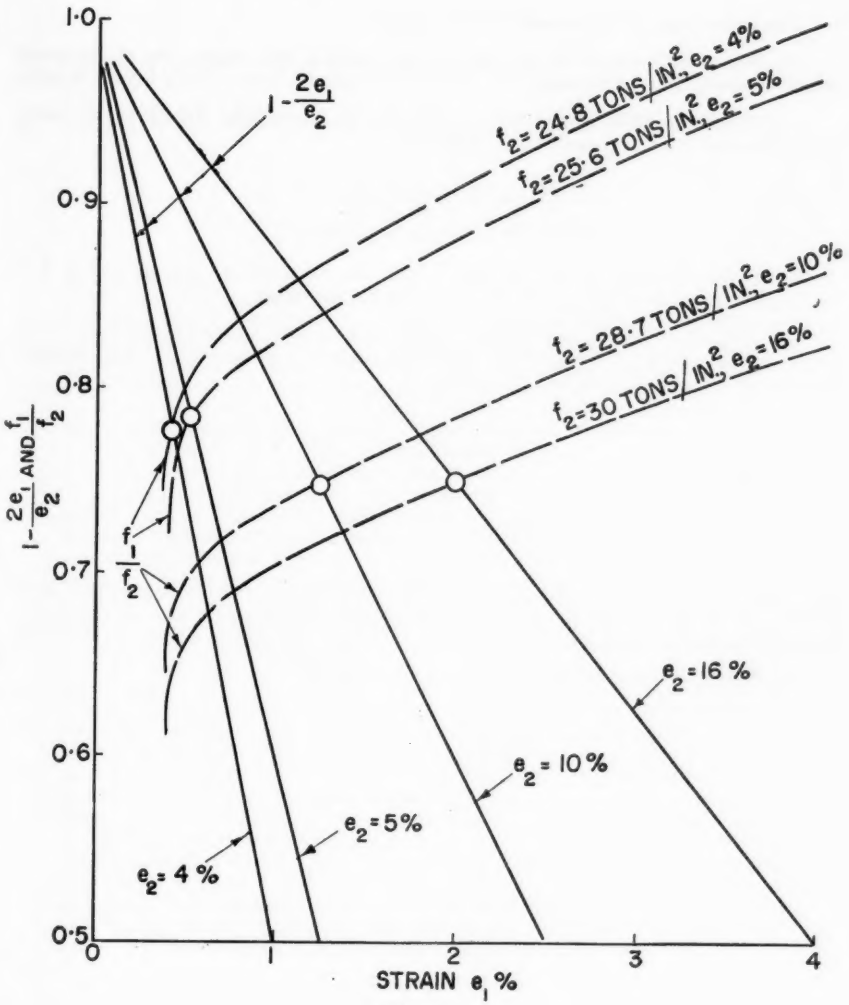

Fig. 14.

Graphical solution of the equation $f_1/f_2 = 1-(K_t-1)\,e_1/e_2$ when $K_t = 3{\cdot}0$.

Appendix II

The equation extracted from Ref. 1 relating purely elastic stress concentration factors with the partially plastic stress concentration factor is

$$K_p = 1+(K_t-1)\frac{E_s}{E_\infty}. \quad . \quad . \quad . \quad . \quad . \quad . \quad (3)$$

This can be re-written

$$\frac{f_2}{f_1} = 1+(K_t-1)\frac{E_s}{E_\infty}. \quad . \quad . \quad . \quad . \quad . \quad . \quad (9)$$

This expression can be solved in three stages:—

(*i*) When the material at the base of the notch is still elastic, the elastic stress concentration factor K_t operates to its full extent and so curve *AB* in Fig. 2 is valid.

(*ii*) When the material at the base of the notch has yielded locally but the body of the material is elastic, equation (9) becomes

$$\frac{f_2}{f_1} = 1 + (K_t - 1)\frac{E_s}{E}.$$

By taking values for f_2 and reading E_s from the stress-strain curve as in Fig. 5, f_1 can be determined in terms of K_t and f_2/f_1 can be calculated.

(*iii*) When the whole material has yielded, a graphical solution is necessary since the relationship between stress and strain is not expressed algebraically. The equation (3) between K_p and K_t can be re-written

$$\frac{f_2}{f_1} = 1 + (K_t - 1)\frac{f_2}{e_2}\frac{e_1}{f_1}.$$

This reduces to

$$\frac{f_1}{f_2} = 1 - (K_t - 1)\frac{e_1}{e_2}.$$

By taking values for f_2 and the corresponding values for e_2 from the stress-strain curve of Fig. 3, both sides of the expression can be plotted against values of e_1 as in Fig. 14. From these curves we can obtain values of f_2/f_1 (*i.e.* K_p) which satisfy the equation.

The values so obtained for K_p are shown in Fig. 6.

Stabilisation of the Aeroplane in Symmetric Flight at Zero or Very Small Air Speeds

W. S. COLEMAN, B.Sc., Ph.D.

(*Blackburn & General Aircraft*)

SUMMARY: The possible use of jet thrust as a source of lift, either by deflection of the force from the normal propulsion axis, or by some other means, raises a new stability problem under conditions of hovering flight and flight at speeds for which the aerodynamic damping becomes insignificant. At the same time, despite the small dynamic pressure, the direct air loads cannot be neglected, for, due to the very large positive or negative incidences peculiar to the motion, the associated coefficients are of a compensatingly high order. Consequently, the problem retains an aerodynamic element, but is principally one of automatic stabilisation, amenable to treatment by ordinary mechanical or electrical circuit theory. The investigation has been restricted to the longitudinal-symmetric motion with virtually the only workable form of automatic control, namely, one responsive to the angular displacement and velocity in pitch, but these conditions undoubtedly embrace all the essentials of any practical application, *e.g.* in take-off and landing by the new technique. The solution to the stability in a gust, or in a succession of disturbances, may then be easily obtained in closed analytical form, but the more general case of unsteady motion, when the displacements are no longer purely oscillatory, necessitates, in part, the use of step-by-step integration. This arises from the added complexity of the aerodynamic terms, due to the appearance of significant changes of incidence, and to the very large and variable values of the resistance derivatives at the angles involved, so that, in the present state of knowledge, the forces determining the motion cannot be expressed functionally. The labour which such calculations entail may be considerably shortened, however, by the application of a procedure based on mean deviations, but it is also found that the conclusions to be drawn from the hovering case remain valid in a number of important respects for the general problem. This feature is demonstrated in the discussion at the end of the paper on a number of examples designed to illustrate the characteristics of the automatic control and the conditions necessary for stability in a variety of circumstances, both when the aircraft is hovering and when its displacement increases continuously with time.

1. Introduction

The sustentation of an aeroplane in the normal flying attitude by means of the thrust from a turbo-jet engine, or a number of such engines, is a development which will probably materialise in a comparatively short time. To obtain the necessary vertical reaction to enable the aeroplane to hover, and to rise and fall, either the engines intended primarily for normal propulsion may be used, in which case the jets must be temporarily deflected, or a battery of small power units, installed exclusively for the production of the necessary lift, might be adopted.

Received March 1954.

As a result of the possibilities which this development offers, much thought is being devoted to the problems involved, both in relation to the engine, and to the control and performance of the aeroplane, under the new conditions which are introduced. The present paper discusses the stability during the stages when the mean air speed is so low that the aerodynamic damping of a disturbance is negligible. Accordingly, stabilisation of a mechanical character is essential, and it is assumed that when the aeroplane is airborne in a condition for which the aerodynamic control and stability are ineffective, there is no intervention on the part of the pilot, the motion being determined purely automatically in terms of the displacements and velocities. Again, for the purpose of the investigation, it is assumed that the system concerned consists of the necessary servo-mechanisms coupled to subsidiary jets disposed at suitable points on the aeroplane. In considering the stability under these conditions, it is also clearly sufficient to stipulate the form of the response without further examination of the detailed functioning of the auto-controls, and in this connection it is assumed that there is a linear correspondence between the input and output signals. At the same time, lag in the system as a whole is taken into account. Lastly, it is manifestly out of the question, within the space of a short paper, to consider more than one or two of the very wide range of ways in which such controls may be designed to function through various measures of the disturbances to which the aircraft is subject. Accordingly, attention is confined here to what would seem to be the two most practical, and commonly used, components, namely, the angular displacement and the angular velocity which, in the present instance, refer essentially to the pitching motion.

Although, as discussed in Appendix I, all the relevant aerodynamic damping terms may be ignored in the immediate problem, this is not the case with respect to the corresponding static forces and moments for, despite the very small air speeds, the incidence is clearly large, tending to the limit $\pm 90°$, and wind tunnel measurements of the lift, drag and pitching moment on a model of a typical high performance aeroplane under such conditions indicate that the coefficients then become so large as to make the actual forces and moments significant. Indeed, if the degree of stability is inadequate, the aircraft rapidly executes a loop into the ground, due to the combination of the thrust and the aerodynamic terms (*see* Section 4.4).

It will also be assumed that the motion is confined to the longitudinal-symmetric state, since this clearly accords in all essentials with the relevant and normal flight conditions. It implies, however, that any gyroscopic yawing couple generated by the rotating parts of the power units and other like sources, when the aircraft pitches, is either negligible or else so damped as to produce no significant departure from two-dimensional motion. This point is considered in detail during the early stages of a disturbance in Appendix II, from which it appears that, for any reasonable magnitude of the couple, the deviations from the truly longitudinal-symmetric state, provided there is adequate stabilisation in both pitch and yaw, will be sufficiently small to satisfy the foregoing assumption.

Because of the small linear velocities which are dealt with, both as regards the horizontal and vertical components, the problem of the stabilisation associated with vertical flight may be largely studied in terms of the hovering aeroplane subject to

a gust of known characteristics. It will be seen that all the essentials of the motion during a typical take-off on jet lift, for example, are exhibited under these simple conditions which yield a solution of the equations of motion in closed analytical form. The results also isolate the effects of the relevant geometrical and inertial characteristics of an aircraft in a very simple manner. On the other hand, if the aircraft is not hovering, and the resultant mean air speed is, in general, an unknown function of the time, the motion can only be determined from a step-by-step solution for each individual case. The labour inherent in such calculations has been much reduced, however, by the mean deviation method fully described in Section 3.2.

The first part of the paper, therefore, is devoted to the hovering case with a variety of disturbances, and these results are amplified later by a selection of the more interesting conclusions from a number of step-by-step analyses of the general case when the displacements of the aircraft are not purely oscillatory.

There remains one other point to consider at this stage. Because the flight path of the aircraft is a primary consideration in the present investigation, fixed axes of reference are more convenient than the customary moving axes of stability theory. At the same time, owing to the symmetric character of the motion, freedom in rotation is confined to pitch, and hence the corresponding inertial term requires no resolution, since the transverse body axis and its counterpart in the fixed reference system remain normal to the plane of symmetry, and therefore parallel to one another. Accordingly, the stationary reference frame has been adopted and the appropriate forms of the equations of motion are considered with respect to it.

NOTATION

x, z	fixed rectangular co-ordinates*, with the x-axis horizontal, the z-axis vertical and the origin at sea level
t	time
τ	dummy time variable
T	period of oscillation of the aircraft
W, m	weight and mass of the aircraft respectively
B	moment of inertia of the aircraft with respect to the transverse axis (normal to the xz-plane) through the centre of gravity
P	total thrust developed by the aircraft
$\overline{M}$	total applied pitching moment with respect to the centre of gravity
L, D, M	aerodynamic lift, drag and pitching moment about the centre of gravity respectively
C_L, C_D	lift and drag coefficients
C_m	moment coefficient
σ	relative air density

*It is convenient to regard the reference axes as fixed relative to the earth, and the motion, apart from the gust conditions investigated, as occurring in still air.

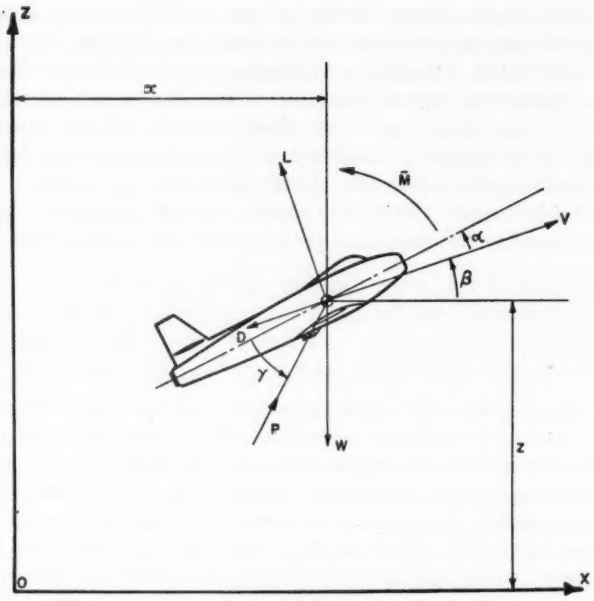

Fig. 1.
Co-ordinate system.

ρ_0 standard sea level air density

V true air speed

S gross wing area

$\bar{c}$ geometrical mean wing chord

α angle of incidence with respect to either wing chord or longitudinal body axis, the two being assumed parallel in the present investigation

β slope of the flight path at any point with respect to the horizontal, taken positively in a climb

γ inclination of the jet pipe axis to the longitudinal body axis, assumed positive when measured downwards from the zero position for normal propulsion

θ angular displacement in pitch relative to the horizontal, *i.e.* $\theta = \alpha + \beta$

w vertical gust velocity

w_1 maximum value of w

T_g duration of a gust

$\omega = \pi / T_g$

K_1 stiffness coefficient of an automatic control which responds linearly with $\dot{\theta}$, *i.e.* the moment generated per unit of angular velocity in pitch

K_2 stiffness coefficient of an automatic control which responds linearly with θ, *i.e.* the moment generated per unit of angular displacement in pitch

$a = -K_1/(2B)$

$s = \sqrt{(-K_2/B)}$

$b = \sqrt{(s^2 - a^2)}$

$\kappa_1 = \sigma\rho_0 w_1^2 S\bar{c}C_m/(2B)$

$\kappa_2 = \sigma\rho_0 w_1^2 SC_D/(2W)$

$\kappa_3 = \kappa_1/(1-2a\varepsilon_1)$

ε_1 time lag of a $\dot{\theta}$-control system

ε_2 time lag of a θ-control system

$a_1 = (2a - s^2\varepsilon_2)/\{2(1-2a\varepsilon_1)\}$

$s_1 = s/\sqrt{(1-2a\varepsilon_1)}$

$b_1 = \sqrt{(s_1^2 - a_1^2)}$

$f(p)$ Laplace transform $\int_0^\infty \theta e^{-pt} dt$

$H(t)$ unit step function

$\mu = \Delta M/B$

ΔM amplitude of a square wave pitching-moment disturbance

q half excitation period of such a disturbance

$\lambda^2 = a^2 - b^2 + 4\omega^2$

$\nu^2 = a^2 + b^2 - 4\omega^2$

$\lambda_1^2 = a_1^2 - b_1^2 + 4\omega^2$

$\nu_1^2 = a_1^2 + b_1^2 - 4\omega^2$

C_1 to C_5 constants of integration defined by equation (17)

C_6, C_7 constants of integration defined by equation (24)

C_1' to C_5' constants of integration defined by equation (17) when the following substitutions are made, namely, C_1' for C_1, C_2' for C_2, etc., and a_1 for a, b_1 for b, κ_3 for κ_3, λ_1 for λ, ν_1 for ν

Ω_1, Ω_2 constants of integration defined by equation (36)

$F(t)$ the variable M/B

h_0, h_1, h_2, h_3 coefficients in the step-by-step expansion of x

g_0, g_1, g_2, g_3 coefficients in the step-by-step expansion of z

2. The Equations of Motion

2.1. Equations of Longitudinal-Symmetric Motion Referred to Fixed Axes

Consider the motion of the aircraft with respect to the fixed rectangular axes defined in the Notation. Then, from Fig. 1, resolving with respect to x and z. we have

$$m\ddot{x} = P\cos(\theta+\gamma) - L\sin\beta - D\cos\beta, \quad . \quad . \quad . \quad . \quad (1)$$

$$m\ddot{z} = P\sin(\theta+\gamma) + L\cos\beta - D\sin\beta - mg, \quad . \quad . \quad . \quad (2)$$

$$B\ddot{\theta} = \overline{M}, \quad . \quad . \quad . \quad . \quad . \quad . \quad . \quad . \quad . \quad (3)$$

and further $$\frac{dz}{dx} = \frac{\dot{z}}{\dot{x}}. \quad . \quad . \quad . \quad . \quad . \quad . \quad . \quad . \quad (4)$$

Moreover, with the conventional notation for derivatives, the elements of P, L, D, $\overline{M}$ for an infinitesimal increment dt of the time are

$$\left.\begin{aligned} dP &= P_z dz + P_V dV, \\ dL &= L_\alpha d\alpha + L_V dV + L_{\dot\theta} d\dot\theta, \\ dD &= D_\alpha d\alpha + D_V dV + D_{\dot\theta} d\dot\theta, \\ d\overline{M} &= M_\alpha d\alpha + M_V dV + (M_{\dot\theta} + K_1)\, d\dot\theta + K_2 d\theta. \end{aligned}\right\} \quad . \quad . \quad . \quad (5)$$

But, as discussed in Appendix I, the aerodynamic terms in $\dot\theta$ may be neglected in the present analysis, stabilisation being then maintained purely through the control terms $K_1\dot\theta$ and $K_2\theta$. Hence, the aerodynamic components of force and moment reduce to the instantaneous static terms while, for P, the characteristics of the turbo-jet engine indicate that, for the small ranges of z and V with which we shall be concerned, P_z and P_V may be regarded as constants. Hence, equations (1), (2) and (3) become

$$m\ddot{x} = (P_0 + P_z z + P_V V)\cos(\theta+\gamma) - \tfrac{1}{2}\sigma\rho_0 V^2 S\,(C_L\sin\beta + C_D\cos\beta), \quad . \quad (6)$$

$$m\ddot{z} = (P_0 + P_z z + P_V V)\sin(\theta+\gamma) + \tfrac{1}{2}\sigma\rho_0 V^2 S\,(C_L\cos\beta - C_D\sin\beta) - mg, \quad . \quad (7)$$

$$B\ddot{\theta} = K_1\dot\theta + K_2\theta + \tfrac{1}{2}\sigma\rho_0 V^2 S\bar{c}C_m, \quad . \quad . \quad . \quad . \quad . \quad . \quad . \quad . \quad (8)$$

where P_0 is the initial (sea level) value of P and $V^2 = \dot{x}^2 + \dot{z}^2$*.

*Where gusts are involved, the value of V, under the conditions of symmetry considered here, must clearly be replaced by $V^2 = (\dot{x}\pm u)^2 + (\dot{z}\pm w)^2$, u and w being, respectively, the horizontal and vertical velocity components of the gust. Equally, β is then given by $\tan\beta = (\dot{z}\pm w)/(\dot{x}\pm u)$.

2.2. Hovering Stability. Behaviour in a Vertical Gust with No Lag of the Control

The simultaneous equations (6), (7), (8) can only be solved numerically in the general case, but when the aircraft is hovering the analysis is appreciably simplified for small displacements of the order which accord with satisfactory stability characteristics. The problem then reduces to one of ordinary mechanical or electrical circuit theory. At the same time, as already noted, and as will be seen in due course, the solution for this particular case reveals all the essential features pertinent to the more complex motion relating to non-stationary flight. Accordingly, the behaviour of the hovering aeroplane is first studied when subject to certain disturbances under the foregoing conditions.

Consider, then, the effect of a gust. Examination of the relative influence of the horizontal and vertical velocity components shows that, for equal strength*, the vertical component has a predominant influence and, to shorten the analysis as much as possible, attention will be confined to the effects of a pure up gust or down gust. Further, to preserve the two-dimensional character of the problem, only the gust which, at a given instant, is everywhere of uniform intensity will be treated and, in accordance with generally accepted practice, its growth and decay will be represented by a sinusoidal function of the time. Relative to the gust velocity, it also appears (*see* Section 4.1) that the linear velocity components of the aircraft induced by the disturbance are sufficiently small to be neglected in so far as the aerodynamic forces and moments are concerned. Hence, the resultant air flow at any instant is assumed to be in the vertical direction while, for simplicity, the body axis is taken to be initially horizontal and the thrust axis vertical, in which case

$$-\alpha=\beta=\gamma=\pi/2.$$

Hence, for a small angular displacement θ with respect to the position of equilibrium, we have, since L then tends to zero and P to mg

$$m\ddot{x}=-P\theta=-mg\theta, \quad . \quad . \quad . \quad . \quad . \quad . \quad . \quad (9)$$

$$m\ddot{z}=-\tfrac{1}{2}\sigma\rho_0 w^2 S C_D, \quad . \quad . \quad . \quad . \quad . \quad . \quad (10)$$

$$B\ddot{\theta}=K_1\dot{\theta}+K_2\theta+\tfrac{1}{2}\sigma\rho_0 w^2 S\bar{c}C_m, \quad . \quad . \quad . \quad . \quad (11)$$

θ being assumed sufficiently small to write $\sin\theta\simeq\theta$, $\cos\theta\simeq 1$. In accordance with the preceding observations, we also write

$$w=w_1\sin\omega t \quad . \quad . \quad . \quad . \quad . \quad . \quad . \quad (12)$$

in the interval $0<t<T_g$, where w_1 is the maximum gust velocity, T_g the duration of the gust and ω the constant π/T_g.

*As is well known, atmospheric turbulence tends to be isotropic, *i.e.* the horizontal and vertical velocity components of a gust are approximately equal in magnitude, and the corresponding frequency distributions are essentially the same.

Then equation (11) may be written as

$$\ddot{\theta}+2a\dot{\theta}+s^2\theta=\kappa_1 \sin^2 \omega t, \quad . \quad . \quad . \quad . \quad . \quad (13)$$

where $a=-\dfrac{K_1}{2B}$, $s^2=-\dfrac{K_2}{B}$, $\kappa_1=\dfrac{\sigma\rho_0 w_1^2 S\bar{c}C_m}{2B}$.

In terms of the Laplace transform

$$f(p)=\int_0^\infty \theta e^{-pt}dt,$$

equation (13) in the interval $0<t<T_g$ takes the form

$$(p^2+2ap+s^2)f(p)=\frac{2\omega^2\kappa_1}{p(p^2+4\omega^2)}+(p+2a)\theta_0+\theta_1,$$

where θ_0, θ_1 are, respectively, the initial values of θ, $\dot{\theta}$, and, since we shall be concerned exclusively with the condition $s^2>a^2$, we write $b^2=s^2-a^2$. Then, factorising the quadratic on the left hand side of the last equation,

$$f(p)=\frac{2\omega^2\kappa_1}{p(p+a+ib)(p+a-ib)(p+2i\omega)(p-2i\omega)}+\frac{(p+2a)\theta_0+\theta_1}{(p+a+ib)(p+a-ib)}. \quad (14)$$

But, when $t=0$, $\theta=\dot{\theta}=0$. Hence, the second term of (14) is zero, and the inverse of (14) is then

$$\theta=2\omega^2\kappa_1\Big[\int_0^t\Big\{\frac{e^{-(a-ib)t}}{2ib(a^2-b^2+4\omega^2-2iab)}+\text{conjugate}\Big\}dt+$$

$$+\int_0^t\Big\{\frac{e^{2i\omega t}}{4i\omega(a^2+b^2-4\omega^2+4ia\omega)}+\text{conjugate}\Big\}dt\Big], \quad . \quad (15)$$

where "conjugate" indicates a similar term with the sign of i changed.

Finally, writing $\lambda^2=a^2-b^2+4\omega^2=2a^2-s^2+4\omega^2$,

$$\nu^2=a^2+b^2-4\omega^2=s^2-4\omega^2,$$

equation (15) yields

$$\theta=e^{-at}(C_1\cos bt+C_2\sin bt)+C_3\cos 2\omega t+C_4\sin 2\omega t+C_5, \quad . \quad (16)$$

with
$$\left.\begin{aligned} C_1 &= -\frac{2\omega^2\kappa_1(\lambda^2+2a^2)}{(\lambda^4+4a^2b^2)(a^2+b^2)}, \\ C_2 &= -\frac{2a\omega^2\kappa_1(\lambda^2-2b^2)}{b(\lambda^4+4a^2b^2)(a^2+b^2)}, \\ C_3 &= -\frac{\nu^2\kappa_1}{2(\nu^4+16a^2\omega^2)}, \\ C_4 &= -\frac{2a\omega\kappa_1}{\nu^4+16a^2\omega^2}, \\ C_5 &= \frac{\kappa_1}{2(a^2+b^2)} = -C_1-C_3. \end{aligned}\right\} \quad . \quad . \quad . \quad . \quad (17)$$

Again, when $t \geqslant T_g$, equation (12), and hence the first term of equation (14), are zero, while the second term of the same equation no longer vanishes, since, for continuity, θ_0, θ_1 now take the values of θ, $\dot{\theta}$ at $t=T_g$. Thus,

$$f(p) = \frac{(p+2a)\theta_0+\theta_1}{(p+a+ib)(p+a-ib)},$$

which yields

$$\theta = e^{-a(t-T_g)}\left[\frac{\theta_1+a\theta_0}{b}\sin b(t-T_g)+\theta_0\cos b(t-T_g)\right], \quad . \quad (18)$$

while, for continuity with (16) when $t=T_g$,

$$\left.\begin{aligned} \theta_0 &= e^{-aT_g}(C_1\cos bT_g+C_2\sin bT_g)+C_3\cos 2\omega T_g+C_4\sin 2\omega T_g+C_5, \\ \theta_1 &= e^{-aT_g}[(aC_1-bC_2)\cos bT_g+(aC_2+bC_1)\sin bT_g]- \\ &\quad -2\omega(C_3\sin 2\omega T_g-C_4\cos 2\omega T_g). \end{aligned}\right\} \quad . \quad (19)$$

Hence, the solution of equation (11) for θ, when w assumes the form of equation (12), is given by equations (16), (17), (18) and (19). The corresponding solutions of equations (9) and (10) follow immediately. Thus, in the case of equation (9), we have

$$\frac{\dot{x}}{g} = -\int \theta\, dt + C_6, \quad . \quad . \quad . \quad . \quad . \quad . \quad . \quad (20)$$

$$\frac{x}{g} = -\int\int \theta\, dt\, dt + C_6 t + C_7, \quad . \quad . \quad . \quad . \quad (21)$$

where C_6, C_7 are the constants of integration. Then, for the interval $0 < t < T_g$ we obtain, on substituting (16) in (20) and (21),

$$\frac{\dot{x}}{g} = \frac{e^{-at}}{a^2+b^2}\left[(aC_1+bC_2)\cos bt+(aC_2-bC_1)\sin bt\right]-\frac{C_3}{2\omega}\sin 2\omega t+\frac{C_4}{2\omega}\cos 2\omega t-C_5 t+C_6, \quad . \quad . \quad . \quad . \quad (22)$$

$$\frac{x}{g} = -\frac{e^{-at}}{(a^2+b^2)^2}\left[\{(a^2-b^2)C_1+2abC_2\}\cos bt+\{(a^2-b^2)C_2-2abC_1\}\sin bt\right]+$$
$$+\frac{C_3}{4\omega^2}\cos 2\omega t+\frac{C_4}{4\omega^2}\sin 2\omega t-\frac{1}{2}C_5t^2+C_6t+C_7, \quad . \quad . \quad . \quad (23)$$

and, when $t=0$, $x=\dot{x}=0$, in which case

$$\left.\begin{aligned} C_6&=-\frac{aC_1+bC_2}{a^2+b^2}-\frac{C_4}{2\omega},\\ C_7&=\frac{(a^2-b^2)C_1+2abC_2}{(a^2+b^2)^2}-\frac{C_3}{4\omega^2}. \end{aligned}\right\} \quad . \quad . \quad . \quad . \quad (24)$$

Again, with respect to equation (10), $\ddot{z}$ may be written as

$$\frac{\ddot{z}}{g} = -\kappa_2 \sin^2 \omega t,$$

in the interval $0<t<T_g$, where $\kappa_2=\sigma\rho_0 w_1{}^2SC_D/(2W)$. Hence,

$$\frac{\dot{z}}{g} = -\kappa_2\left\{\frac{1}{2}t-\frac{\sin 2\omega t}{4\omega}\right\}+D_1,$$
$$\frac{z}{g} = -\kappa_2\left\{\frac{1}{4}t^2+\frac{\cos 2\omega t}{8\omega^2}\right\}+D_1t+D_2,$$

and when $t=0$, $z=\dot{z}=0$, therefore

$$D_1=0, \qquad D_2=\frac{\kappa_2}{8\omega^2},$$

so that

$$\frac{z}{g}=\frac{\kappa_2}{4}\left[\frac{1}{2\omega^2}(1-\cos 2\omega t)-t^2\right]. \quad . \quad . \quad . \quad (25)$$

Clearly, equations (9) and (10) are not adequate approximations when $t>T_g$, for then both x and z increase linearly with time, apart from a small oscillation of x which will be insignificant unless $a\longrightarrow 0$. In reality, however, the displacements will slowly decay due to the small aerodynamic resistance which has been neglected, and, equally, the corresponding damping in pitch will modify the solution (18) to equation (11). This, nevertheless, will only be significant if a is vanishingly small, when the solution given leads to an oscillation of constant amplitude instead of one which is slightly damped. After the gust has subsided, however, the motion is of no particular interest, for it is only the conditions prevalent in the interval $0<t<T_g$ which are characteristic of the problem under investigation, and it is then that the stability or instability of the aircraft will be decided. In the remainder of the discussion relating to pure gusts, therefore, attention will be confined to the interval $0<t<T_g$.

2.3. Hovering Stability. Effect of Control Lag in a Vertical Gust

The effect of lag in the control system could have been included in Section 2.2, but to avoid unnecessary elaboration it will be dealt with separately in the present section. Suppose that the time lags of the θ and $\dot{\theta}$ responses may be expressed serially. Then, provided that the lag is a small proportion of the period of oscillation of the aeroplane, we may neglect all but first order terms and so replace $\dot{\theta}$ by $(\dot{\theta}-\varepsilon_1\ddot{\theta})$ and θ by $(\theta-\varepsilon_2\dot{\theta})$, ε_1 being the lag of the $\dot{\theta}$ system and ε_2 that of the θ system. Hence, equation (13) becomes

$$\ddot{\theta}+2a(\dot{\theta}-\varepsilon_1\ddot{\theta})+s^2(\theta-\varepsilon_2\dot{\theta})=\kappa_1\sin^2\omega t,$$

$$\text{or}\qquad \ddot{\theta}+2a_1\dot{\theta}+s_1^2\theta=\kappa_3\sin^2\omega t, \qquad (26)$$

$$\text{where}\quad 2a_1=\frac{2a-s^2\varepsilon_2}{1-2a\varepsilon_1}, \quad s_1^2=\frac{s^2}{1-2a\varepsilon_1}, \quad \kappa_3=\frac{\kappa_1}{1-2a\varepsilon_1}, \qquad (27)$$

Thus, writing

$$b_1^2=s_1^2-a_1^2,$$
$$\lambda_1^2=a_1^2-b_1^2+4\omega^2=2a_1^2-s_1^2+4\omega^2,$$
$$\nu_1^2=a_1^2+b_1^2-4\omega^2=s_1^2-4\omega^2,$$

equation (16) has the modified form

$$\theta=e^{-a_1t}(C_1'\cos b_1t+C_2'\sin b_1t)+C_3'\cos 2\omega t+C_4'\sin 2\omega t+C_5', \qquad (28)$$

for which equations (17) hold when C_1 is replaced by C_1', C_2 by C_2' etc., and a_1 is written for a, b_1 for b, κ_3 for κ_1, λ_1 for λ and ν_1 for ν. The equations corresponding to (18), (19), (22), (23), (24) then follow immediately, as is obvious, by making these substitutions. It is also evident that, on the basis of the present treatment, lag of the system introduces no change in the form of the differential equation defining the longitudinal stability, *i.e.* equations (13) and (26) only differ in the magnitudes of the constant coefficients. It is, therefore, immaterial, for the purpose of general discussion, whether lag is considered to be present or not, and accordingly, attention is confined to equation (13) in the development which follows.

2.4. Hovering Stability. Characteristics of Controls Responsive to θ or $\dot{\theta}$ Exclusively

It is of some interest to consider automatic controls which respond either to θ or to $\dot{\theta}$ only, since the resulting analysis shows clearly the essential contributions made by each of these elements to a control which will be satisfactory in a general manner. The former condition is merely a particular case ($a=0$) of the solutions

obtained in Sections 2.2, 2.3, so that no further consideration is necessary in this instance. On the other hand, the control purely responsive to $\dot{\theta}$ requires separate treatment. Equation (13) then reduces to

$$\ddot{\theta}+2a\dot{\theta}=\kappa_1 \sin^2\omega t, \quad . \quad . \quad . \quad . \quad . \quad (29)$$

or, on integrating once, to

$$\dot{\theta}+2a\theta=\kappa_1\left(\frac{t}{2}-\frac{\sin 2\omega t}{4\omega}\right), \quad . \quad . \quad . \quad . \quad (30)$$

the constant being zero since $\theta=\dot{\theta}=0$ when $t=0$. Hence, solving this first order linear differential equation to satisfy the initial condition $\theta=0$, $t=0$, we obtain, finally, over the interval $0<t<T_g$,

$$\theta=\frac{\kappa_1}{4}\left[\frac{1}{a}\left(t-\frac{1}{2a}\right)+\frac{1}{2(a^2+\omega^2)}\left\{\frac{\omega^2}{a^2}e^{-2at}+\cos 2\omega t-\frac{a}{\omega}\sin 2\omega t\right\}\right]. \quad (31)$$

Again, after the gust has subsided, *i.e.* for $t>T_g$, equation (29) becomes

$$\ddot{\theta}+2a\dot{\theta}=0 \quad . \quad . \quad . \quad . \quad . \quad . \quad (32)$$

$$\text{or} \quad \dot{\theta}+2a\theta=\text{constant}=\Omega, \text{ say}, \quad . \quad . \quad . \quad . \quad (33)$$

so that, on integration of (33),

$$\theta=\frac{\Omega}{2a}+\frac{\text{constant}}{e^{2a(t-T_g)}}. \quad . \quad . \quad . \quad . \quad . \quad (34)$$

Then Ω and the constant of integration in equation (34) may be determined from the conditions for continuity, namely, by substituting the relations for θ and $\dot{\theta}$ given by (30) and (31) when $t=T_g$ in (33) and (34). It is then found that

$$\theta=\Omega_1\{1-e^{-2a(t-T_g)}\}+\Omega_2 e^{-2a(t-T_g)} \quad . \quad . \quad . \quad . \quad (35)$$

where Ω_1, Ω_2 are constants having the values

$$\left.\begin{aligned}\Omega_1&=\frac{\Omega}{2a}=\frac{\kappa_1}{4a}\left(T_g-\frac{\sin 2\omega T_g}{2\omega}\right),\\ \Omega_2&=\frac{\kappa_1}{4}\left[\frac{1}{a}\left(T_g-\frac{1}{2a}\right)+\frac{1}{2(a^2+\omega^2)}\left\{\frac{\omega^2}{a^2}e^{-2aT_g}+\cos 2\omega T_g-\frac{a}{\omega}\sin 2\omega T_g\right\}\right].\end{aligned}\right\} \quad (36)$$

Finally, in the interval $0<t<T_g$, we have from equations (20), (21) and (31),

$$\frac{\dot{x}}{g}=\frac{\kappa_1}{8a}\left[\left(\frac{1}{a}-t\right)t+\frac{1}{2a^2\omega^2(a^2+\omega^2)}\left\{a^4\left(1-\cos 2\omega t-\frac{\omega}{a}\sin 2\omega t\right)-\omega^4(1-e^{-2at})\right\}\right], \quad . \quad . \quad . \quad . \quad (37)$$

$$\frac{x}{g}=\frac{\kappa_1}{8a}\left[\left(\frac{1}{2a}-\frac{t}{3}\right)t^2-\frac{1}{4a^3\omega^3(a^2+\omega^2)}\left\{a^4\omega\left(1-\cos 2\omega t+\frac{a}{\omega}\sin 2\omega t\right)-\right.\right.$$

$$\left.\left.-\omega^5(1-e^{-2at})-2a\omega(a^4-\omega^4)t\right\}\right]. \quad . \quad (38)$$

in which the constants of integration are determined to satisfy the initial conditions $x=\dot{x}=0$ when $t=0$.

2.5. Hovering Stability. Disturbances in the Form of a Succession of Sharp Pulses

Another type of disturbance of some practical interest which can be dealt with quite simply when the resultant air speed is zero, is one which persists with more or less regular frequency. For example, if the control jets are arranged in groups so disposed to give the requisite stabilising couples, it is possible that certain jets in a group may fail to operate correctly in that they introduce disturbing moments of a cyclical character through some fault in the servo-mechanism. Again, although the main jet-lift pipes may be arranged to give zero net thrust moment with respect to the centre of gravity of the aeroplane when the engines are functioning normally, any uneven running of one or more engines will tend to have a similar effect. Further, if moderate pulses of this kind occur with resonance frequency, they are liable to produce undesirably large displacements in a relatively short time should the automatic control be weak, but not necessarily inadequate, to meet other conditions. Inevitably such disturbances will have a very complex spectrum, but it is assumed here that the fundamental term is predominant, and can be represented by a periodic function which, in view of the essentially spasmodic nature of the disturbance, will be considered to have a discontinuous wave form.

Under the present conditions, equations (6), (7) and (8) reduce to

$$m\ddot{x}=-P\theta, \quad . \quad . \quad . \quad . \quad . \quad . \quad . \quad (39)$$

$$m\ddot{z}=P-mg, \quad . \quad . \quad . \quad . \quad . \quad . \quad . \quad (40)$$

$$B\ddot{\theta}=K_1\dot{\theta}+K_2\theta+\Delta M, \quad . \quad . \quad . \quad . \quad . \quad . \quad (41)$$

where P may now be a function of the time and ΔM is the disturbing moment about the axis, normal to the xz-plane, through the centre of gravity. In addition, as already seen in Section 2.2 on the evidence given in Section 4.1, the linear displacements x, z and their derivatives are of second order significance compared with the corresponding terms in pitch, so that essentially equation (41) remains. Then, in accordance with the foregoing remarks regarding the nature of the disturbance, we write

$$\ddot{\theta}+2a\dot{\theta}+s^2\theta=\mu\left\{H(t)+2\sum_{r=1}^{\infty}(-1)^rH(t-rq)\right\}, \quad . \quad . \quad (42)$$

where $H(t)$ is the unit step function, $\mu=\Delta M/B$ and $2q$ is the excitation period. Thus, writing for the moment, $\phi(t)$ for the function on the right hand side of (42), we have

$$(D^2+2aD+s^2)\,\theta=\phi(t),$$

$$\text{or} \qquad \{D+(a+ib)\}\,\{D+(a-ib)\}\,\theta=\phi(t). \qquad . \quad . \quad . \quad (43)$$

For convenience, let $\theta_1(t)$ represent the complementary function and $\theta_2(t)$ the particular integral of equation (43). Then,

$$\theta_1(t)=e^{-at}(A\cos bt+B\sin bt), \qquad . \quad . \quad . \quad . \quad (44)$$

with A, B as arbitrary constants, while, from the general relation for the particular integral of a second order inhomogeneous ordinary linear differential equation

$$\theta_2(t)=\frac{e^{-(a-ib)t}}{2ib}\int_0^t e^{(a-ib)\tau}\phi(\tau)\,d\tau-\frac{e^{-(a+ib)t}}{2ib}\int_0^t e^{(a+ib)\tau}\phi(\tau)\,d\tau,$$

$$=\frac{\mu e^{-(a-ib)t}}{2ib\,(a-ib)}\left[H(t)\left\{e^{(a-ib)t}-1\right\}+2\sum_{r=1}^{\infty}(-1)^r H(t-rq)\left\{e^{(a-ib)t}-e^{(a-ib)rq}\right\}\right]-$$

$$-\frac{\mu e^{-(a+ib)t}}{2ib\,(a+ib)}\left[H(t)\left\{e^{(a+ib)t}-1\right\}+2\sum_{r=1}^{\infty}(-1)^r H(t-rq)\left\{e^{(a+ib)t}-e^{(a+ib)rq}\right\}\right]$$

which, on reduction, yields finally

$$\theta_2(t)=\frac{\mu}{a^2+b^2}\left[H(t)\left\{1-\frac{1}{b}e^{-at}(a\sin bt+b\cos bt)\right\}+\right.$$

$$\left.+2\sum_{r=1}^{\infty}(-1)^r H(t-rq)\left\{1-\frac{1}{b}e^{-a(t-rq)}[a\sin b(t-rq)+b\cos b(t-rq)]\right\}\right]$$

$$. \quad . \quad . \quad (45)$$

Then $$\theta=\theta_1(t)+\theta_2(t). \qquad . \quad . \quad . \quad . \quad . \quad (46)$$

But, when $t=0$, $H(t)=H(t-rq)=0$. Hence, the particular integral and its derivatives are all zero at $t=0$. Thus, θ is then equal to the complementary function $\theta_1(t)$, and, since $\theta=\dot{\theta}=0$ when $t=0$, it is seen from equation (44) and its first derivative that

$$A=B=0.$$

Therefore, $$\theta=\theta_2(t), \qquad . \quad . \quad . \quad . \quad . \quad . \quad (47)$$

as given by equation (45).

3. The Case of Non-Stationary Flight

3.1. Numerical Solutions of Equations (6), (7) and (8)

We will now consider the general condition when the aircraft has vertical and horizontal velocity components other than the values arising from a disturbance. In this case, the aerodynamic forces and couples become indeterminable functions of the time, and the simultaneous equations (6), (7) and (8) can only be solved approximately step-by-step. Take, first, equation (8). This may be written as

$$\ddot{\theta}+2a\dot{\theta}+s^2\theta=F(t), \quad . \quad . \quad . \quad . \quad . \quad (48)$$

where $F(t)$ defines the quantity M/B. Then equation (48) has the solution

$$\theta=e^{-at}\left[A_1\cos bt+B_1\sin bt+\frac{1}{b}\int_0^t F(\tau)\,e^{a\tau}\sin b(t-\tau)\,d\tau\right],$$

and by the rule for the differentiation of a definite integral

$$\dot{\theta}=-e^{-at}\left[(bA_1+aB_1)\sin bt+(aA_1-bB_1)\cos bt+\frac{1}{b}\left\{a\int_0^t F(\tau)\,e^{a\tau}\sin b(t-\tau)\,d\tau-\right.\right.$$

$$\left.\left.-b\int_0^t F(\tau)\,e^{a\tau}\cos b(t-\tau)\,d\tau\right\}\right],$$

A_1, B_1 being the constants of integration. But, when $t=0$, $\theta=\dot{\theta}=0$.

Therefore $A_1=B_1=0$, and hence,

$$\theta=\frac{e^{-at}}{b}\int_0^t F(\tau)\,e^{a\tau}\sin b(t-\tau)\,d\tau,$$

$$=\frac{e^{-at}}{b}\left[\sin bt\int_0^t F(\tau)\,e^{a\tau}\cos b\tau d\tau-\cos bt\int_0^t F(\tau)\,e^{a\tau}\sin b\tau d\tau\right], \quad . \quad . \quad (49)$$

the latter form for the solution of θ being more convenient in the present discussion. Suppose now that over the time interval $0<t<t_k$, k equal sub-intervals r are taken, so that $t_k=kr$. Also, let r be so small that, to a sufficient approximation, $F(t)$ may be regarded as constant during the time lapse r and equal to its mean value. Thus, for $(j-1)r<t<jr$, write

$$[\overline{F(t)}]_{j-1}^{j}=\tfrac{1}{2}[F\{(j-1)r\}+F\{jr\}]$$

as the mean value of $F(t)$ at the mean time $\frac{1}{2}(2j-1)r$, where $j=1, 2, 3, \ldots k$.

Then, substituting $\overline{F(t)}$ in (49), integrating over a sub-interval and summing over the total interval $0<t<t_k$, we obtain, on writing $t_{j-1}\equiv(j-1)r$, $t_j\equiv jr$,

$$\theta_k=\frac{e^{-at_k}}{b(a^2+b^2)}\Big[\sin bt_k\sum_{j=1}^{k}[\overline{F(t)}]_{j-1}^{j}\{e^{at_j}(a\cos bt_j+b\sin bt_j)-$$
$$-e^{at_{j-1}}(a\cos bt_{j-1}+b\sin bt_{j-1})\}-$$
$$-\cos bt_k\sum_{j=1}^{k}[\overline{F(t)}]_{j-1}^{j}\{e^{at_j}(a\sin bt_j-b\cos bt_j)-e^{at_{j-1}}(a\sin bt_{j-1}-b\cos bt_{j-1})\}\Big], \quad (50)$$

from which it will be seen that, if t_k is equated to the period $2\pi/b$,

$$\theta_k=-\frac{e^{-at_k}}{b(a^2+b^2)}\sum_{j=1}^{k}[\overline{F(t)}]_{j-1}^{j}\{e^{at_j}(a\sin bt_j-b\cos bt_j)-e^{at_{j-1}}(a\sin bt_{j-1}-b\cos bt_{j-1})\}, \quad (51)$$

while, when $K_1=a=0$, there is the further simplification

$$\theta_k=\frac{1}{b^2}\sum_{j=1}^{k}[\overline{F(t)}]_{j-1}^{j}\{\cos bt_j-\cos bt_{j-1}\}. \quad (52)$$

Equally, when $t_k=\pi/b$, θ_k is again given by equation (51), but the sign of the expression must be changed. The same condition applies in the case of equation (52). As will be seen in Section 3.2, where the numerical procedure is discussed, equations (51) and (52) can be used with great advantage to lighten the labour of computation.

Now consider equations (6) and (7). In the interval $0<t<t_k$*, let x and z be represented by the quartics

$$x=h_0+h_1t+\frac{1}{2}h_2t^2+\frac{1}{6}h_3t^3, \quad (53)$$

$$z=g_0+g_1t+\frac{1}{2}g_2t^2+\frac{1}{6}g_3t^3. \quad (54)$$

Then, by successive differentiation of (53) and (54) it follows that

$$\left.\begin{array}{lll} h_0=x_0, & h_1=(\dot{x})_0, & h_2=(\ddot{x})_0, \\ g_0=z_0, & g_1=(\dot{z})_0, & g_2=(\ddot{z})_0, \end{array}\right\} \quad (55)$$

where the suffix 0 denotes an initial value, *i.e.* the value of a quantity at the beginning of a step, and given, therefore, by the end value of the preceding step.

*It will be clear that, in a succession of such intervals, the origin is taken, for convenience, to shift from step to step.

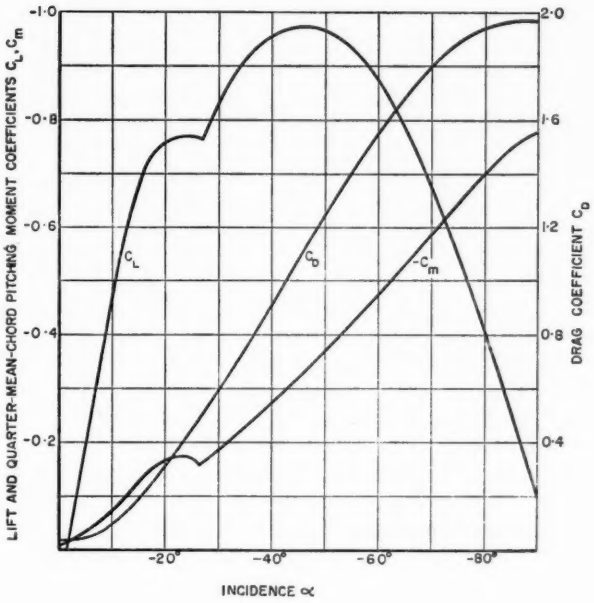

Fig. 2.
Experimental lift, drag and pitching moment data in a down gust.

Further, $\tan\beta=\dfrac{\dot{z}}{\dot{x}}$, $\sin\beta=\dfrac{\dot{z}}{\sqrt{(\dot{x}^2+\dot{z}^2)}}$, $\cos\beta=\dfrac{\dot{x}}{\sqrt{(\dot{x}^2+\dot{z}^2)}}$, . (56)

and $V^2=\dot{x}^2+\dot{z}^2$, ... (57)

while the aerodynamic coefficients

$$C_L=f_1(\alpha), \qquad C_D=f_2(\alpha), \qquad C_m=f_3(\alpha), \quad . \quad . \quad . \quad (58)$$

where $\alpha=\theta-\beta$ are assumed to be given empirically. Hence, through the first and second derivatives of equations (53) and (54), together with equations (56), (57) and (58), we obtain, on substitution in equations (6) and (7), two relations for h_3, g_3 which may be expressed formally in terms of the given initial conditions as

$$h_3=\chi_1\{x_0, (\dot{x})_0, (\ddot{x})_0, z_0, (\dot{z})_0, (\ddot{z})_0, t_k\}, \quad . \quad . \quad . \quad . \quad (59)$$

$$g_3=\chi_2\{x_0, (\dot{x})_0, (\ddot{x})_0, z_0, (\dot{z})_0, (\ddot{z})_0, t_k\}. \quad . \quad . \quad . \quad . \quad (60)$$

Unfortunately, equations (59) and (60) prove to be too involved for direct solution, but the values of h_3, g_3 at each step may be obtained quite rapidly by successive approximation, provided that the aircraft is stable. This point is considered further in the following section.

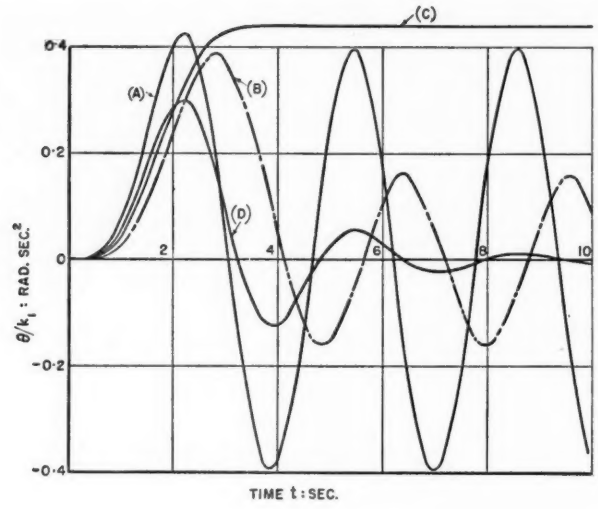

Fig. 3.

(A) $a=0$, $b=2$ sec.$^{-1}$, $T_g=3$ sec.
(B) $a=0$, $b=2$ sec.$^{-1}$, $T_g=5$ sec.
(C) $a=1{\cdot}7$ sec.$^{-1}$, $b=0$, $T_g=3$ sec.
(D) $a=0{\cdot}5$ sec.$^{-1}$, $b=2$ sec.$^{-1}$, $T_g=3$ sec.

3.2. Numerical Procedure. Method of Mean Deviations

Given the initial values of x, z, θ, together with the first derivatives of x, z, and taking P_z, P_V, $f_1(\alpha)$, $f_2(\alpha)$, $f_3(\alpha)$ to be known empirically, the step-by-step solution of equations (6), (7) and (8) may be obtained as follows. Values of h_3 and g_3 in the interval concerned are first assumed*. Then x, z at the end of the interval follow from (53) and (54) respectively, and $\dot{x}$, $\dot{z}$ by differentiation of the series, while the corresponding values of β and V are given by (56) and (57). Next assume a value of α, and so determine C_L, C_D, C_m. Now divide the step into a suitable number of equal sub-intervals r, calculate $\overline{F(t)}$ for each sub-interval and thence a first approximation for θ from (50), or (51) and (52) when the conditions permit (*see* later). Hence, a second approximation for α follows from the relation $\alpha=\theta-\beta$. Finally, evaluate $\ddot{x}$, $\ddot{z}$ at the end of the interval by substitution in (6) and (7), and so, by double differentiation of (53) and (54), obtain second approximations for h_3, g_3. The calculations must then be repeated with the improved values of h_3, $\dot{g}_3$, α until the approximations coincide to a satisfactory order of accuracy.

*As the calculations develop, first approximations may be obtained by extrapolation from the data established, but in the early stages, when this is not a very reliable procedure, it is sufficient to start a new step with h_3, g_3 assigned the values obtained finally in the preceding step.

When the control has a strongly damped element, as, for example, in Fig. 3 ($a=0{\cdot}5$ sec.$^{-1}$, $b=2{\cdot}0$ sec.$^{-1}$), or in Fig. 12 ($a=0{\cdot}55$ sec.$^{-1}$, $b=1{\cdot}80$ sec.$^{-1}$), the most convenient choice of interval is the natural period of oscillation $2\pi/b$, or some integral multiple of it, since the simplified equation (51) may then be used to calculate θ. If, however, there is an appreciable tendency to oscillation, as in the undamped, but stable, condition (*e.g. see* Fig. 3, $a=0$, $b=2{\cdot}0$ sec.$^{-1}$ and Fig. 12, $a=0$, $b=1{\cdot}80$ sec.$^{-1}$), the interval has to be reduced considerably, so greatly adding to the labour involved. The difficulty may be circumvented, however, by the following procedure* which results in a substantial economy of computation without loss of accuracy.

Suppose that an approximate solution to the problem is first obtained by ignoring the oscillations in θ, and that any convenient integral multiple of the natural period is again taken as interval. Then, the values of x, z and $F(t)$ so obtained are strictly valid for a distribution of θ given, for example, by the lower envelope to the curve of Fig. 12 when $a=0$. Equally the upper envelope to θ is determined by calculating the half-periodic values. Both these estimates may be performed rapidly, since the much simplified relation (52) then holds. Finally, the mean deviation θ_m, as indicated by the chain curve in Fig. 12, is used to re-calculate $F(t)$, x, z as before, the process being continued until successive approximations agree with the requisite accuracy. In point of fact, it is found that the variations in θ, β and V, upon which the aerodynamic pitching moment, and hence $F(t)$, depend, so combine as to make the second approximation to $F(t)$ in very close agreement with the first. Hence, in practice, it is unlikely that the calculations need be repeated more than once.

This method has also been carefully checked over one period against sample calculations which follow the actual oscillations of θ (the steps in this case were reduced to 1/10 of the period with sub-intervals of 1/60 of the period), and the comparisons, even for a severe gust, proved to be in agreement with an accuracy which is probably better than the general accuracy of the step-by-step method.

This procedure of working on the mean deviation of θ, when the motion is strongly oscillatory, involves little more time and labour than does the simpler calculation in the case of a control giving appreciable damping.

4. Discussion of the Control Characteristics and the Conditions for Stabilisation

4.1. General Properties of θ and $\dot{\theta}$ Controls

Some examples illustrating the characteristics peculiar to the type of automatic control under consideration are now presented, and an examination is made of the conditions necessary for adequate stabilisation of the aeroplane when the normal aerodynamic damping becomes negligible. The results are divided into two groups.

*Although the procedure has been found to give satisfactory convergence in the present calculations, and accords well with the checks referred to at the end of the section, no investigation has been made as to its general suitability and validity in step-by-step calculations of an oscillatory character.

The first set (*see* Figs. 3 to 8 inclusive; also Table I) refer to the hovering case, and the second (Figs. 9 to 14 inclusive) to some of the more interesting points arising from step-by-step calculations of the take-off flight path in a specific instance.

As will be clear from Sections 2.2 to 2.5, the motion in hovering flight is proportional to the coefficients κ_1, κ_2, μ which connect the mass and inertial characteristics of the aircraft with the forces and moments generated aerodynamically, or through some source of the kind discussed in Section 2.5. The calculations, therefore, under such conditions, may be expressed quite generally, and accordingly, the relevant results, as presented in Figs. 3 to 8 and Table I, are independent of the geometry and mass distribution of the aircraft, and of the magnitude of the disturbance. On the other hand, when the aircraft is subject to a continuous displacement in addition to one of an oscillatory character, the aerodynamic loads, as already observed, then become dependent variables, and in these circumstances, the motion can only be analysed step-by-step for specific initial conditions. Those relating to Figs. 9 to 14 refer to an aircraft considered tentatively as a means of conducting some full-scale experiments on the type of stability problem discussed herein. The essential data were as follows: weight of the aircraft at take-off 2,600 lb.; corresponding wing loading 60 lb./ft.^{2}; sea level thrust (assumed to act, except where otherwise stated, at an angle γ of 72·5°) 2,850 lb.; and thrust variations P_z, P_V of, respectively, $-0{\cdot}0720$ lb. ft.$^{-1}$, valid for $0 < z < 5{,}000$ ft., and $-1{\cdot}325$ lb. sec. ft.$^{-1}$, tenable over the range $0 < V < 150$ ft./sec.

Figure 2 also gives the lift, drag and quarter-chord pitching moment data upon which all the step-by-step calculations were based. These measurements do not refer to the aircraft in question, but were taken from some unpublished records of wind tunnel experiments on a model of similar form at a mean chord Reynolds number of $0{\cdot}6 \times 10^6$. The curves shown represent the average values of the coefficients from observations with (*a*) the normal wing, (*b*) the same wing with the span reduced by 25 per cent. In each case the sets of coefficients differed very little when based on the respective wing areas.

The first point to which attention will be drawn relates to the characteristics of the θ and $\dot{\theta}$ components, and to the ways in which they are important for satisfactory stabilisation. Fig. 3 shows the oscillations in pitch under hovering conditions as the result of a vertical gust. Curves (A) and (B) are for a pure θ control, curve (C) for a $\dot{\theta}$ control only and curve (D) for a combination of the two. Ignoring, for the moment, the effect of lag, a control responsive to θ alone will, provided that it is of sufficient strength, preserve stability, but the aircraft continues to oscillate after the disturbance has ceased. Owing to the neglect of air resistance, this residual motion appears as a continuous oscillation of constant amplitude, whereas, in reality, it will decay, but, at the low velocities concerned, the damping will be so gradual that it will not materially alter the tendency of the aircraft to hunt. Fig. 12 also illustrates this characteristic very well during take-off in gusty conditions with the same form of control. Again, an adequate $\dot{\theta}$ control provides stability during a disturbance, but in contrast to the θ control, which preserves the original attitude of equilibrium, the $\dot{\theta}$ control causes the aircraft to assume a new steady state, so that, unless correction is applied by manual intervention or by a

monitoring system, there will be a gradual divergence in, for example, a succession of gusts. The combination of θ and $\dot{\theta}$ response clearly avoids these disadvantages, and the less disturbed behaviour of an aircraft with the double form of control, as compared with that depending on θ only, during flight through a number of down gusts is well illustrated in Fig. 12.

Of further interest is the way an aircraft reacts to gusts which persist for varying lengths of time. From Section 2.2, it is easily seen that, with zero damping ($a=0$), the effect of a gust will be a maximum when the duration of the gust is equal to the natural period of oscillation, *i.e.* when $T_g=2\pi/b$, or $\omega=b/2$. Thus, a dominant gust exists for every value of b. Examples demonstrating this feature are given in Fig. 4, from which it will be noted that, relative to the most severe condition, there is a much more pronounced variation of response to gusts of short existence than there is with long period gusts. Other calculations when $a=1$ sec.$^{-1}$ display essentially the same result, namely, a dominant gust which, for any value of b within the limits indicated in Fig. 4, has about the same duration as that corresponding to zero damping. Equally, there is, again, a greater variation of response to sharp gusts than to those of a more prolonged nature. It appears, therefore, that the aircraft exhibits a general uniformity of behaviour to gusts of various lengths over the ranges of a and b here considered, and that the value of T_g for the dominant gust is virtually a function of b only.

Figs. 5, 6, 7 present general curves of the displacements θ_{max}, $x(T_g)$ and $z(T_g)$, the first being the maximum value attained in the dominant gust* and the other two the values at the end of a gust. Estimates of κ_1, κ_2 based on data from Ref. 1 for w_1 and Ref. 2 for B, and on the results of Fig. 2 for C_D, C_m, indicate that κ_1 is not often likely to exceed about 0·1 sec^{-2}, while κ_2, which is non-dimensional, also has a maximum limit in the region of 0·1. Thus, for instance, when $b=1{\cdot}5$ sec.$^{-1}$, the displacements of the aircraft in the dominant gust, for which $T_g=4{\cdot}2$ sec., are: $\theta_{max}=4{\cdot}3°$, $x(T_g)=6{\cdot}4$ ft., $z(T_g)=13{\cdot}5$ ft. when $a=0$, and $\theta_{max}=1{\cdot}7°$, $x(T_g)=3{\cdot}1$ ft., $z(T_g)=13{\cdot}5$ ft. when $a=1$ sec.$^{-1}$, *i.e.* the average values of $\dot{x}$, $\dot{z}$ during the gust period range from 1 to 3 ft./sec. Hence, since w_1 appropriate to the above example is of the order of 50 ft./sec., the assumption made in Section 2.2 that the components $\dot{x}$ and $\dot{z}$ are aerodynamically insignificant, given adequate control, is quite justified.

4.2. Effect of Lag

The crucial point from this aspect of the investigation is the absolute necessity for some degree of $\dot{\theta}$ control if stability is to be preserved when lag is present. This is evident from the first of equations (27) which shows that there is a critical value of ε_2 for which the stability is neutral, *i.e.* for $a_1=0$ or $a=\frac{1}{2}s^2\varepsilon_2$, so that when the response to $\dot{\theta}$ is absent ($a=0$), the aircraft is inevitably unstable however small the lag.

*As already stated, the value of T_g for the dominant gust proves to be virtually independent of a, and may, therefore, be taken as equal to the value $2\pi/b$ appropriate to $a=0$. In this case, however, equations (16) and (23) for θ, x respectively become indeterminate, since λ, ν are then both zero. Nevertheless, as Fig. 4 shows, the variation of θ with T_g for values close to $2\pi/b$ is trivial, and the calculations were based on the gust times indicated by the curve AA of Fig. 4.

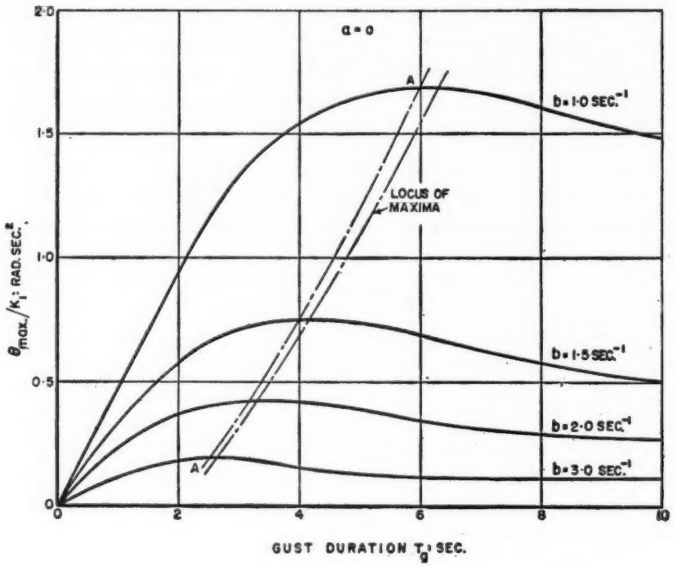
a = 0
A
b = 1·0 SEC.⁻¹
LOCUS OF MAXIMA
b = 1·5 SEC.⁻¹
b = 2·0 SEC.⁻¹
b = 3·0 SEC.⁻¹
A
2·0
1·5
1·0
0·5
0
0
2
4
6
8
10
θmax./K1 : RAD. SEC.²
GUST DURATION Tg : SEC.

Fig. 4.

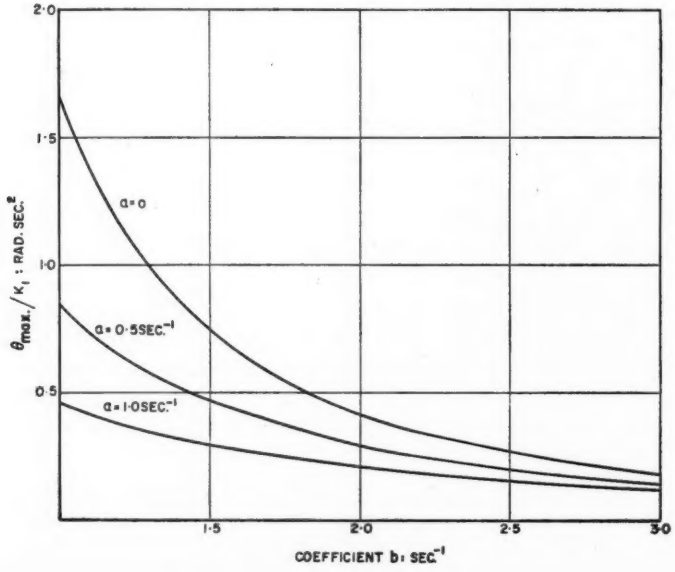
2·0
1·5
1·0
0·5
a = 0
a = 0·5 SEC.⁻¹
a = 1·0 SEC.⁻¹
1·5
2·0
2·5
3·0
θmax./K1 : RAD. SEC.²
COEFFICIENT b : SEC.⁻¹

Fig. 5.

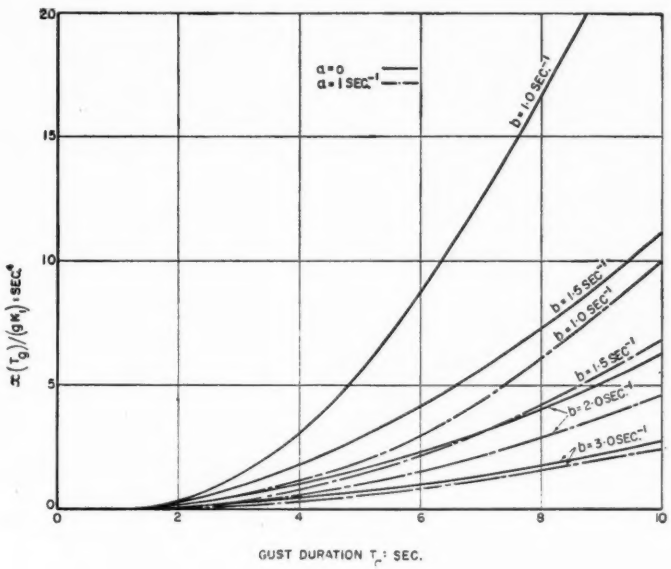
a=0
a=1 SEC.⁻¹
b=1·0 SEC.⁻¹
b=1·5 SEC.⁻¹
b=1·0 SEC.⁻¹
b=1·5 SEC.⁻¹
b=2·0 SEC.⁻¹
b=3·0 SEC.⁻¹
x (T_g)/(gK_x) : SEC.⁴
GUST DURATION T_g : SEC.

Fig. 6.

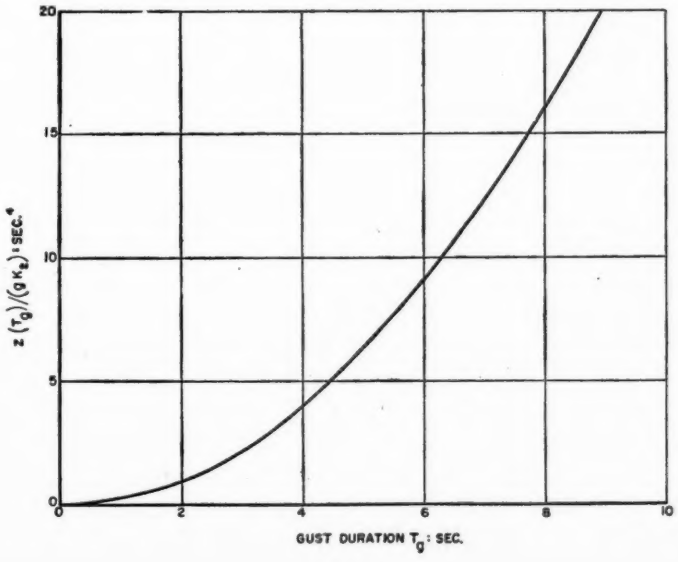
z (T_g)/(gK_z) : SEC.⁴
GUST DURATION T_g : SEC.

Fig. 7.

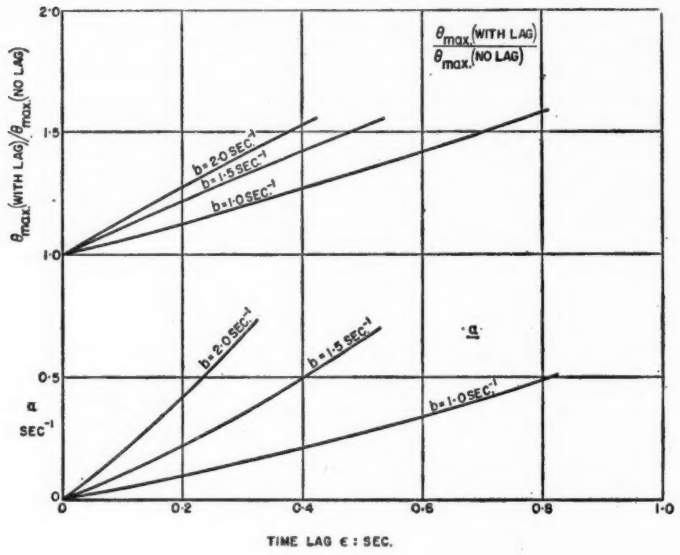

Fig. 8.

Thus, for any values of a and b, we have, since $s^2 = a^2 + b^2$,

$$\varepsilon_2\,(\text{crit}) = \frac{2a}{a^2+b^2}, \qquad \ldots \quad (61)$$

and further, for neutral stability,

$$b_1^2 = \frac{a^2+b^2}{1-2a\varepsilon_1}. \qquad \ldots \quad (62)$$

Hence, given a and b, the critical lag and the corresponding behaviour of the aircraft to a known disturbance may be determined according to the analysis of Section 2.3. Some examples based on the reasonable assumption that $\varepsilon_1 = \varepsilon_2 = \varepsilon$, say, are recorded in Fig. 8. For a typical degree of lag, the minimum value of a to give neutral stability is not large, and increases roughly in proportion to both ε and b. Equally, the corresponding ratio of the displacement θ_{max} with lag to that for zero lag is very nearly a linear function of ε, but is not markedly dependent on b at the higher values. In the normal range of b, say 1·5 to 2·0 sec.$^{-1}$, and for a lag of 0·5 sec., θ_{max} in the limiting case of neutral stability will be about 50-65 per cent. larger than the value when lag is absent. This is, perhaps, an extreme condition, but it illustrates the need for adequate damping from the control.

In the further discussion, lag will again be ignored.

TABLE I

(*a*) RESONANCE. LIMITING CONDITIONS FOR AN AMPLITUDE IN PITCH NOT EXCEEDING $\pm 10°$

$a=0, b=1{\cdot}047$			$a=0, b=2{\cdot}094$			$a=0, b=3{\cdot}142$		
No. of half-cycles r	*Time lapse rq* sec.	μ sec.$^{-2}$	*No. of half-cycles r*	*Time lapse rq* sec.	μ sec.$^{-2}$	*No. of half-cycles r*	*Time lapse rq* sec.	μ sec.$^{-2}$
1	3	0·0955	2	3	0·1910	3	3	0·2865
2	6	0·0478	4	6	0·0956	6	6	0·1434
3	9	0·0318	6	9	0·0636	9	9	0·0954
4	12	0·0239	8	12	0·0478	12	12	0·0717
5	15	0·0191	10	15	0·0382	15	15	0·0573
6	18	0·0159	12	18	0·0318	18	18	0·0477
7	21	0·0136	14	21	0·0272	21	21	0·0408
8	24	0·0119	16	24	0·0238	24	24	0·0357
9	27	0·0106	18	27	0·0212	27	27	0·0318
10	30	0·0096	20	30	0·0192	30	30	0·0288

(*b*) DAMPED CONDITION. AMPLITUDE IN DEGREES AFTER A LAPSE OF 10 SEC.

$b=1{\cdot}047$			$b=2{\cdot}094$			$b=3{\cdot}142$		
μ sec.$^{-2}$	$a=0{\cdot}5$	$a=1{\cdot}0$	μ sec.$^{-2}$	$a=0{\cdot}5$	$a=1{\cdot}0$	μ sec.$^{-2}$	$a=0{\cdot}5$	$a=1{\cdot}0$
0·0955	6·40	2·89	0·1910	6·57	3·20	0·2865	6·60	3·26
0·0478	3·20	1·45	0·0956	3·29	1·60	0·1434	3·30	1·63
0·0318	2·13	0·96	0·0636	2·19	1·07	0·0954	2·19	1·09
0·0239	1·60	0·72	0·0478	1·65	0·80	0·0717	1·65	0·82
0·0191	1·28	0·58	0·0382	1·32	0·64	0·0573	1·32	0·65
0·0159	1·07	0·48	0·0318	1·10	0·53	0·0477	1·10	0·54
0·0136	0·91	0·41	0·0272	0·94	0·46	0·0408	0·94	0·47
0·0119	0·80	0·36	0·0238	0·82	0·40	0·0357	0·82	0·41
0·0106	0·71	0·32	0·0212	0·73	0·37	0·0318	0·73	0·37
0·0096	0·65	0·29	0·0192	0·66	0·32	0·0285	0·66	0·32

Note: a and b are given in radian measure and have the dimension sec.$^{-1}$.

4.3. Stability During a Succession of Sharp Pulses

The influence of a repetitive disturbance, as discussed in Section 2·5, also demonstrates the importance of providing damping ($a \neq 0$) under certain conditions, namely, when the frequency of excitation approaches the natural frequency.

In Table I(*a*), the allowable disturbing moment per unit moment of inertia for a pure θ control (system with no damping), such that the angle of pitch shall not exceed $\pm 10°$ after a specified number of oscillations, is recorded over a range of b. Inversely, Table I(*b*) gives the amplitude, with various degrees of damping, after a lapse of 10 sec. from the onset of the disturbance. Thus, whereas, for example, the undamped angle of pitch reaches 10° after 3 sec. when $\mu=0{\cdot}191$ sec.$^{-2}$ and $b=2{\cdot}094$ sec.$^{-1}$*, the corresponding damped displacement at the same values of μ and b is only 6·6° after 10 sec. when $a=0{\cdot}5$ sec.$^{-1}$, or 3·2° when $a=1{\cdot}0$ sec.$^{-1}$.

*The values of b given in Table I were adopted for convenience in order to make the excitation period $2q=2\pi/b$ a whole number.

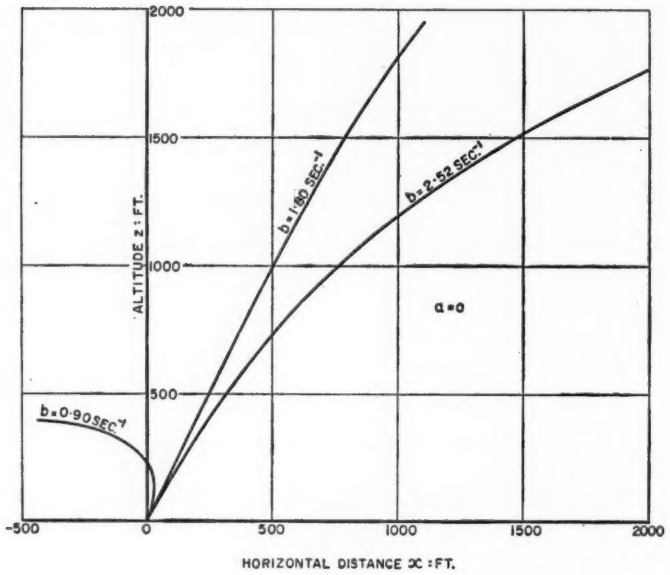

Fig. 9.

4.4. Stability Features Peculiar to the Case When the Displacements are Not Purely Oscillatory

So far only the hovering condition has been discussed, when θ, x, z are purely oscillatory, and $\dot{x}$, $\dot{z}$ may normally be ignored compared with the gust velocity w, but there are certain features of general interest when x, z exhibit a continuous positive or negative variation throughout the motion, *e.g.* during take-off or landing. As to the displacement θ, it has been noted that this aspect of the motion is much the same whether the aircraft is hovering or moving under its own power (*cf.* Figs. 3, 12), and it is very useful that the simple hovering condition leads to results in this respect of wide application, since the stability of the aircraft (always, of course, with the restriction that the resultant air speed is sufficiently small to make the aerodynamic damping negligible) is primarily dependent on the pitching motion generated. What happens with inadequate automatic control is portrayed in Figs. 9, 10, 11. Thus, in Fig. 9 take-off flight paths have been plotted for the undamped condition ($a=0$) with, respectively, values of b equal to 0·90, 1·80 and 2·52 sec.$^{-1}$*. In the first instance, the motion is clearly unstable. Due to the inadequate control moment, the pitch angle increases rapidly. As a consequence, the thrust inclination approaches the vertical (*see* Fig. 1), and then slopes in the opposite direction.

*Again, as in the calculations relating to Table I, values of a and b for the step-by-step calculations were so chosen that the period, and therefore the interval, were whole numbers. This much simplifies the numerical work. Also, a was made zero, in order to shorten the calculations, whenever the immediate point under discussion was not significantly dependent on a.

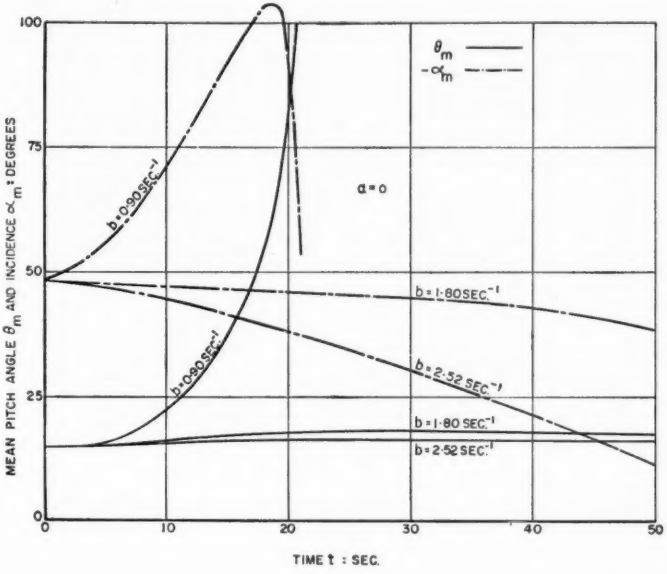
MEAN PITCH ANGLE θ_m AND INCIDENCE α_m : DEGREES
TIME t : SEC.
θ_m
$-\alpha_m$
a = 0
b = 0·90 SEC.$^{-1}$
b = 1·80 SEC.$^{-1}$
b = 2·52 SEC.$^{-1}$
b = 0·90 SEC.$^{-1}$
b = 1·80 SEC.$^{-1}$
b = 2·52 SEC.$^{-1}$
0
25
50
75
100
10
20
30
40
50

Fig. 10.

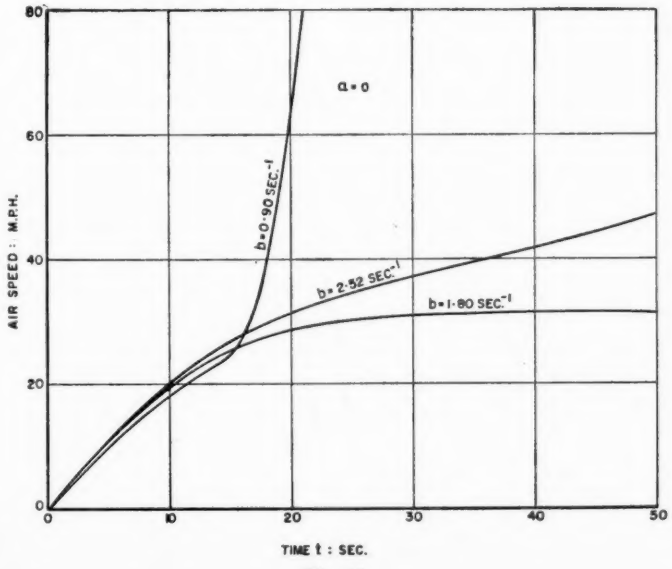
AIR SPEED : M.P.H.
TIME t : SEC.
a = 0
b = 0·90 SEC.$^{-1}$
b = 2·52 SEC.$^{-1}$
b = 1·80 SEC.$^{-1}$
0
20
40
60
80
10
20
30
40
50

Fig. 11.

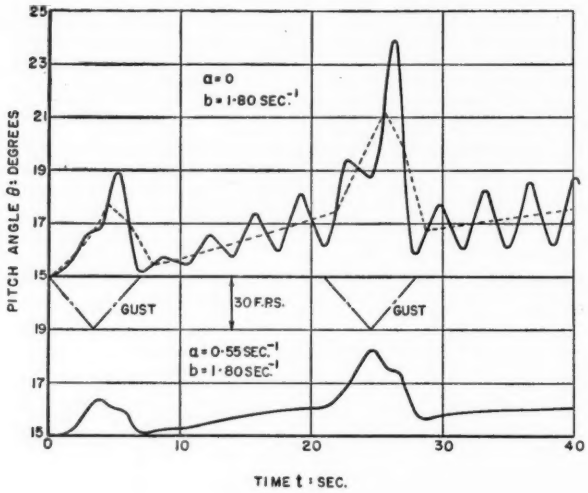

Fig. 12.

Correspondingly, there is a decrease to zero of the horizontal thrust component, followed subsequently by a rapid increase in the reverse sense, while the vertical component remains very nearly constant at first, diminishes to zero as the body axis becomes normal to the flight path, and finally changes sign. It will be seen, therefore, that the initial forward and upward motion is steadily converted into one in a rearward and downward direction, so that the flight path takes the form of a loop, as indicated, with the aircraft in roughly the inverted position at the top of the trajectory. When, however, the control is adequate, θ varies very little (*see*, further, Fig. 10). Consequently, the horizontal and vertical thrust components remain of the same sign, and the flight path takes the desired form. Nevertheless, although the difference of θ between the controls with $b=1{\cdot}80$ and $b=2{\cdot}52$ sec.$^{-1}$ is very small, it is evident from Fig. 9 that the corresponding changes of flight path are much larger. This is due principally to the sensitivity of the horizontal thrust component to small variations of θ. It is also obvious that, in the unstable case ($b=0{\cdot}90$ sec.$^{-1}$), there will be a maximum for α, as shown in Fig. 10, in the region where the aircraft body axis has become roughly normal to the direction of motion. Beyond this point the incidence will decrease again as the aircraft becomes inverted. At about the same time, the resultant air speed increases rapidly (*see* Fig. 11), since the thrust then acts principally along the flight path. Finally, had the calculations been extended to the culminating stage (an undertaking which would have involved a very considerable increase of labour owing to the rapid changes taking place), it is clear that they would have indicated a strong downward curvature of the flight path under the combination of gravity and inverse vertical thrust.

The close accordance of the pitch characteristics, whether the aircraft is hovering or in general motion, has already been noted from Figs. 3 and 12. Equally, the earlier observation with respect to the small effect of a gust on x and z is again

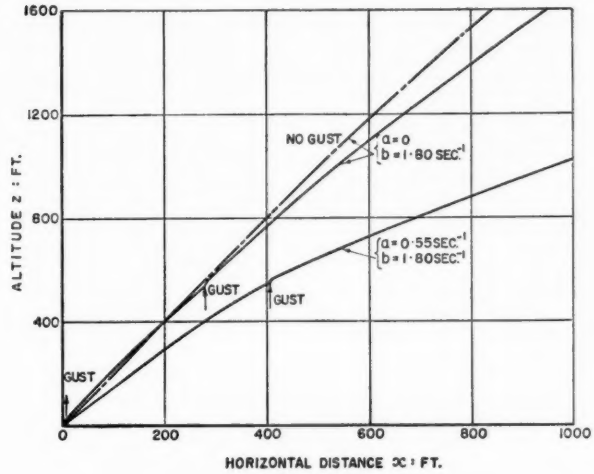

Fig. 13.

apparent when translation of the aircraft is considered. To illustrate this point, an example is given in Fig. 13 of the flight path in calm and gusty air* when $a=0$, $b=1{\cdot}80$ sec.$^{-1}$. The close proximity of the curves agrees very well with the earlier conclusion derived from the analysis of the simple hovering case. Fig. 12 describes the corresponding pitching motion of the aircraft under the gust conditions. Of additional interest is the effect of adding some damping ($a=0{\cdot}55$ sec.$^{-1}$) to the control. Here, the appreciable diminution of the oscillations in pitch (Fig. 12) results, for the reason given earlier, in a larger horizontal thrust component, and therefore the forward speed and displacement of the aircraft are increased relative to the corresponding undamped conditions. On the other hand, the motion vertically remains practically unchanged. Hence, the flight path becomes less steep. In general, therefore, any increase of damping or stiffness in the control leads to a more curved, *i.e.* a flatter, trajectory.

Finally, in regard to this last feature, an interesting point is raised in Fig. 14†, namely, the sensitivity of the initial flight direction β to the thrust angle γ. This, of course, is again explained by the appreciable changes in the conditions horizontally for small differences of either θ or γ. Practically, it suggests that, where, for example, a take-off has to be made in a confined space, careful attention must be given to the setting of the jet pipes and ground angle of the aeroplane. Other discrepancies of possible significance, not here considered, may arise from lack of coincidence of the line of action of the jet thrust with the pipe axis (the most natural practical datum to assume) due to ground interference and asymmetry of the gas flow before discharge.

*Triangular gusts were considered in contrast to the sinusoidal distribution assumed when hovering, since they are more convenient in the step-by-step calculations. Either form has substantially the same quantitative effect.

†In this case, it is quite adequate, for the purpose of demonstration, to assume infinite stiffness of the control (θ constant), when the calculations are particularly simple.

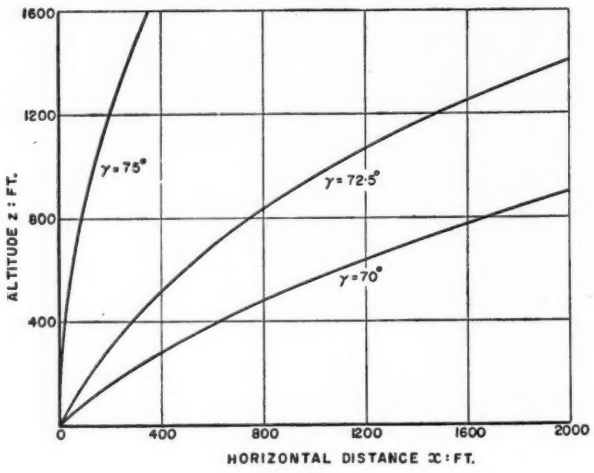

Fig. 14.

ACKNOWLEDGMENT

The author is indebted to Mr. P. Bellerby who kindly undertook the labour of the numerical calculations.

REFERENCES

1. DONELY, P. Summary of Information Relating to Gust Loads on Airplanes. N.A.C.A. Report 997, 1950.

2. The Staff of the Structures Department, R.A.E. Empirical Formulae for Moments of Inertia of Aircraft. R.A.E. Report Structures 28, 1948.

Appendix I

ORDER OF THE TERMS IN $\dot{\theta}$ IN EQUATIONS (5)

To show that the terms in $\dot{\theta}$ of equations (5) may be ignored under the conditions pertinent to the present investigation, it is noted first that either they are demonstrably negligible even under normal conditions of flight, or else that they arise predominantly from the action of the tailplane. To obtain the order of magnitude of the terms concerned, therefore, contributions from other parts of the aircraft will be neglected.

Consider, now, the case when there is steady angular velocity $\dot{\alpha}$ and β is constant. Then the tailplane experiences an increment of incidence

$$\delta\alpha' = \frac{l_T \dot{\alpha}}{V} - \delta\varepsilon, \quad . \quad . \quad . \quad . \quad . \quad . \quad . \quad (63)$$

where α' is the angle of incidence of the tailplane, l_T is the distance of the tailplane lifting line from the centre of gravity and ε is the downwash.

Further, by the usual assumption regarding downwash lag, namely that the instantaneous value of the downwash at the tailplane is the same as that appropriate to the lifting line of the wing at the instant when it occupied the spatial position now held by the tailplane, we have

$$\delta\varepsilon = -\frac{d\varepsilon}{d\alpha}\frac{l_T\dot{\alpha}}{V}, \qquad (64)$$

so that

$$\delta\alpha' = \frac{l_T\dot{\alpha}}{V}\left(1+\frac{d\varepsilon}{d\alpha}\right). \qquad (65)$$

Again, when there is steady angular velocity $\dot{\beta}$, with α constant, the increment of tailplane incidence is

$$\delta\alpha' = \frac{l_T\dot{\beta}}{V}, \qquad (66)$$

so that when both α and β are varying, we have, combining equations (65) and (66),

$$\left.\begin{aligned} L_{\dot{\theta}}\delta\dot{\theta} \simeq L'_{\dot{\theta}}\delta\dot{\theta} &= \frac{\partial L'}{\partial\alpha'}\frac{l_T}{V}\left\{\left(1+\frac{d\varepsilon}{d\alpha}\right)\dot{\alpha}+\dot{\beta}\right\}, \\ D_{\dot{\theta}}\delta\dot{\theta} \simeq D'_{\dot{\theta}}\delta\dot{\theta} &= \frac{\partial D'}{\partial\alpha'}\frac{l_T}{V}\left\{\left(1+\frac{d\varepsilon}{d\alpha}\right)\dot{\alpha}+\beta\right\}, \\ M_{\dot{\theta}}\delta\dot{\theta} \simeq M'_{\dot{\theta}}\delta\dot{\theta} &= \frac{\partial M'}{\partial\alpha'}\frac{l_T}{V}\left\{\left(1+\frac{d\varepsilon}{d\alpha}\right)\dot{\alpha}+\dot{\beta}\right\}, \end{aligned}\right\} \qquad (67)$$

where L', D', M' are the lift, drag and pitching moment respectively contributed by the tailplane. If, further, we write

$$L',\ D' = \tfrac{1}{2}\sigma\rho_0 V^2 S\,(C_L',\ C_D'),$$

$$M' = \tfrac{1}{2}\sigma\rho_0 V^2 S\bar{c}\,C_m',$$

where primes again denote measures related to the tailplane, neglect the downwash variation on account of the very high incidences involved and assume, for simplicity, that the tailplane chord is parallel to the wing chord, *i.e.* α' becomes equal to α, we have for the instantaneous values of L, D, M

$$\left.\begin{aligned} L &\simeq \tfrac{1}{2}\sigma\rho_0 V^2 S\left(C_L+\frac{dC_L'}{d\alpha}\frac{l_T\dot{\theta}}{V}\right), \\ D &\simeq \tfrac{1}{2}\sigma\rho_0 V^2 S\left(C_D+\frac{dC_D'}{d\alpha}\frac{l_T\dot{\theta}}{V}\right), \\ M &\simeq \tfrac{1}{2}\sigma\rho_0 V^2 S\bar{c}\left(C_m+\frac{dC_m'}{d\alpha}\frac{l_T\dot{\theta}}{V}\right). \end{aligned}\right\} \qquad (68)$$

The magnitudes of the various terms in equations (68) are now evaluated under the most severe conditions which can reasonably be expected. Whether they relate to a small but responsive aircraft, or to one of greater size and comparative sluggishness, the

value of $l_T\dot{\theta}/V$ during a disturbance is unlikely to exceed 0·06. From tailplane experiments on the model referred to in Section 4.1 under the conditions there indicated, it also appears that over the interval $30° < \alpha < 70°$ the coefficients C_L', C_D', C_m' are roughly linear functions of α with $dC_L'/d\alpha \simeq \pm 0{\cdot}20$ per rad.*, $dC_D'/d\alpha \simeq 0{\cdot}38$ per rad. and $dC_m'/d\alpha \simeq -0{\cdot}17$ per rad. Accordingly, the following maxima are obtained for the $\dot{\theta}$ terms in equations (68):

$$\frac{dC_L'}{d\alpha}\frac{l_T\theta}{V} = \pm 0{\cdot}012, \quad \frac{dC_D'}{d\alpha}\frac{l_T\dot{\theta}}{V} = 0{\cdot}023, \quad \frac{dC_m'}{d\alpha}\frac{l_T\dot{\theta}}{V} = -0{\cdot}010.$$

Relative to the maximum values of C_L, C_D, C_m (Fig. 2), the corresponding terms above are all of the order of one per cent., so that even when the latter quantities are halved, which occurs when the incidence is about 80° for lift and 40° to 50° for drag and pitch, *i.e.* when considering virtually the full flight range of incidence, the error in neglecting the $\dot{\theta}$ terms is unlikely to be more than two per cent.

Appendix II

Gyroscopic Yawing Couple Due to Pitching of the Aircraft

When the aircraft pitches, a yawing couple N_g may be produced by revolving parts such as the impeller, or impellers, of the turbo-jet power system. This effect depends upon the disposition of the various units. In general, if OX, OY, OZ are any set of rectangular axes with OX as the relevant axis of rotation, then, when the system as a whole experiences an angular velocity about OY, there will be a gyroscopic couple with respect to OZ. Hence, in the case of the pitch and yaw interaction, the moment will be principally generated by those units for which OX is substantially parallel to, but not necessarily in, the plane of symmetry, while, if N_g is measured about the normal to the longitudinal axis of the aircraft, only those revolving elements for which OX is parallel, or approximately parallel, to the longitudinal axis will be significant†. Accordingly, in the following brief analysis, which is merely concerned with the order of the effect, secondary terms are ignored and the problem is regarded as essentially determined by the foregoing approximations relating to the disposition of reference axes and to the selection of significant mechanical units. Then, the magnitude of the couple N_g with respect to OZ is

$$N_g = pI\dot{\theta}, \quad . \quad . \quad . \quad . \quad . \quad . \quad . \quad (69)$$

where p is the angular velocity of the rotating parts (assumed constant and of the same magnitude and sense for each component), and I is the total polar moment of inertia. On the assumption, therefore, that the disturbance in pitch arises from a two-dimensional vertical gust, as discussed in Section 2.2, and further, that any subsequent lateral motion may be treated independently of the longitudinal motion (an argument which is reasonably valid during the short interval of a disturbance), we have, when the

*The lift curve has a sharp maximum at about $\alpha = 50°$, such that, for $30° < \alpha < 50°$, $dC_L'/d\alpha \simeq 0{\cdot}20$ per rad., and for $50° < \alpha < 70°$, $dC_L'/d\alpha \simeq -0{\cdot}20$ per rad.

†Normally, the longitudinal axis will not be appreciably displaced from the horizontal, so that N_g then refers roughly to the vertical, or OZ, axis of the fixed reference frame adopted in the main part of the paper.

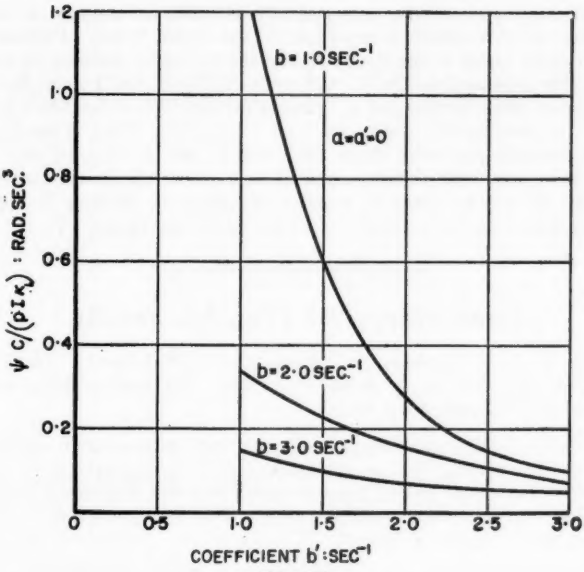

Fig. 15.
Yaw due to gyroscopic action.

yawing motion due to N_g is reacted by automatic controls similar to those discussed in the case of pitch, the companion equation to (8), namely,

$$C\ddot{\psi}=K_1'\dot{\psi}+K_2'\psi+N_g,$$

or
$$\ddot{\psi}+2a'\dot{\psi}+s'^2\psi=F'(t), \qquad . \quad . \quad . \quad . \quad . \quad (70)$$

where C is the moment of inertia of the aircraft about OZ, ψ is the angle of yaw, K_1', K_2' the control stiffness coefficients proportional to $\dot{\psi}$ and ψ respectively and

$$a'=-\frac{K_1'}{2C}, \qquad s'^2=-\frac{K_2'}{C}, \qquad F'(t)=\frac{N_g}{C}=\frac{pI\dot{\theta}}{C}.$$

Then the solution to (70) follows immediately from (49) simply by substituting ψ for θ, a' for a, b for b, $F'(t)$ for $F(t)$ and the value of $\dot{\theta}$ in (69) by the differentiation of (16). The result may be expressed as

$$\frac{C\psi}{pI\kappa_1}=\frac{e^{-a't}}{b'}\left[\sin b't\int_0^t e^{a'\tau}\Theta(\tau)\cos b'\tau d\tau-\cos b't\int_0^t e^{a'\tau}\Theta(\tau)\sin b'\tau d\tau\right], \qquad . \quad (71)$$

where

$$\Theta(\tau)=-\frac{e^{-a\tau}}{\kappa_1}\{(aC_1-bC_2)\cos b\tau+(bC_1+aC_2\sin b\tau\}-\frac{2\omega}{\kappa_1}(C_3\sin 2\omega\tau-C_4\cos 2\omega\tau).$$

Fig. 15 is a plot of $C\psi_{max}/(pI\kappa_1)$ as a function of b and b' when $a=a'=0$ and $1<b$, $b'<3$, ψ_{max} being the maximum angle of yaw in the gust.

value of $l_T\dot{\theta}/V$ during a disturbance is unlikely to exceed 0·06. From tailplane experiments on the model referred to in Section 4.1 under the conditions there indicated, it also appears that over the interval $30° < \alpha < 70°$ the coefficients C_L', C_D', C_m' are roughly linear functions of α with $dC_L'/d\alpha \simeq \pm 0{\cdot}20$ per rad.*, $dC_D'/d\alpha \simeq 0{\cdot}38$ per rad. and $dC_m'/d\alpha \simeq -0{\cdot}17$ per rad. Accordingly, the following maxima are obtained for the $\dot{\theta}$ terms in equations (68):

$$\frac{dC_L'}{d\alpha}\frac{l_T\theta}{V} = \pm 0{\cdot}012, \quad \frac{dC_D'}{d\alpha}\frac{l_T\dot{\theta}}{V} = 0{\cdot}023, \quad \frac{dC_m'}{d\alpha}\frac{l_T\dot{\theta}}{V} = -0{\cdot}010.$$

Relative to the maximum values of C_L, C_D, C_m (Fig. 2), the corresponding terms above are all of the order of one per cent., so that even when the latter quantities are halved, which occurs when the incidence is about 80° for lift and 40° to 50° for drag and pitch, *i.e.* when considering virtually the full flight range of incidence, the error in neglecting the $\dot{\theta}$ terms is unlikely to be more than two per cent.

Appendix II

Gyroscopic Yawing Couple Due to Pitching of the Aircraft

When the aircraft pitches, a yawing couple N_g may be produced by revolving parts such as the impeller, or impellers, of the turbo-jet power system. This effect depends upon the disposition of the various units. In general, if OX, OY, OZ are any set of rectangular axes with OX as the relevant axis of rotation, then, when the system as a whole experiences an angular velocity about OY, there will be a gyroscopic couple with respect to OZ. Hence, in the case of the pitch and yaw interaction, the moment will be principally generated by those units for which OX is substantially parallel to, but not necessarily in, the plane of symmetry, while, if N_g is measured about the normal to the longitudinal axis of the aircraft, only those revolving elements for which OX is parallel, or approximately parallel, to the longitudinal axis will be significant†. Accordingly, in the following brief analysis, which is merely concerned with the order of the effect, secondary terms are ignored and the problem is regarded as essentially determined by the foregoing approximations relating to the disposition of reference axes and to the selection of significant mechanical units. Then, the magnitude of the couple N_g with respect to OZ is

$$N_g = pI\dot{\theta}, \quad . \quad . \quad . \quad . \quad . \quad . \quad . \quad (69)$$

where p is the angular velocity of the rotating parts (assumed constant and of the same magnitude and sense for each component), and I is the total polar moment of inertia. On the assumption, therefore, that the disturbance in pitch arises from a two-dimensional vertical gust, as discussed in Section 2.2, and further, that any subsequent lateral motion may be treated independently of the longitudinal motion (an argument which is reasonably valid during the short interval of a disturbance), we have, when the

*The lift curve has a sharp maximum at about $\alpha = 50°$, such that, for $30° < \alpha < 50°$, $dC_L'/d\alpha \simeq 0{\cdot}20$ per rad., and for $50° < \alpha < 70°$, $dC_L'/d\alpha \simeq -0{\cdot}20$ per rad.

†Normally, the longitudinal axis will not be appreciably displaced from the horizontal, so that N_g then refers roughly to the vertical, or OZ, axis of the fixed reference frame adopted in the main part of the paper.

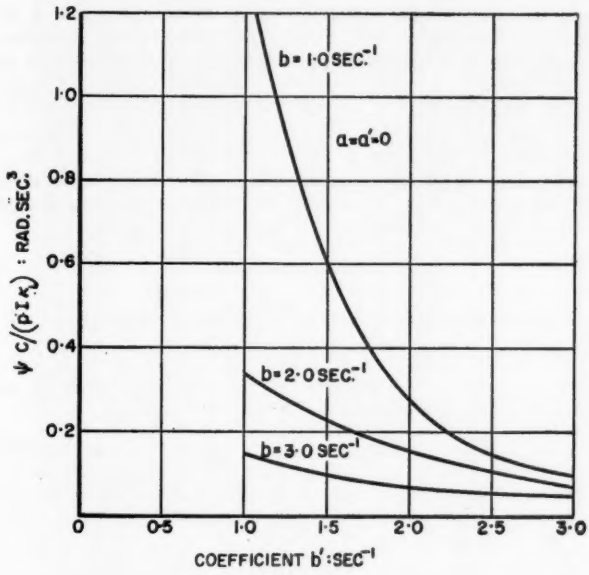

Fig. 15.
Yaw due to gyroscopic action.

yawing motion due to N_g is reacted by automatic controls similar to those discussed in the case of pitch, the companion equation to (8), namely,

$$C\ddot{\psi}=K_1'\dot{\psi}+K_2'\psi+N_g,$$

or
$$\ddot{\psi}+2a'\dot{\psi}+s'^2\psi=F'(t), \qquad . \quad . \quad . \quad . \quad . \quad . \quad (70)$$

where C is the moment of inertia of the aircraft about OZ, ψ is the angle of yaw, K_1', K_2' the control stiffness coefficients proportional to $\dot{\psi}$ and ψ respectively and

$$a'=-\frac{K_1'}{2C}, \qquad s'^2=-\frac{K_2'}{C}, \qquad F'(t)=\frac{N_g}{C}=\frac{pI\dot{\theta}}{C}.$$

Then the solution to (70) follows immediately from (49) simply by substituting ψ for θ, a' for a, b for b, $F'(t)$ for $F(t)$ and the value of $\dot{\theta}$ in (69) by the differentiation of (16). The result may be expressed as

$$\frac{C\psi}{pI\kappa_1}=\frac{e^{-a't}}{b'}\left[\sin b't\int_0^t e^{a'\tau}\Theta(\tau)\cos b'\tau d\tau-\cos b't\int_0^t e^{a'\tau}\Theta(\tau)\sin b'\tau d\tau\right], \qquad . \quad (71)$$

where

$$\Theta(\tau)=-\frac{e^{-a\tau}}{\kappa_1}\{(aC_1-bC_2)\cos b\tau+(bC_1+aC_2\sin b\tau\}-\frac{2\omega}{\kappa_1}(C_3\sin 2\omega\tau-C_4\cos 2\omega\tau).$$

Fig. 15 is a plot of $C\psi_{max}/(pI\kappa_1)$ as a function of b and b' when $a=a'=0$ and $1<b$, $b'<3$, ψ_{max} being the maximum angle of yaw in the gust.

From an examination of the data on current turbo-jet engines, it would appear that the quantity pI/P varies between about 1 and 2 rad.ft.sec. Further, taking the weight W as roughly equal to the thrust P, and the radius of gyration in yaw from the data of Ref. 2, it is estimated that pI/C will not normally exceed 1·5 rad. sec.$^{-1}$. Hence, with the maximum value assigned to κ_1, namely 0·1 sec.$^{-2}$ (*see* Section 4.1), a figure of 0·15 rad. sec^{-3} is obtained for the upper limit to $pI\kappa_1/C$. Thus, from Fig. 15, it will be seen that at roughly the lower limits for b and b', say, $b=b'=1{\cdot}5$ sec.$^{-1}$, the value of ψ_{max} is not likely to exceed about 5°, and when $a \neq 0$ it will be even smaller. Hence, the assumption of two-dimensional motion advanced in Section 1 appears to be reasonably justified.

Errata—May 1955 (Vol. VI, Part 2)

In the paper by E. W. GRAHAM, B. J. BEANE and R. M. LICHER, "*The Drag of Non-Planar Thickness Distributions in Supersonic Flow*," the authors have asked for the following addition to be made on p. 111:—

> "In Figure 7, the equivalent Sears-Haack body of revolution should be of fineness ratio 5. The central body of revolution should be approximately double-conical in shape (*i.e.* two cones placed base to base), and the maximum thickness of the central body, for the given wing geometry, is approximately half the maximum thickness of the Sears-Haack body."

In the paper by G. N. LANCE, "*The Lift of Twisted and Cambered Wings*," the following corrections are necessary:—

p. 154: The argument of the $\cosh^{-1}$ in (15) should read $\left|\frac{a}{\theta}\right|$.

p. 155: Insert a minus sign on the right hand side of (18).

p. 156: The left hand sides of the equations on lines 9, 10 and 11 and 13 should read b_0/α_{11}, b_2/α_{11}, c_2/α_{11}, and $+\eta$ respectively.
The right hand side of (25) should be -1.

p. 157: Replace (27) and (28) with

$$ab_0'[2a^2\mathrm{K}-(1+a^2)\mathrm{E}]+ab_2'[a^2\mathrm{K}(5a^2-3)+2\mathrm{E}(3-5a^2+a^4)]+ +a^2c_2'[2a^4\mathrm{K}-\mathrm{E}(3a^2-1)]=0 \quad . \quad . \quad (27)$$

$$ab_0'[a^2\mathrm{K}(5-3a^2)+2\mathrm{E}(3a^4-5a^2+1)]+ab_2'[2a^4\mathrm{K}-(a^2+a^4)\mathrm{E}]+ +a^2c_2'[a^2\mathrm{K}(3-a^2)-2\mathrm{E}]=0 \quad . \quad . \quad (28)$$

The left hand sides of (30) and (31) should read $-\pi b_0'$ and $+\pi b_2'$ respectively.

p. 161: In the expression for ϕ_{11}, the first α_{11} should be preceded by a minus sign and the term $-2\eta^2$ should read $+2\eta^2$.

The author wishes to express his thanks to Mr. Julian Kainer and Mr. Hitch for drawing his attention to these errors.

INDEX TO VOLUME VI

AERODYNAMICS

See also Channel Flow, Compressor Blades, Photography, Stability, Sting Supports.

Note on a Null Method for the Direct Measurement of Pressure Coefficients, L. H. Tanner, p. 241 (November 1955).

On an Approximate Method of Calculating Pressures on Non-lifting Head Shapes at Supersonic Speeds, H. K. Zienkiewicz, p. 31 (February 1955).

On the Unsteady Motion of a Slender Body through a Compressible Fluid, L. E. Fraenkel, p. 59 (February 1955).
Errata, p. 164 (May 1955).

Supersonic Flow Past Slender Bodies with Discontinuous Profile Slope, L. E. Fraenkel and H. Portnoy, p. 114 (May 1955).

The Distribution of Pressure on an Aerofoil, in a Stream with a Spanwise Velocity Gradient, W. A. Mair, p. 1 (February 1955).

The Drag of Non-Planar Thickness Distributions in Supersonic Flow, E. W. Graham, B. J. Beane and R. M. Licher, p. 99 (May 1955).
Addendum, p. 240 (August 1955).
Erratum, p. 328 (November 1955).

The Lift of Twisted and Cambered Wings in Supersonic Flow, G. N. Lance, p. 149 (May 1955).
Erratum, p. 328 (November 1955).

BEANE, B. J., E. W. GRAHAM and R. M. LICHER

The Drag of Non-Planar Thickness Distributions in Supersonic Flow, p. 99 (May 1955).
Addendum, p. 240 (August 1955).
Erratum, p. 328 (November 1955).

BISHOP, R. E. D. and D. C. JOHNSON

Some Properties of Nodes in Vibrating Systems, p. 46 (February 1955).

CHANNEL FLOW

Compressible Subsonic Flow in Two-dimensional Channels, L.C. Woods.
Part I: Basic Mathematical Theory, p. 205 (August 1955).
Part II: The Application of the Theory to Problems of Channel Flow, p. 254 (November 1955).

COLEMAN, W. S.

Stabilisation of the Aeroplane in Flight at Zero or Very Small Air Speeds, p. 295 (November 1955).

COMPRESSOR BLADES

Some Effects of Mechanical Damping on the Self-Induced Aeroelastic Oscillations of an Axial Compressor Blade, I. M. Davidson, p. 81 (May 1955).

DAVIDSON, I. M.

Some Effects of Mechanical Damping on the Self-Induced Aeroelastic Oscillations of an Axial Compressor Blade, p. 81 (May 1955).

DONALDSON, I. S.

The Effect of Sting Supports on the Base Pressure of a Blunt-Based Body in a Supersonic Stream, p. 221 (Aug. 1955).

ELECTRICAL ANALOGUE

See Structures.

ELLIOTT, D. E.

The Measurement of High Speed Air Velocity and Temperature using Sound Wave Photography, p. 181 (August 1955).

FATIGUE

See also Photoelasticity.

Effect of Yielding on the Fatigue Properties of Test Pieces containing Stress Concentrations, K. Gunn, p. 277 (November 1955).

FRAENKEL, L. E.

On the Unsteady Motion of a Slender Body through a Compressible Fluid, p. 59 (February 1955).
Errata, p. 164 (May 1955).

FRAENKEL, L. E. and H. PORTNOY

Supersonic Flow Past Slender Bodies with Discontinuous Profile Slope, p. 114 (May 1955).

GODFREY, D. E. R.

Normal Loading on a Wedge-Shaped Plate, p. 196 (August 1955).

GRAHAM, E. W., B. J. BEANE and R. M. LICHER

The Drag of Non-Planar Thickness Distributions in Supersonic Flow, p. 99 (May 1955).
Addendum, p. 240 (August 1955).
Erratum, p. 328 (November 1955).

GUNN, K.

Effect of Yielding on the Fatigue Properties of Test Pieces containing Stress Concentrations, p. 277 (November 1955).

HOLISTER, G. S., H. T. JESSOP and C. SNELL

Photoelastic Investigation in Connection with the Fatigue Strength of Bolted Joints, p. 230 (August 1955).

INTERPLANETARY FLIGHT

Dynamic Problems of Interplanetary Flight, Derek F. Lawden, p. 165 (August 1955).

INDEX

JESSOP, H. T., C. SNELL and G. S. HOLISTER

Photoelastic Investigation in Connection with the Fatigue Strength of Bolted Joints, p. 230 (August 1955).

JOHNSON, D. C. and R. E. D. BISHOP

Some Properties of Nodes in Vibrating Systems, p. 46 (February 1955).

LANCE, G. N.

The Lift of Twisted and Cambered Wings in Supersonic Flow, p. 149 (May 1955). *Erratum*, p. 328 (November 1955).

LAWDEN, DEREK F.

Dynamic Problems of Interplanetary Flight, p. 165 (August 1955).

LICHER, R. M., E. W. GRAHAM and B. J. BEANE

The Drag of Non-Planar Thickness Distributions in Supersonic Flow, p. 99 (May 1955).
Addendum, p. 240 (August 1955).
Erratum, p. 328 (November 1955).

MAIR, W. A.

The Distribution of Pressure on an Aerofoil, in a Stream with a Spanwise Velocity Gradient, p. 1 (February 1955).

PALMER, P. J. and S. C. REDSHAW

Experiments with an Electrical Analogue for the Extension and Flexure of Flat Plates, p. 13 (February 1955).

PHOTOELASTICITY

Photoelastic Investigation in Connection with the Fatigue Strength of Bolted Joints, H. T. Jessop, C. Snell and G. S. Holister, p. 230 (August 1955).

PHOTOGRAPHY

The Measurement of High Speed Air Velocity and Temperature using Sound Wave Photography, D. E. Elliott, p. 181 (August 1955).

PORTNOY, H. and L. E. FRAENKEL

Supersonic Flow Past Slender Bodies with Discontinuous Profile Slope, p. 114 (May 1955).

REDSHAW, S. C. and P. J. PALMER

Experiments with an Electrical Analogue for the Extension and Flexure of Flat Plates, p. 13 (February 1955).

REVIEWS

Linearized Theory of Steady High-Speed Flow, by G. N. Ward. Reviewed by W. A. Mair, p. 240 (August 1955).

Studies in Mathematics and Mechanics, presented to Richard von Mises, edited by Garrett Birkhoff, Gustav Kuerti and Gabor Szegö. Reviewed by M. J. Lighthill, p. 164 (May 1955).

ROBINSON, J. R.

The Buckling and Bending of Orthotropic Sandwich Panels With All Edges Simply-Supported, p. 125 (May 1955).

SANDWICH PANELS

The Buckling and Bending of Orthotropic Sandwich Panels With All Edges Simply-Supported, J. R. Robinson, p. 125 (May 1955).

SNELL, C., H. T. JESSOP and G. S. HOLISTER

Photoelastic Investigation in Connection with the Fatigue Strength of Bolted Joints, p. 230 (August 1955).

STABILITY

Stabilisation of the Aeroplane in Flight at Zero or Very Small Air Speeds, W. S. Coleman, p. 295 (November 1955).

STING SUPPORTS

The Effect of Sting Supports on the Base Pressure of a Blunt-Based Body in a Supersonic Stream, I. S. Donaldson, p. 221 (August 1955).

STRUCTURES

See also Fatigue, Photoelasticity, Sandwich Panels.

Experiments with an Electrical Analogue for the Extension and Flexure of Flat Plates, P. J. Palmer and S. C. Redshaw, p. 13 (February 1955).

Normal Loading on a Wedge-Shaped Plate, D. E. R. Godfrey, p. 196 (August 1955).

TANNER, L. H.

Note on a Null Method for the Direct Measurement of Pressure Coefficients, p. 241 (November 1955).

VIBRATION

See also Compressor Blades

Some Properties of Nodes in Vibrating Systems, R. E. D. Bishop and D. C. Johnson, p. 46 (February 1955).

WOODS, L. C.

Compressible Subsonic Flow in Two-dimensional Channels.
Part I: Basic Mathematical Theory, p. 205 (August 1955).
Part II: The Application of the Theory to Problems of Channel Flow, p. 254 (November 1955).

ZIENKIEWICZ, H. K.

On an Approximate Method of Calculating Pressures on Non-lifting Head Shapes at Supersonic Speeds, p. 31 (February 1955).